LEOPARDSAT CONSTELLATION

Low Earth Orbit Phased Array Radar Detection satellite constellation for the Royal Netherlands Air Force

Benedicto Rinaudo T.	4234979	Klapwijk J.	4023560
Boerdijk T.	1506714	Nieuwenhuijsen M.P.	4102274
Coolen D.L.	4156803	Schroyen D.J.P.	4214269
Jaberi S. al	4040570	Zeeuw W. de.	4221230
Jacobse R.	4141385	**GROUP S19**	

Final Report

Design Synthesis Exercise

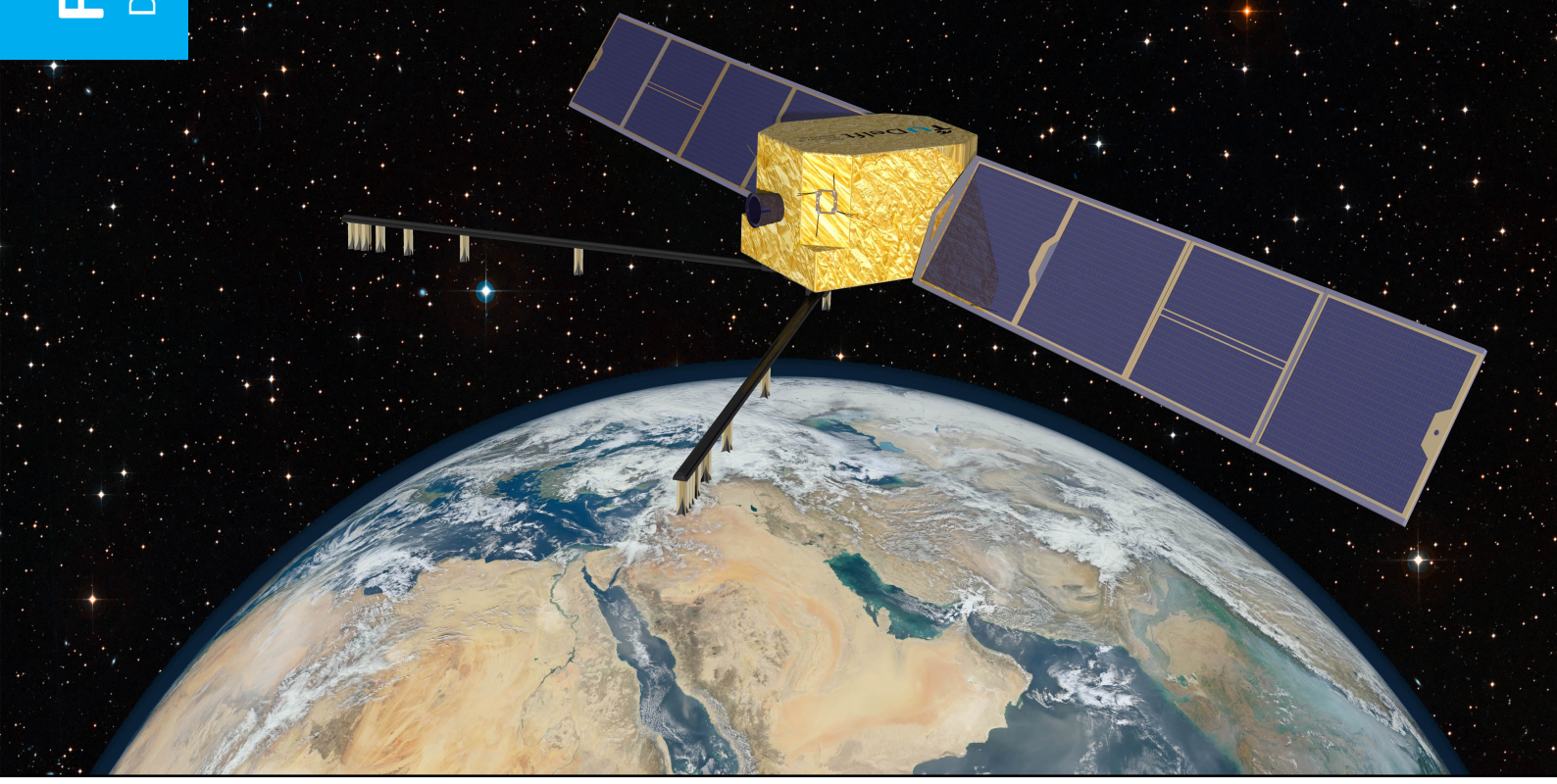

TU Delft Delft University of Technology

Faculty of Aerospace Engineering

June 30, 2015

Change Record

Issue	Revision	Reason for Change	Date	Paragraph(s)
1	0	First Issue of Document	23/06/2015	all
2	0	New version to implement comments and to comply with page limit regulation	30/06/2015	all

Team Members


Tomas Benedicto Rinaudo


Tom Boerdijk

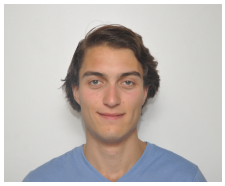
Danny Coolen


Salwan al Jaberi


Ruben Jacobse


Jeffrey Klapwijk


Maarten Nieuwenhuijsen


Dries Schroyen


Willem de Zeeuw

External Relations

	Name	Organisation
Customer	Capt. F.A. Matser	RNLAF
External experts	Bertil Oving	NLR
	Bert-Johan Vollmuller	NLR
	Matthijs de Haan	Terma
	Ruut Neubauer	SSBV
	Max Pastena	SSBV

Preface

This report is the third and final report written by DSE Group 19 at the Delft University of Technology (TU Delft). The DSE is the closing project for the Bachelor of Science (BSc) curriculum at the Faculty of Aerospace Engineering of the Delft University of Technology. Over the course of eleven weeks, a group of nine students worked on the design of an aerospace system as the final assessment before obtaining their BSc.

This project was set up in cooperation with the RNLAF. Our customer, RNLAF Captain Frank Matser, has expressed the need to decrease the dependence on foreign intelligence services. Because the Dutch MoD does not have any space assets of its own, there is a partial dependence on other states to gather ELINT. Captain Matser has tasked the team with investigating the feasibility of creating a Dutch space asset to provide an in-house source of intelligence gathered from space.

Readers who are particularly interested in RF signal detection and localisation are referred to Chapter 6 and Chapters 11 to 13. Part III of this report is of particular interest to readers looking for the resulting design of this project. For an overview of the system characteristics of the satellites, the reader is recommended to read Chapter 10. Readers who seek more information on the DSE project in general and the organisation of the project are referred to Chapter 2.

A number of employees from the TU Delft and professionals from the aerospace industry have provided their assistance to our DSE project, for which we are very thankful. Firstly, we would like to express our gratitude to Captain Frank Matser for acting as the customer in this project and for enabling us to collaborate with experts from the aerospace industry.

Secondly, our sincere thankfulness goes out to Trevor Watts, Jacco Geul and Ping Liu from the Delft University of Technology for their dedicated guidance, advice and feedback. Their help has provided us with the means to set course towards a successful completion of this DSE project.

Furthermore, we would like to thank Ruut Neubauer and Max Pastena from SSBV for their aid and advice during this project. We appreciate that they hosted us for a full afternoon and arranged a meeting with SSBV engineers at their office in Noordwijk.

We thank Matthijs de Haan from Terma for bringing us into contact with Terma's specialists, which was of great value to the team and the project. The help we got from Terma's engineers Benny Hede and Kim Plauborg has proven to be very useful.

Next to SSBV and Terma, the NLR has also provided their assistance during the project. We would like to thank Bertil Oving and Bert-Johan Vollmuller from the NLR for their help and the elaborate feedback they gave on our reports.

Lastly, we would like to express our appreciation for all the help we got from employees within the TU Delft. A special thanks goes out to professor Alexander Yarovoy of the Microwave Sensing, Signals and Systems section at the Faculty of Electrical Engineering, Mathematics and Computer Science for his help with the antenna design.

Delft, June 30th 2015
DSE Group 19

Summary

This document presents a feasibility study and a concept design of a constellation of small spacecraft capable of detecting, identifying, and locating radars and Global Positioning System jammers for the Royal Netherlands Air Force for a mission lifetime of five years. These actions are performed in the context of the Design Synthesis Exercise.

The spacecraft are required to detect radar signals from 1 GHz to 4 GHz and from 8 GHz to 12 GHz, since most radar systems of interest operate within these frequency bands. The frequency band used by GPS jammers is the L1-band, which falls within these frequency bands.

Several concepts were proposed and compared to each other. The concept that was chosen to be designed to the subsystem level consists of four identical spacecraft, flying in a rectangular formation made up of two orbital planes. The spacecraft will process the data from the payload on-board and will need a crosslink to the other satellites to exchange some of the payload data in order to perform its geolocation function.

Starting from this description of the concept, the subsystems of the spacecraft have been designed, as well as the orbit. The design was performed using concurrent engineering and iterations.

The constellation consists of four spacecraft, orbiting at an altitude of 500 km in two orbital planes, which are both inclined at 100° and divided by a right ascension of the ascending node of 6°.

Using these orbital characteristics, the geolocation performance of the system is the following: Radar sources can be localised, using a single observation angle of arrival method. For this, two antenna arrays of 2.4 m are used. This method produces location results with an accuracy within 5 km for elevation angles above 30°. At such elevations, side-lobe detection of radar systems is required. Using this method, global coverage is achieved for the geolocation of radars. On the other hand, to locate GPS jammers, four observations of the same signal need to be obtained. From these, the Joint Time Difference of Arrival-Frequency Difference of Arrival method can be used to locate the jamming source with an accuracy of 200 m up to 70° latitude.

The spacecraft use several arrays of antennas and signal processing equipment to detect the signals of interest. To successfully locate the GPS jammers, due to the geolocation method selected, the spacecraft need to exchange the frequency spectrum and time stamp of the received signal. This is achieved through UHF-band crosslinks.

The wet mass of an individual spacecraft is 130 kg. Its average power consumption is 346 W with a peak power of 672 W. The estimated cost of the entire program, excluding launch, is € 88 million.

Finally, with the aforementioned specifications, the system is compliant or partially compliant to all set requirements, except for the cost requirement, which was set at € 45 million.

Contents

List of Symbols

A_r	Ram area	[m^2]
A_s	Sunlit surface area	[m^2]
a_D	Acceleration due to aerodynamic drag	[m s^{-2}]
B	Bandwidth	[Hz]
B	Magnetic field strength	[T]
C_D	Drag coefficient	[−]
c	Speed of light ($c = 3 \times 10^8$)	[m s^{-1}]
cm	Centre of mass	[m]
cp	Centre of pressure	[m]
cp_a	Centre of aerodynamic pressure	[m]
cp_s	Centre of solar radiation pressure	[m]
D	Distance between first and last antenna elements	[m]
D	Residual dipole moment	[A m^2]
DOD	Battery depth of discharge	[−]
d	Arm of c.m. to panel	[m]
d	Distance between transmitter and receiver	[m]
E	Eccentric anomaly	[rad]
E_b	Energy per bit	[dBJ]
e	Eccentricity	[−]
$F(S)$	Fraction of cost consumed	[−]
f	Frequency	[Hz]
f_b	Transmission frequency of the beacon	[Hz]
G	Covariance matrix of the unknowns in the TDOA-FDOA method	[−]
G_{RX}	Receiving antenna gain	[dBi]
G_{TX}	Transmitting antenna gain	[dBi]
g	Load factor on spacecraft during launch	[−]
g_0	Gravitational acceleration on Earth	[m s^{-2}]
H	Angular momentum	[N m s]
H_{FDOA}	Derivatives w.r.t. time of the position angles observer w.r.t. reference observer	[rad s^{-1}]
H_{TDOA}	Position angles of the observer relative to the reference observer	[rad]
H_a	Angular momentum due to aerodynamic torques	[N m s]
H_g	Angular momentum due to gravity gradient torques	[N m s]
H_m	Angular momentum due to magnetic torques	[N m s]
H_{res}	Residual angular momentum after orbit insertion	[N m s]
H_s	Angular momentum due to solar radiation pressure torques	[N m s]
H_{th}	Angular momentum due to thruster misalignment torques	[N m s]
H_{tot}	Total angular momentum	[N m s]
h_c	Panel core thickness	[m]
I	Mass moment of inertia	[kg m^2]
i	Inclination	[rad]
J	Jacobian matrix of the emitter positions w.r.t. to the observer positions	[−]
K	Stiffness matrix	[N m^{-1}]
k	Stiffness of spring	[N m^{-1}]
k	Boltzmann constant ($k = 1.38065 \cdot 10^{-23}$)	[m^2 kg s^{-2} K^{-1}]
L_{AT}	Atmospheric absorption loss	[dB]
L_{FS}	Free space path loss	[dB]
L_{IO}	Ionospheric loss	[dB]
L_{PM}	Polarisation mismatch loss	[dB]
$L_{P,RX}$	Receiving antenna pointing loss	[dB]
L_{RA}	Rain loss	[dB]
L_{TR}	Total receiver losses	[dB]
L_{TT}	Total transmitter losses	[dB]
$L_{P,TX}$	Transmitting antenna pointing loss	[dB]
M	Earth's magnetic moment multiplied by the magnetic constant ($M = 7.96 \cdot 10^{15}$)	[T m^3]
M	Mean anomaly	[rad]

$\mathbf{M}$	Mass matrix	[kg]
M_{cm}	Moment about centre of mass	[N m]
m	Mass	[kg]
m_p	Propellant mass	[kg]
N_0	Noise power spectral density	[dBm s]
n	Iteration variable	[−]
P_{RX}	Receiver input power	[dBm]
P_{TX}	Transmitter power	[dBm]
P_e	Required power during eclipse	[W]
P_{in}	Input power	[W]
P_{out}	Output power	[W]
p	Pressure	[N m^{-2}]
q	Dimensionless reflectance factor	[−]
R	Bit rate	[bps]
R	Distance from the Earth's centre	[m]
R	Distance from transmitter	[m]
R_i	Magnitude of the relative distance of the observer relative to the emitter	[m]
$\dot{R}_i$	Magnitude of the velocity of the observer relative to the emitter	[m s^{-1}]
$\mathbf{r}_{gs}$	Ground station position vector	[m]
$\mathbf{r}_{s/c}$	Spacecraft position vector	[m]
S	Fraction of time consumed	[−]
T	Torque	[N m]
T_S	System noise temperature	[K]
T_a	Atmospheric drag torque	[N m]
T_{cont}	Control torque	[N m]
T_g	Gravity gradient torque	[N m]
T_m	Magnetic torque	[N m]
T_s	Solar radiation pressure torque	[N m]
T_{th}	Thruster misalignment torque	[N m]
$\mathbf{T}_x$	Transformation matrix for rotation about x-axis	[−]
$\mathbf{T}_z$	Transformation matrix for rotation about z-axis	[−]
t	Time	[s]
t_a	Time required for damping the residual angular momentum	[s]
t_d	Time required for momentum dumping	[s]
t_e	Eclipse time	[hr]
t_f	Panel face sheet thickness	[m]
V	Orbital velocity	[m s^{-1}]
Wh_b	Energy storage capacity of battery	[W h]
x_{em}	Position of the emitter in the x-direction	[m]
x_{2d}	x-coordinate of the spacecraft position in the orbital plane	[m]
$\dot{x}_i$	Velocity of observer i in the x-direction	[m s^{-1}]
x_i	Position of observer i in the x-direction	[m]
y_{em}	Position of the emitter in the y-direction	[m]
y_{2d}	y-coordinate of the spacecraft position in the orbital plane	[m]
$\dot{y}_i$	Velocity of observer i in the y-direction	[m s^{-1}]
y_i	Position of observer i in the y-direction	[m]
z_{em}	Position of the emitter in the z-direction	[m]
$\dot{z}_i$	Velocity of observer i in the z-direction	[m s^{-1}]
z_i	Position of observer i in the z-direction	[m]
α	Spacecraft angle above the horizon	[rad]
β	Safety factor	[−]
γ	Phase error due to noise	[rad]
ϵ_{err}	Misalignment of the thrust vector with the thrust axis	[rad]
η	Efficiency	[−]
θ	Azimuth angle with respect to the satellite	[rad]
θ	Off-boresight angle	[rad]
λ	Dimensionless function of the magnetic latitude	[−]
λ	Wavelength	[m]

μ	Earth's gravitational constant	[$m^3\ s^{-2}$]
ρ	Atmospheric density	[$kg\ m^{-3}$]
ρ_p	Density of the propellant	[$kg\ m^{-3}$]
ρ_t	Density of the tank material	[$kg\ m^{-3}$]
σ	Standard deviation	[−]
σ_α	Standard deviation of the elevation angle	[rad]
σ_{FDOA}	Standard deviation of the FDOA measurement	[Hz]
σ_θ	Standard deviation of the azimuth angle	[rad]
σ_{HorPos}	Standard deviation of the position estimate of the beacon	[m]
σ_p	Stress in panel	[$N\ m^{-2}$]
σ_{TDOA}	Standard deviation of the TDOA measurement	[s]
σ_{x_i}	Standard deviation of the position of the observer in the x-direction	[m]
σ_y	Yield strength	[$N\ m^{-2}$]
σ_{y_i}	Standard deviation of the position of the observer in the y-direction	[m]
σ_{z_i}	Standard deviation of the position of the observer in the z-direction	[m]
Φ	Solar radiation flux	[$W\ m^{-2}$]
ϕ	Incidence angle of the Sun	[rad]
ϕ	Phase	[rad]
Ω	Right ascension of the ascending node	[rad]
ω	Argument of perigee	[rad]
ω_{res}	Residual angular velocity after orbit injection	[$rad\ s^{-2}$]

-

List of Abbreviations

AOA Angle of Arrival
AOCS Attitude and Orbit Control System
APR Array Power Regulation
BCDR Battery Charge/Discharge Regulation
BCR Battery Charge Regulation
BDR Battery Discharge Regulation
BER Bit Error Rate
BLR Baseline Report
BPSK Binary Phase-Shift Keying
C/A Coarse/Acquisition
C&DH Command and Data Handling
CBS Cost Breakdown Structure
CDR Critical Design Review
COM centre of mass
COTS Commercial Off-The-Shelf
CW Continuous Wave
DOD Depth-of-Discharge
DPDT Double-Pole, Double-Throw
DSE Design Synthesis Exercise
ECEF Earth-Centred, Earth-Fixed
ECI Earth-Centred, Inertial
ECSS European Cooperation for Space Standardization
EDAC Error Detection and Correction
EIRP Equivalent Isotropically Radiated Power
ELINT Electronic Signals Intelligence
EMC Electromagnetic Compatibility
EOL End-of-life
EPD Equipment Power Distribution
EPS Electric Power System
ESA European Space Agency
ESM Electronic Support Measures
FBS Functional Breakdown Structure
FDOA Frequency Difference of Arrival
FFD Functional Flow Diagram
FOA Frequency of Arrival
FR Final Report
FSK Frequency-Shift Keying
FY Fiscal Year
GPS Global Positioning System
HILT Hardware in the Loop Test
I&T Integration and Test
ICDs Interface Control Documents
IF Intermediate Frequency
IMU Inertial Measurement Unit
IR Infrared
ISL Inter-Satellite Link
ISR Intelligence, Surveillance, and Reconnaissance
ITAR International Traffic in Arms Regulations
ITU International Telecommunication Union
LEO Low Earth Orbit
LEOP Launch and Early Orbit Phase
LEOPARDSAT Low Earth Orbit Phased Array Radar Detection Satellite
LNA Low Noise Amplifier
LVC Launch Vehicle Catalogue
MAIT Manufacturing, Assembly, Integration, and Test
MLI Multilayer Insulation
MoD Ministry of Defence
MOSAIC Modular Solar Arrays with Integrated Construction
MPPT Maximum Power Point Tracking
MSK Minimum-Shift Keying
MTR Midterm Report
NASA National Aeronautics and Space Administration
NATO North Atlantic Treaty Organisation
OBC On-Board Computer
OBS Organisational Breakdown Structure
PCDU Power Conditioning and Distribution Unit
PD&D Program Design and Development
PDR Preliminary Design Review
PFM Protoflight Model
PMF Production Master File
PP Project Plan
PPU Power Processing Unit
PRI Pulse Repetition Interval
PRN Pseudo Random Noise
PV Photovoltaic
QPSK Quadrature Phase-Shift Keying
RAAN Right Ascension of the Ascending Node
RAM Random Access Memory
RAMS Reliability, Availability, Maintainability, and Safety
RF Radio Frequency
RMS Root Mean Square
RNLAF Royal Netherlands Air Force
RWR Radar Warning Receiver
S/C Spacecraft
SADA Solar Array Drive Assembly
SAR Search and Rescue
SEB Single Event Burnout
SEE Single Event Effects
SEGR Single Event Gate Rupture
SEL Single Event Latchup
SEU Single Event Upset
SMAD Space Mission Analysis and Design
SNR Signal-to-Noise Ratio
SSCM Small Spacecraft Cost Model
STK Systems Tool Kit
SvalSat Svalbard Satellite Station
TBD To Be Determined
TDMA Time Division Multiple Access
TDOA Time Difference of Arrival
TDOA-FDOA Joint Time Difference of Arrival-Frequency Difference of Arrival
TOA Time of Arrival
TT&C Telemetry, Tracking, and Command
UHF Ultra High Frequency
V&V Verification and Validation
VHF Very High Frequency
WGS Wideband Global SATCOM

1 | Introduction

For decades, the Dutch Ministry of Defence has been using foreign satellite services for its military operations. Since The Netherlands does not possess any space assets of its own, it makes the Dutch armed forces more dependent and therefore vulnerable. Space is increasingly used by defence departments all over the world for three main purposes: navigation, communication and (Earth) observation. Nowadays, defence without the use of assets in space has become almost unthinkable. Therefore, space is said to be the fourth operational domain of the Ministry of Defence (MoD) next to land, sea and air [1]. The use of space for navigation, communication and Earth observation enables the Dutch armed forces to take quick and effective military actions worldwide.

Earth observation capabilities of satellites are also used by Dutch intelligence services to analyse the activities of foreign states and groups. Because the MoD does not possess its own intelligence spacecraft, it is partially dependent on foreign states to gather this intelligence. Since the use of assets in space is free and unrestricted, satellite Earth observation delivers an eminent opportunity to gather intelligence on and enhance awareness of foreign activities of interest [2]. Activities of gathering data and information on an object or in an area of interest fall under the general term Intelligence, Surveillance, and Reconnaissance (ISR).

The Royal Netherlands Air Force (RNLAF) has expressed the need to decrease its dependence on foreign intelligence services by strengthening their own independent ISR position. In order to establish a stronger ISR position, the RNLAF has requested to study the feasibility of creating their own space assets for Electronic Signals Intelligence (ELINT) purposes.

This report is the last report in a series of reports on this feasibility study of an ELINT space asset for the RNLAF. The previously written reports include the Project Plan [3], the Baseline Report [4], and the Midterm Report [5]. With the requirements and constraints set by the RNLAF, a preliminary design for a space asset was created down to the subsystem level. On the basis of literature and with assistance from industry professionals the design for a ELINT space mission was generated. The purpose of the Final Report is to provide the conclusions of the performed research into this space asset, designed to gather ELINT for the Dutch MoD. The content of the report aims at providing an overview of the complete study as well as a more detailed description of the generated design and an analysis of the feasibility of this design. In this way, the report addresses the capabilities of a ELINT mission taking ito account the requirements and constraints set by the customer.

The Final Report consists of five main parts. The first part, *Mission Analysis*, includes the mission description and an assessment of the mission requirements and system functionalities. In the second part, *Design Process*, the process leading to the selection of the final concept is described. The detailed description of the preliminary design is given in part three, *Spacecraft Constellation*. An analysis of the preliminary design is provided in part four, *Systems Engineering*. This part discusses the breakdown of the budgets, sensitivity analyses, requirements compliance, and Verification and Validation (V&V). The fifth part, *Project Management*, consists of a post-project development logic, considerations with respect to sustainability, and a risk analysis. Afterwards, the conclusions of this study are provided and recommendations concerning the mission at hand are given to the customer.

2 | DSE Project Description

This chapter offers a concise overview of the project in terms of its background and organisation.

2.1 Design Synthesis Exercise

The Design Synthesis Exercise (DSE) is a third year project that aims at realising a synthesis between all courses and projects offered in the Aerospace Engineering Bachelor and as such wraps up the Bachelor study program. The DSE project lasts eleven weeks and the project group consists of nine students. In these eleven weeks this group of students is supposed to organise themselves as an engineering team. As a team they have to come up with a design, taking all steps usually found in real design projects. Besides taking part in the technical aspects of the design process, the team has to carry out the management tasks involved with the project as well. The goal of this project is to generate a conceptual design up to subsystem level of a constellation able to deliver ELINT to the RNLAF from 2019 onward. This design has to be documented in a Final Report (FR). Finally the concept has to be presented at the Final Review and at the DSE symposium.

In the next sections the group organisation will be explained in more detail as well as the way in which the work was organised.

2.2 Group Organisation

The group organisation is represented in the Organisational Breakdown Structure (OBS) shown in Figure 2.1. The tasks have been split in organisational and technical tasks and to each task a group member was assigned. The figure clearly shows how all technical divisions work under the supervision of the system engineers and how the contacts with the supporting staff and the customer are the responsibility of the project manager.

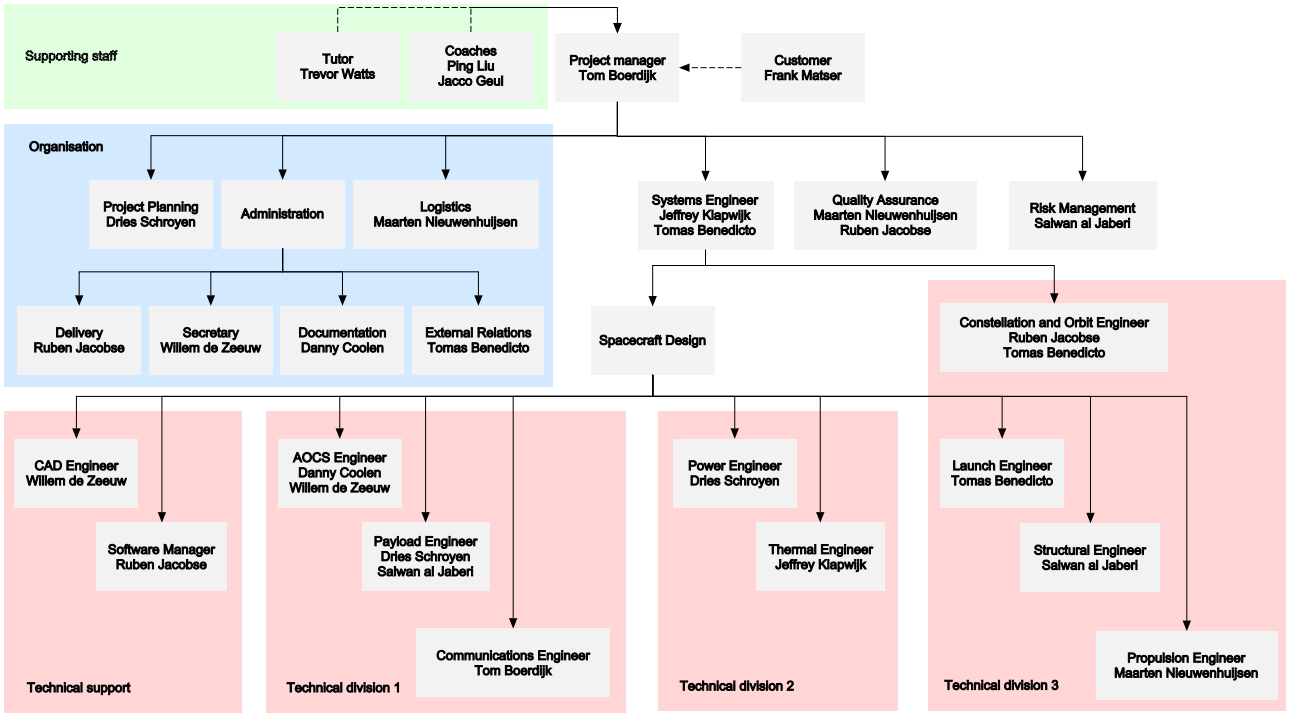

Figure 2.1: Group organisation of DSE S19.

2.3 Work Flow and Deliverables

The work that had to be done was divided in six work packages, each of them producing one or more deliverables. Figure 2.2 shows the work packages and the corresponding deliverables. Figure 2.3 on the other hand provides an overview of the same work packages with more detail and the proper order of the flow. It details the different aspects of the work packages, and shows the same deliverables as presented in Figure 2.1.

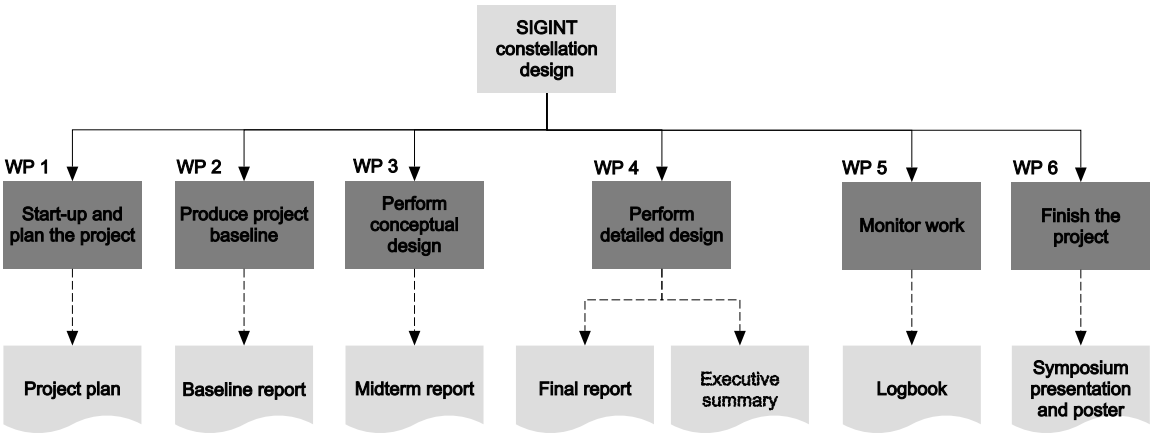

Figure 2.2: Overview of the work breakdown of the DSE project and the corresponding deliverables.

The Project Plan (PP) [3] reported on the organisational aspects, the Baseline Report (BLR) [4] presented the requirements and feasibility study, the Midterm Report (MTR) [5] focused on concept selection and finally this report presents the final findings. Besides that an executive summary, logbook and poster were made.

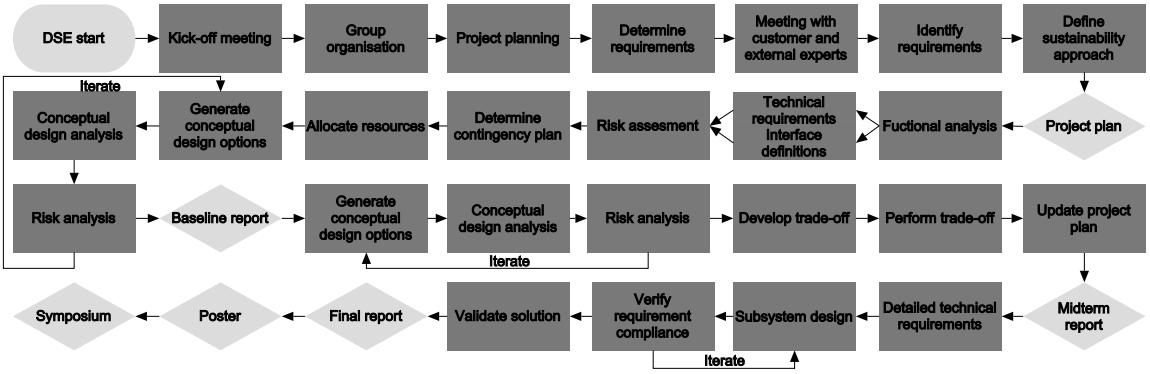

Figure 2.3: Overview of the work flow of the DSE project and the corresponding reviews.

Part I

Mission Analysis

3 | Mission Description

This chapter provides a short overview of the mission. It includes the customer need statement, the mission statement and a description of the mission itself.

3.1 Customer Need Statement

This project was started in response to a request by the RNLAF. Their request has been expressed as the costumer need statement presented below.

To gain independence of other countries and sources in the sector of intelligence, the RNLAF needs a low-cost, global, durable, reliable, and accurate signal intelligence system that is able to detect, recognise, and locate target signal sources.

3.2 Mission Statement

This DSE project is dedicated to providing more insight into the feasibility of the request as posed by the RNLAF. The following statement describes the objective of this study.

This ELINT satellite constellation project will, over the course of eleven weeks, study the feasibility of and generate a conceptual design for a space asset capable of detecting, recognising, and locating target signal sources (L-, S- and X-band radar, and Global Positioning System (GPS) jammers) and providing the RNLAF with this data from 2019 onward at a total constellation cost of less than € 45 million (excluding launch and operating costs).

In this study, a conceptual design is made for the space segment consisting of the spacecraft and constellation geometry. Other aspects, such as production, ground segment and support segment are discussed more briefly at the end of the report in Part V.

4 | Mission Requirements

This chapter aims at stating and explaining the preliminary requirements and the process behind the discovery of the system and subsystem requirements. First, the labelling and tracking conventions are stated. This is followed by the preliminary requirements discovery, including a list of the preliminary requirements and an elaboration on their discovery. Finally, the discovery of system and subsystem requirements is covered.

4.1 Requirement Labelling Convention

To support requirement traceability all requirements have been uniquely labelled. Each label consists of three letters, two numbers, and optionally another combination of a letter and two numbers. The first three letters indicate the subsystem to which the requirements belong. The two numbers following that are meant for designating a unique label to order them. If a requirement is split down further a letter and two numbers are added. The letter is a 'F' or 'C', indicating a functional requirement or a constraint respectively. The two number following that, again assign a unique order to the sub requirements. For example the requirement labelled AOC-11-F02 is the second functional sub requirement belonging to the eleventh Attitude and Orbit Control System (AOCS) requirement. A list of all requirements that have been specified can be found in Appendix A.

4.2 Tracing Requirement Changes

During the course of the project some requirements have changed. To maintain traceability during the project a requirement changelog has been created. The changelog first lists the date at which the change was introduced, then the old and new label are indicated. Finally, the last two columns give the old and new description of the requirement. By combining the list of requirements and the changelog, all issued versions of the requirements can be linked. The changelog can be found in Section A.13.

4.3 Preliminary Requirements Discovery

The preliminary requirements were derived from the project guide and the first status meeting with the customer [6]. In order to obtain a complete set of requirements that would encompass the whole mission, a requirements discovery tree was drawn, as can be seen in Figure 4.1. From the requirements discovery tree, the list of preliminary requirements shown below was generated.

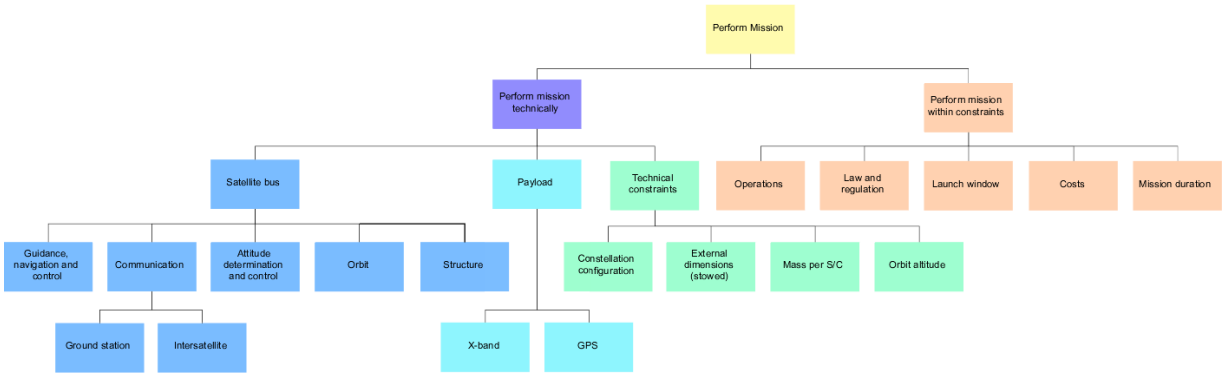

Figure 4.1: Higher-level requirements discovery tree. Note that the NGC, communication, AOCS and structure requirements are subsystem requirements and are therefore displayed in Appendix A.

4.3.1 General Requirements (GEN)

GEN-01 The constellation shall consist of 5 to 7 S/C.

GEN-02 The constellation shall be capable of accommodating extra S/C.

GEN-03 Each S/C shall meet the requirements specified by the launcher.

- GEN-03-F01: The S/C shall withstand the mechanical loads during launch.
- GEN-03-C01: Each S/C shall fit within a cylinder of 1 m length and 1 m diameter.
- GEN-03-C02: The maximum weight of each S/C shall be 200 kg.

GEN-04 The mission shall have a minimum lifetime of five years.

GEN-05 The maximum cost of the mission shall be € 45 million, excluding launch and operations costs.

GEN-06 The launch window of the mission is between 2017 and 2019.

GEN-07 The satellites shall be removed from orbit no later than 25 years after end of mission.

GEN-08 Intercepted RF signals shall be processed to identify target signals.

- GEN-08-F01: A library of target signals shall be available for the constellation and ground operations system.
- GEN-08-F02: Target signals shall be identified by matching with the signal library.
- GEN-08-F03: The signal library shall be up-datable.

4.3.2 Payload Requirements (PAY)

PAY-01 The constellation shall detect RF signals in the 1-4 GHz and 8-12 GHz bands.

PAY-03 RF signal sources shall be located with an accuracy better than 5000 m.

PAY-04 The constellation shall detect GPS jammers with an EIRP of 40 mW.

PAY-05 GPS jammer positions shall be determined with an accuracy better than 200 m.

From the above-mentioned requirements list, three types of requirements can be identified:

- **Key requirements** GEN-04, GEN-05, GEN-06, GEN-07. They belong to this selection due to their high level of importance since they affect the value of the product or were derived from strict regulations that could lead to judicial repercussions in case of non-compliance.
- **Driving requirements** GEN-05, PAY-01, PAY-03, PAY-04, PAY-05. These requirements drive the design of the mission since they set important guidelines on the performance of the systems.
- **Killer requirements** GEN-05, PAY-03. These are killer requirements since they set unachievable expectations. The budget has been discussed with the customer since it does not match the performance expected from the system. The same can be said about PAY-03 before it was changed (see Section A.13). Even after the change, it creates strain on the budget requirement.

4.4 System and Subsystem Requirements Discovery

The full list of requirements, up to subsystem level, is displayed in Appendix A. In Part III of this report, the subsystems use the preliminary requirements and requirements derived from other subsystems to, in turn, derive requirements for other subsystems. These derived requirements are the inputs used in the models that define the performance of the subsystem. Figure 4.2, showing the interaction between the subsystems, was used to structure the iterative design process of the constellation.

Orbit	EIRP [PAY-08/09/10] Aperture angle [PAY-06]	EIRP Aperture angle Up-downlink [TTC-06/07/08]	Eclipse time, Energy storage	Perturbations	Altitude maintenance/ Station keeping [PRO-01/03]	Launch loads [STR-04]	Sun flux Albedo/Infrared	De-orbit ΔV Type of de-orbit	Launch ΔV Type of trajectory Type of launcher Launch location	Required separation [CON-05/06]
Downlink [CON-02]	**Payload**	Interference [PAY-14]	Required power	Pointing accuracy/ stability [AOC-24/25/26/27/29] Slew rate [AOC-12]		Space allocation [PAY-11,12,13] Vibration analysis	Temperature range [TML-03]			Type of geoloc. Max separation [PAY-06]
Up-downlink [CON-02]	Interference	**TT&C**	Required power	Pointing accuracy/ Stability [AOC-28]		Space allocation Vibration analysis	Temperature range [TML-05]			
Eclipse time	Power budget [PWR-01]	Power budget [PWR-01]	**Power**	Power budget [PWR-01] Orientation of solar array [AOC-22/23]		Space allocation Vibration analysis	Temperature range/distribution [TML-04/06]			
			Power required [PWR-01]	**AOCS**		Space allocation Vibration analysis Force distributions [STR-06]	Temperature range			
	Electric field interference [PRO-05]		Power required [PWR-01]	Thrust duration, levels & vectors [AOC-21] Frequency [AOC-30]	**Propulsion**	Vibration analysis Space allocation [PRO-07/08] Force distribution [STR-06]	Temperature range/distribution [TML-01/02]			
	Size constraints [GEN-03]	Size constraints [GEN-03]	Size constraints [GEN-03]	Moment of inertia Centre of gravity Size constraints	Structural limits [PRO-08]	**Structures**	Size constraints		S/C mass/volume	
	Thermal expansion [PAY-11]		Power required [PWR-01]	Pointing requirement [AOC-22/23]	Temperature requirement	Thermal conductivity [STR-08/09] Vibration analysis	**Thermal**			
			Passivation		Passivation De-orbit ΔV [PRO-12]	Space allocation Vibration analysis		**EOL**		
			De-tumbling & start-up power	LEOP [AOC-9/10] Max angular rate	LEOP In-orbit commissioning ΔV [PRO-02]	Vibration modes Launch loads Ground handling [STR-05]	Temperature distribution		**Launch**	
Altitude [CON-01] S/C separation [CON-05/06] Global coverage [CON-03/04]	Aperture angle [AAR-01] Angular accuracy [PAY-06] Frequency error [PAY-15]	Intersatellite link data	Power required [PWR-01]	Navigation accuracy [AOC-11/31] Time synchronisation [AOC-32]	Formation keeping ΔV [PRO-01]				Number of orbital planes	**Geolocation**

Figure 4.2: Table displaying the inter-relations between the subsystems. It is used to orchestrate the iterative design process. All requirements are followed by their code. The entries without codes were not deciding factors in the design of the system and are therefore not requirements.

5 | Functional Analysis

The goal of this chapter is to clarify how the different functions of the Spacecraft (S/C) are organised, both hierarchically and time wise ordered. Besides that, it offers an overview of the ways in which the subsystems interact in order to fulfil the options mentioned before.

5.1 Functional Breakdown Structure

Figure 5.1 shows the Functional Breakdown Structure (FBS). It presents all the functions that the S/C has to perform in a hierarchical order. The hierarchical order allows tracing the interdependence of the functions [5].

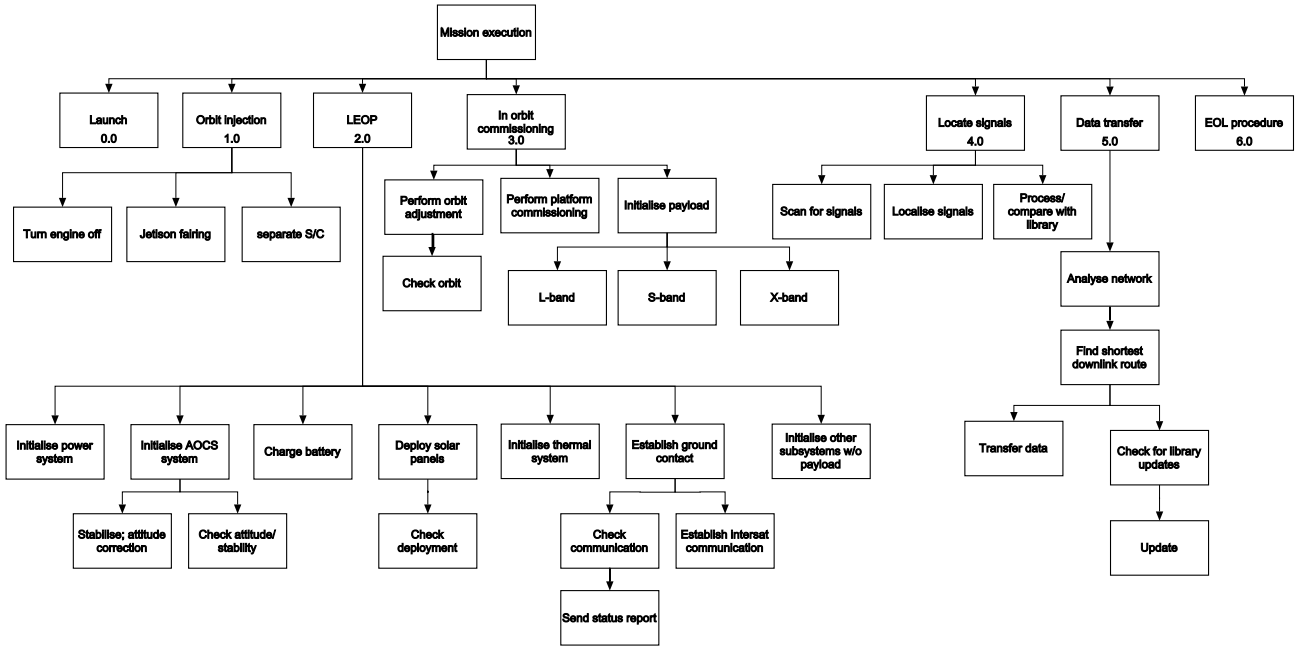

Figure 5.1: Hierarchical representation of the functions that have to be performed by the S/C.

As can be seen, the main mission elements are Launch and Early Orbit Phase (LEOP), in orbit commissioning, locating signals, data transfer, and the End-of-life (EOL) procedure. These elements together form the mission timeline. For each element the main functions that have to be performed during that phase of the mission have been listed in a tree, and if necessary they have been expanded further.

5.2 Functional Flow Diagram

The Functional Flow Diagram (FFD) displays the time sequenced flow of all the functions the system has to perform. The FFD allows to see how the functions presented in the FBS relate to the more detailed mission timeline [5].

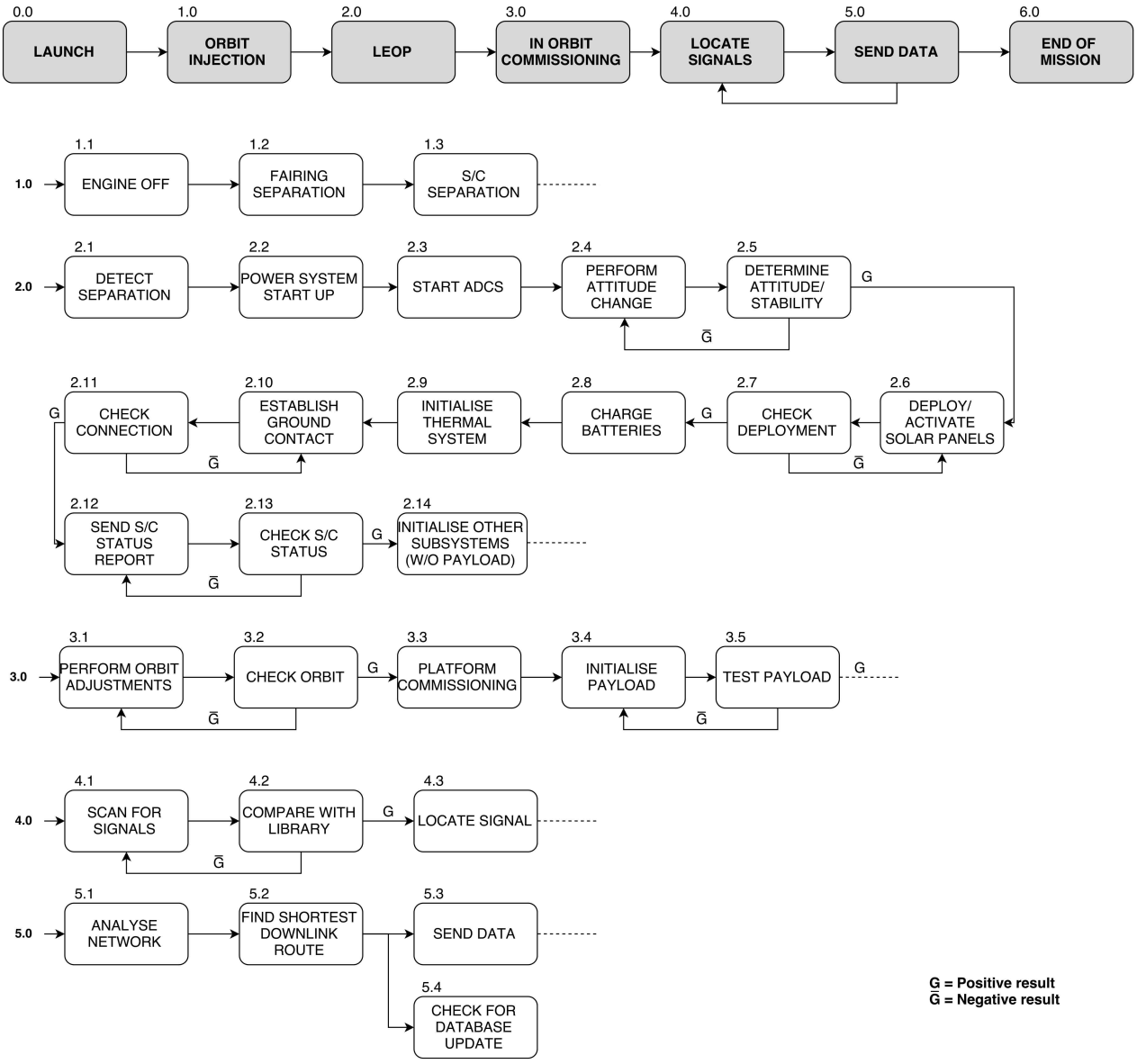

Figure 5.2: Time wise represented analysis of the functions of the S/C.

As can be seen, the numbers in Figure 5.1 and Figure 5.2 correspond. By comparing the two figures, one can relate the order in which the functions are performed to the way in which they depend on each other. Note that the functions listed under 4.0 and 5.0 are periodically repeated during the nominal mission.

5.3 N2 Chart

Figure 5.3 shows the N2 chart generated for this project. The N2 chart has been structured after an example by Prof. Dr. E.K.A. Gill [7]. It shows the subsystem interactions encountered during operations.

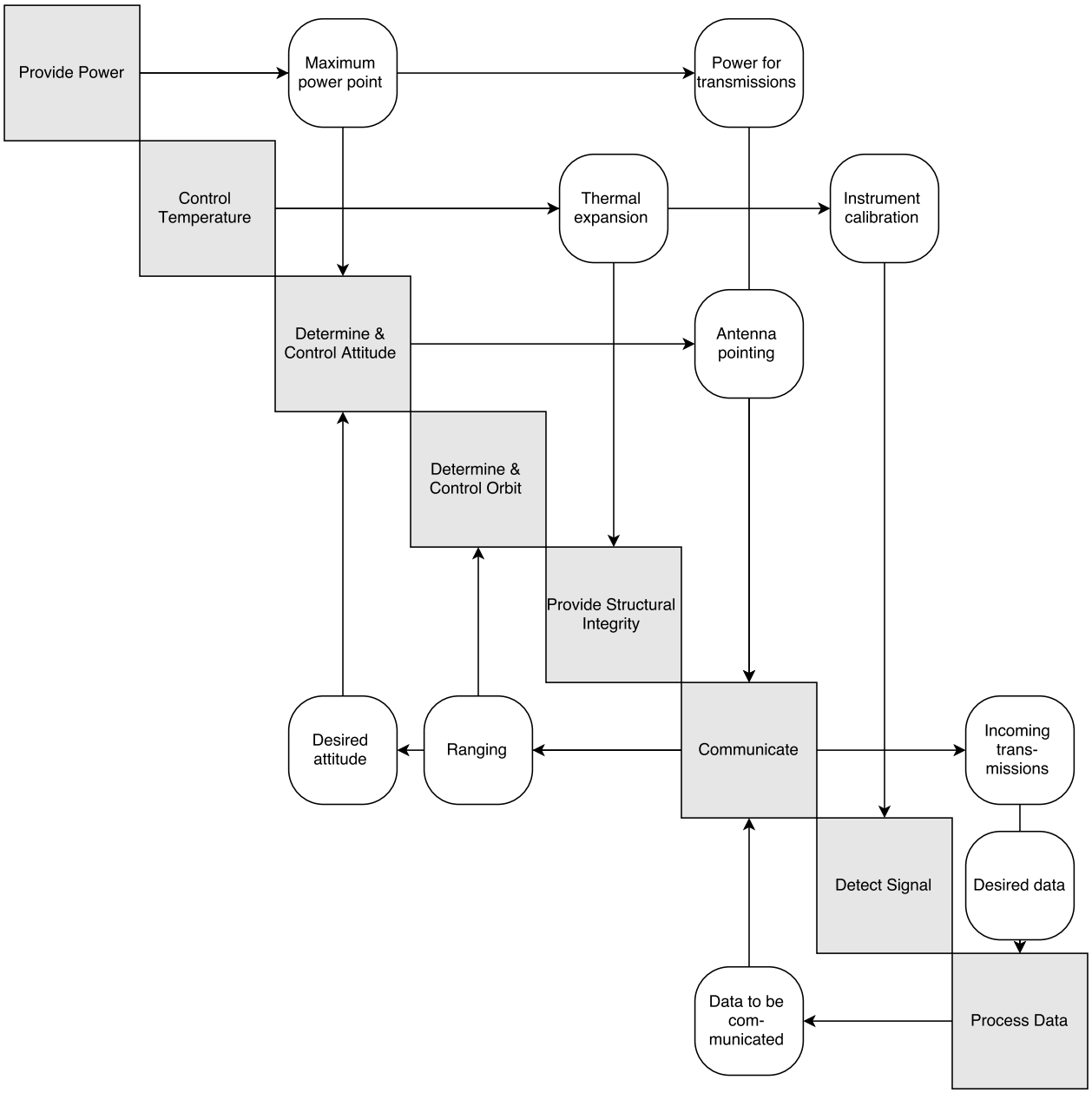

Figure 5.3: N2 chart showing the subsystem interactions.

From the figure it is easily derived that some subsystems are driving the design of other subsystems. The signal detection for example influences the data processing and the attitude control, while the structure mainly provides the required functions, but does not influence the other subsystems' performance.

6 | Signal Characteristics

In this chapter firstly the GPS jammer signal characteristics are discussed. Secondly the signal characteristics of radars are analysed.

6.1 GPS Jammer Signal Characteristics

GPS jamming is the act of transmitting a Radio Frequency (RF) signal that is meant to prevent receivers in a target area from tracking GPS signals, as stated in a 2001 report by the John A. Volpe National Transportation Systems Center [8]. Besides jamming, the report also distinguishes methods called spoofing and meaconing. Spoofing is a method that does not necessarily deny service to receivers, but rather sends out a false GPS signal that causes a receiver to think it is tracking a satellite and as a result comes up with a wrong solution for its position. Meaconing is the method of confusing a receiver by rebroadcasting a received signal with a delay. According to the Volpe report spoofing and meaconing are much harder to detect than jamming for a user that is being targeted, though these methods may disrupt GPS service in a larger area.

For interference purposes there are two GPS navigation frequencies that can be interfered with: the L1 and L2 frequencies at 1575.42 and 1227.60 MHz, respectively. On the L1 frequency the Coarse/Acquisition (C/A) code is transmitted together with the precision P(Y)-code, on the L2 frequency the same P(Y) code is transmitted [9]. Additionally, a new military code (M-code) and two new civilian codes (L1C and L2C) are being added and will be fully operational in 2018[1,2].

Because most current civil receivers only use the C/A code on the L1 frequency, their tracking of GPS signals will be prevented by jamming just the L1 frequency. For effective denial of service to a military GPS receiver that uses both the L1 and L2 frequencies, signals on both these frequencies need to be jammed. Because for both civilian and military receivers the L1 frequency needs to be jammed it is assumed that all jammers that need to be located by this mission are at least capable of jamming on this frequency. This means that for jammer localisation it is sufficient to localise the source of jamming signals on the L1 frequency.

6.1.1 Jamming

The characteristics of a number of commercial GPS jammers are analysed in series of papers produced at Cornell University [10], [11], and [12]. The GPS jammers studied in these papers all jam on or near the L1 frequency whereas only a few jam on or near the L2 frequency. The power of these jammers varies between approximately 0.1 and 640 mW. Due to a lack of data on military GPS jamming equipment it is assumed that the working of those installations is similar to that of commercially available GPS jamming devices.

All jammers analysed have a sawtooth pattern in the frequency-time domain, producing a so-called 'chirp' pulse on or near the L1 frequency. The bandwidth of the signals, although dependent on the type of jammer, ranges up to approximately 50 MHz. Due to lack of better information, it is assumed that this will be the case for all jammers.

It has to be noted that other non GPS-specific jamming signals exist and may be encountered. A few are given by Holmes but these are not discussed in this report due to lack of further information [9].

6.1.2 Spoofing

Similar to the situation with the jamming equipment there is also little information available on military GPS spoofing installations. An example of a spoofing attack is given by Humphreys [13]. It is assumed that all spoofing signals behave similar to the one studied in this paper. Even though spoofing generally only works against one target, the Pseudo Random Noise (PRN)-code transmitted by the spoofer may be strong enough to jam signals and could act as a jammer. It is assumed that the spoofing signal looks like the GPS PRN-code it is pretending to be.

6.1.3 Meaconing

No relevant sources on meaconing of GPS signals could be found, but given the definition in the Volpe report it is assumed that the signal equals that of the GPS signal it is rebroadcasting, though slightly shifted in time. This means that the signal can be used to confuse GPS receivers. It can be located by filtering the real GPS signal out and then applying the Joint Time Difference of Arrival-Frequency Difference of Arrival (TDOA-FDOA) method on the remaining false signal.

[1] http://www.gps.gov/systems/gps/modernization/civilsignals [Accessed on 05/06/2015]
[2] http://www.gps.gov/systems/gps/space/#generations [Accessed on 05/06/2015]

6.2 Radar Signal Characteristics

Modern radars are designed to either operate in several modes or in one specific mode. Each mode has a characteristic emission to meet the required function. When some of the emission of a radar is directed into the sky at a large elevation, it can be detected from space. Surveillance radars scan between 0° and 40° elevation. The radar emits for an extended period of time to scan a particular area for threats. An example of a surveillance radar emission sequence is shown in Figure 6.1. The radar illuminates a sector in the sky following a predetermined sequence. The example shown in Figure 6.1 is of a 3D surveillance radar where not only the radial range relative to the radar is computed, but also the elevation of the target. Radars that only determine the radial distance are 2D radars. These radars produce a narrow beam in azimuth, but a wide beam in elevation.

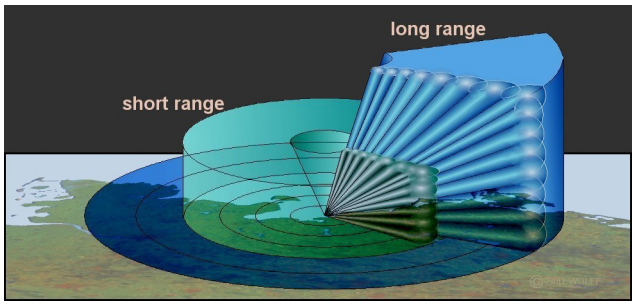

Figure 6.1: Example of emission sequence of a surveillance radar[3].

6.2.1 Radar Emission Waveform

Most radars emit a series of pulses and 'listen' for a reflection of one or more of the pulses and are therefore called pulsed radars. In this configuration the transmitter and receiver share one antenna. Continuous Wave (CW) radars emit a wave with varying frequency and have a separate antenna for the transmitter and receiver. CW radars are more difficult to detect, but technically more difficult to implement, so less used for surveillance radars. CW radars are not used for applications that are likely to be detected by the constellation.

Detectability of a radar is crucial in military radars and much effort is made to ensure the radar emission is difficult to detect. This is done by reducing the emitted power and selecting a suitable waveform. Reducing the emitted power is not always an option, because it is needed to achieve a certain range. But spreading the emitted signal over a large frequency band is an option. In this case the signal will become more difficult to distinguish from background noise. An example of three signals pulses are shown in Figure 6.2. In the figure, wave (a) is a standard sine wave pulse, (b) is a linear frequency modulated pulse, and (c) is a biphase pulse. It is important to be able to identify a wave, so that the return time can be computed. Pulse (b) in Figure 6.2 is an example of a wide frequency band pulse. Pulse (b) and (c) also have the advantage of increasing the range resolution of the radar, which is inversely proportional to the pulse width. These pulses can be decomposed in shorter pulses.

In practice one pulse is not enough to obtain enough information about a target. More information is required and thus several pulses are emitted in a sequence. The time between pulses is called the Pulse Repetition Interval (PRI). During this time the radar receiver is turned on to 'listen' to the reflected signals. In practice, a pulse train consisting of 16 to 20 pulses are emitted in one scan [14]. Modern radars have a varying PRI, because this is one of the parameters used by ELINT interceptors to identify a radar.

Military radars must be designed to operate in a high-interference environment. This interference originates from other radars or jammers. In case of the latter, emissions are generated with the goal of degrading the radar performance. Therefore, most modern radars are designed to hop between frequencies during operation. This way consecutive series of pulses can be sent at different frequency bands. A separate antenna can be used to monitor emissions from the environment and to select a frequency band which has low interference.

[3] http://www.radartutorial.eu/19.kartei/pic/pic1112p.jpg [Accessed on 05/06/2015]

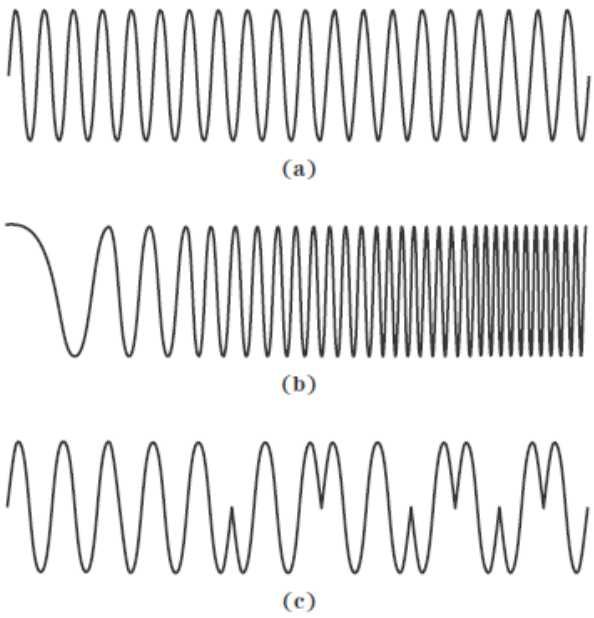

Figure 6.2: Three examples of a radar pulse: a) sine wave b) chirp pulse c) biphase coded pulse [14].

Part II

Design Process

7 | Preliminary Budget Breakdown

The purpose of this chapter is to provide the preliminary budgets as established at the beginning of the project in the BLR [4]. A top-down approach is used to establish the preliminary budgets. The complete system is broken down into different subsystems and an estimation of the budget per subsystem is given. The preliminary electrical power, mass and cost budgets are given in this chapter.

7.1 Preliminary Electrical Power Budget

The preliminary electrical power budget is established with the use of reference data. From this reference data, which consists of LEO spacecraft with a propulsion system, it is estimated that the available power will be 812 W. In Table 7.1, the total available power is broken down to the subsystem level [15].

Table 7.1: Preliminary electrical power budgets.

Subsystem	Percentage of total power	Budgeted power
AOCS	9.2%	75.0 W
Propulsion	1.5%	12.5 W
TT&C	8.5%	68.7 W
Thermal	6.9%	56.2 W
Power	6.9%	56.2 W
Payload	35.4%	287.3 W
Structures & mechanisms	0.8%	6.2 W
C&DH & other	10.8%	87.4 W
Subtotal	**80.0%**	**649.6 W**
Contingency	**20%**	**162.4 W**
Total	**100.0%**	**812 W**

7.2 Preliminary Mass Budget

The preliminary mass budget is based on Requirement **GEN-03-C02**, which states the maximum mass of the spacecraft shall be 200 kg. The mass is broken down with the use of reference data. Assuming the propellant mass is 19% of the total mass of a Low Earth Orbit (LEO) satellite, the total dry mass of the satellite is estimated to be 162 kg [15]. Including a contingency margin of 20% before the preliminary design is started, the total allocated dry mass of the satellite is 129.6 kg. In Table 7.2, the total dry mass budget is further broken down to allocate mass budgets to the satellite's subsystems. Due to the potential integration of Inter-Satellite Link (ISL), the contributions of AOCS and communications are increased. Because of the development of lighter materials for spacecraft structures, the contribution of the structure to the total mass is decreased.

Table 7.2: Preliminary dry mass allocation.

Subsystem	Percentage of dry mass	Budgeted mass
AOCS	8.1%	13.0 kg
Propulsion	4.5%	7.4 kg
TT&C	4.4%	7.1 kg
Thermal	2.2%	3.6 kg
Power	19.1%	30.9 kg
Payload	22.2%	35.9 kg
Structures & mechanisms	16.8%	27.2 kg
C&DH & other	2.8%	4.5 kg
Subtotal	**80.0%**	**129.6 kg**
Contingency	**20%**	**32.4 kg**
Total	**100%**	**162 kg**

7.3 Preliminary Cost Estimation

The preliminary cost estimation is derived with the Small Spacecraft Cost Model (SSCM). The resulting cost estimates from this model are given in 2010 US dollars. The obtained estimates are corrected for inflation and converted to Euros. The resulting preliminary cost estimation in Euros for 2015 is given in Table 7.3.

Table 7.3: Preliminary SSCM cost estimation excluding contingencies.

Cost contributors	**Cost estimate FY15**
AOCS	3,333,000 €
Propulsion	1,250,000 €
TT&C	1,952,000 €
Thermal	296,000 €
Power	5,402,000 €
Structures	1,667,000 €
C&DH	1,082,000 €
Spacecraft bus	**14,983,000 €**
Payload	7,491,000 €
Integration & assembly	15,620,000 €
Program level	4,289,000 €
Flight support	1,124,000 €
Ground support equipment	1,236,000 €
Total	**44,743,000 €**

It is assumed that the use of Commercial Off-The-Shelf (COTS) products will decrease the cost of every subsystem with approximately 20% due to lower development costs per unit.

In short, three budgets have been established in this chapter. The total power of the system was estimated to be 812 W. Including a contingency margin of 20% and assuming a propellant mass of 19%, the dry mass of the satellite was determined to be around 162 kg. The total cost budget for the development of six satellites was modelled. The model estimated the total cost to be approximately € 45 million. Since these budgets are preliminary, they are subject to change. After the preliminary design is finished, new budgets will be established. These budgets can be found in Chapter 24.

8 | Design Options

This chapter aims to provide an overview of the design options considered during the conceptual design phase. As such it serves as an introduction to Chapter 9 in which several generated concepts are presented.

Table 8.1: Overview of all design options used for the concept generation.

Payload								
Identical payloads				Distributed payload				
Hierarchical network			Level network	Hierarchical network			Level network	
Orbits								
LEO								
Low inclination				High inclination				
Constellation								
Formation flying						Swarms		
Identical S/C			Fractioned S/C			Swarms		
Processing								
On board			On ground			Combined		
Propulsion							No propulsion	
Mass expulsion							No propulsion	
Cold gas		Chemical thrust		Electric thrust			No propulsion	
Electrical power								
Solar panels								
Deployable				Fixed				
Attitude control								
Active			Passive					
Thrusters	Reaction wheels	Magne-torquers	Gravity gradient	Magnetic dipole	Aerodyn. stabilization	Solar radiation	Pure/ dual spin	Momentum wheel
Attitude determination								
Optical					Non-optical			
Earth horizon sensor	Sun sensor	Star sensor	CESS	Light & temp.	Magneto-meter	Gyroscope	GNSS	Radio-frequency beacons
Positioning								
On board								
GPS				DORIS				
Up- and Downlink communication								
RF								
WGS-relay				Direct RF				
Inter-satellite communication								
Optical			RF					
Optical			WGS-relay			Direct RF		
Data storage								
Solid state								
Volatile			Non-volatile			Hybrid		
De-orbiting								
Re-entry								
Active				Passive				
Propulsion		Electrodynamic tether		Natural			Drag modification	
Antenna								
Aperture				Travelling wave		Patch		
Horn		Synthetic aperture		Spiral		Patch		

Table 8.1 shows the design options that were determined from the feasibility study presented in the MTR [5]. Note that for some subsystems, the final design will encompass a combination of the mentioned options, rather than one specific option.

Payload
Four options have been identified for the payload. The payload can be identical on all S/C or not, and the system can be hierarchical or level. All options allow for the required geolocation accuracies, but the selected option will have a large impact on the remainder of the design.

Orbits
Only low Earth orbits are a viable option. At higher altitudes the coverage would increase, but the received signal strength would decrease, which poses problems for the detection.

Constellation
The constellation could either be a formation or a swarm. The latter is generally cheaper, but deviations in the constellation cannot be corrected. The two options under formation flying correspond to identical and non-identical S/C.

Processing
Like for payload, all options – on-board, on-ground, and combined – can be used, but the selected option will have a large impact on the design.

Propulsion
Multiple options were considered for the propulsion. The ones that are presented both fit the mass budget and are proven technologies. The more experimental methods of propulsion have been removed from the design phase based on cost and reliability.

Electrical Power
The options shown for the electrical power system were selected based on mass.

Attitude Control
The attitude control sections shows all conventional options, as those are proven designs and readily available COTS.

Attitude Determination
The attitude determination options show all conventional options for the same reason as given for the attitude control.

Positioning
The positioning options are all options that would fit the mass budget, technological readiness level and do not require frequent uplink opportunities.

Up- and Downlink Communication
The up- and downlink communication section shows the main options for these communications links. A direct RF link and using the Wideband Global SATCOM (WGS) were considered as viable options.

Inter-satellite Communication
The communication between the different S/C can use the same options as listed for the up- and downlinks. Optical communication was also considered tor the ISL.

Data Storage
The data storage design options were selected on basis of the current technological state of space data storage systems.

De-orbiting
The de-orbit options list the most common options used on other S/C.

Payload Antenna
The options shown for the antenna design were selected on their aperture angle, gain, and bandwidth.

9 | Concept Selection

This chapter focuses on the concepts that were generated from the design options presented in the previous chapter. First it explains which parameters were varied, then it presents the concepts, and finally it explains which concept was chosen to be designed in more detail.

9.1 Concept Generation

During the design phase, four concepts where generated. The main distinction between the concepts was the processing method. A brief overview of the concepts is presented below

- Identical S/C: constellation of identical or non-identical S/C. Using identical S/C will lower design and manufacturing costs, but using non identical S/C will allow to optimise each individual S/C.
- Payload distribution: identical or non-identical payload in each S/C. Using identical payload improves redundancy, but non identical payload allows larger antenna per S/C
- Processing: on-board or (partially) on-ground. On-board processing decreases the required downlink, but doing it partially on-ground allows for the use of more powerful computer algorithms to improve the accuracy of the geolocation.
- Downlink/ISL: downlink/ISL capabilities

As some combinations are mutually exclusive, four concepts were generated from this approach.

9.2 Concepts

The generated concepts are presented in Table 9.1. Concept A is cheaper to manufacture as the S/C and payload are identical for all of them. Because the S/C send their data to the ground individually, no ISL link is required. This solution is highly redundant and offers the opportunity to use more powerful, Earth based computers to do the calculation. Concept B is more expensive as the S/C and their payload are non-identical, the main advantage of this solution over solution A is the possibility to make larger antennas on each individual S/C to improve their combined performance. Concept C consists of identical S/C that do on board processing. One spacecraft takes the role of master and does all calculations and downlink. The advantage of this concept is redundancy and a low downlink data rate. Finally Concept D uses non identical S/C with one master capable of doing the computations. The main advantage is that one S/C can be optimised for computing, minimising the degree of over-design for the other S/C.

Table 9.1: Overview of the four high-level concepts.

	Concept A	**Concept B**	**Concept C**	**Concept D**
Description	Low cost solution, identical S/C with on ground processing	Non-identical payload with on ground processing	Identical constellation in which every S/C can take the role of master S/C	Hierarchical non-identical constellation with central on board processing
Identical S/C	Yes	No	Yes	No
Payload distribution	Identical payload	Non-identical payload	Identical payload	Non-identical payload
Processing	On ground	On ground	On board	On board
Inter Satellite Link required	No	No	Yes	Yes

9.3 Concept Selection

To asses which concept is the most outstanding, several design criteria where devised which are discussed below:

- **Cost:** There is a cost requirement from the customer, which means that cost is a dominant design criterion.
- **Mass:** Designing for low mass has priority in general, since lower mass reduces cost and spacecraft dimensions.
- **Performance:** The constellation's ability to detect and process a signal of interest. This is a dominant criterion since this directly determines the usefulness of the constellation. A subdivision has been made:
  - **Ability to grow:** Future application of the constellation might require longer lifetime and implementation of new S/C. This criterion verifies the concept's ability to grow.
  - **System latency:** The time required to transfer the gathered data from the S/C to a ground station. This is a less important criterion since the acquired intelligence is not immediately used.
  - **Localisation accuracy:** The ability to localise a signal, better algorithms can result in better accuracy.
  - **Orbital measurement time:** The amount of time the constellation can measure during one orbit. Depending on the orbit and processing type, it is possible that detection can only be done part-time.
- **Reliability:** The overall reliability of the constellation. This is a dominant criterion, since this affects the usefulness of the constellation. This also includes the capability to continue operations after a S/C failure (redundancy).

Not all the criteria listed above are equally important. Based on the customer needs, there is an emphasise on orbital measurement time, system latency, cost and localisation accuracy. During the trade-off process it turned out that Concept A and C where the most promising solutions. It is estimated that the cost, mass and reliability for both concepts will be roughly the same. With this in mind, the downlink data rate and orbital measurement time make Concept C superior over the other concepts. A more detailed design for concept C is therefore presented in this report.

Part III

Spacecraft Constellation

10 | System Overview

This chapter offers a summary of the characteristics of the Low Earth Orbit Phased Array Radar Detection Satellite (LEOPARDSAT) constellation. The design processes for the various subsystems are discussed in detail in Chapters 11 through 21.

The constellation consists of four satellites, called LEOPARDSATs, oriented in a near-rectangular formation in a low Earth orbit. These S/C shall execute their mission for at least five years. All four S/C are identical. A drawing of a LEOPARDSAT can be seen in Figure 10.1.

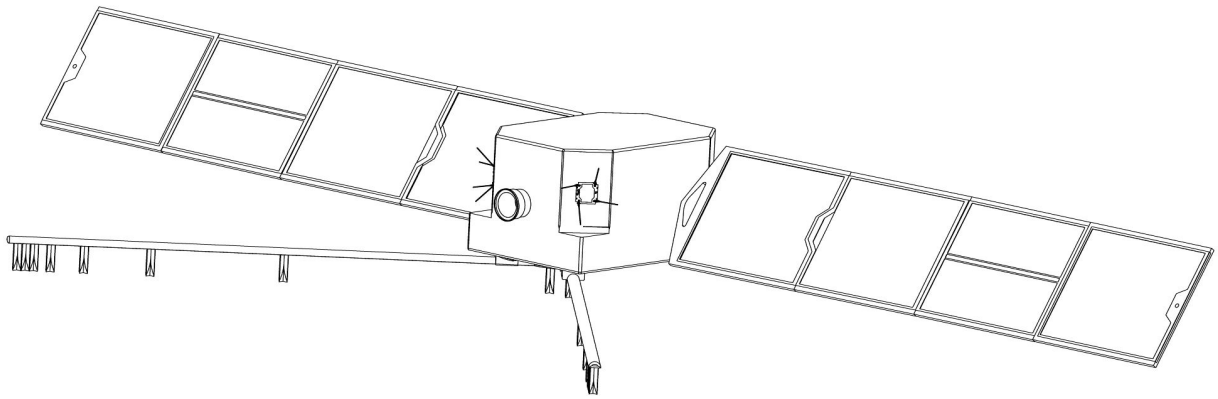

Figure 10.1: Isometric drawing of a LEOPARDSAT.

Each S/C hosts an ELINT payload, consisting of several antenna arrays connected to signal processing equipment. This payload is capable of detecting, identifying, and locating radars and GPS jammers. It achieves this by measuring the angle of arrival of radar signals, and by comparing the time of arrival and frequency of arrival of the GPS jammer signals.

All S/C will be launched using a single Vega launcher. They will be launched from the Guiana Space Centre into two circular orbital planes at an altitude of 500 km and with an inclination of 100°. The Right Ascension of the Ascending Node (RAAN) of the orbital planes are 6° apart to attain a near-rectangular formation. Within each orbital plane the two S/C are 500 km apart. At the end of the mission, the S/C will actively de-orbit themselves.

The AOCS subsystem provides the 3-axis stability and control required by the payload. It achieves a pointing accuracy of 0.04° and a position accuracy of 10 m.

The power subsystem consists of two solar arrays with a combined area of 3.1 m^2 and a battery with a capacity of 562 W h.

The Telemetry, Tracking, and Command (TT&C) subsystem provides telecommunication links with ground stations and the other S/C in the constellation. Ground stations in Breda and Bonaire are used to minimise the time between communication opportunities throughout the orbits.

The propulsion subsystem uses an ion thruster with xenon propellant to maintain the orbit and to de-orbit the S/C at the end of the mission. It provides 5 mN of thrust and has a total ΔV budget of 502 ms^{-1}.

The Command and Data Handling (C&DH) subsystem provides commands to all other subsystems. It also ensures that the incoming transmissions are decrypted and outgoing transmissions are encrypted.

A list of S/C and constellation specifications is given in Table 10.1.

Table 10.1: Specifications of the LEOPARDSAT constellation.

Launch	
Launch date	Mid 2018
Launch vehicle	Vega
Launch site	Guiana Space Centre, Kourou
Orbit	
Orbit altitude	500 km
Orbit type	Circular, 100° inclination
Orbital period	94 minutes
End-of-life strategy	Active de-orbiting and passivation
Mission lifetime	Five years
Physical properties	
Dimensions (without solar array)	550 mm x 700 mm x 900 mm
Mass	Wet: 130 kg, dry: 124 kg
Payload	
Instruments	L-, S-, and X-band signal processing
Coverage	Global for radars, ± 70° latitude for GPS jammers
Minimum detectable GPS jammer power	40 mW
Minimum geolocation accuracy	5.0 km for radars and 200 m for GPS jammers
Attitude Determination and Control	
ADCS method	3-axis stabilised
ADCS sensors	Star trackers, IMUs, magnetometers
ADCS actuators	Magnetorquers, reaction wheels
Pointing accuracy	0.04°
Pointing knowledge	0.004°
GPS position accuracy	10 m
Agility	x: 0.0078° s^{-2}, y: 0.0307° s^{-2}, z: 0.0068° s^{-2}
Power	
Power system	Solar arrays and batteries
Solar array	3.1 m^2 triple junction solar cells
Battery capacity	562 W h
Peak power	673 W
Single orbit average power	346 W
Telemetry, Tracking, and Command	
Downlink	115.2 kbps, 2250 MHz, 13.2 dB margin
Uplink	1200 bps, 437 MHz, 43.6 dB margin
Inter-satellite crosslink	4800 bps, 437 MHz, 15.5 dB margin
Ground stations	Breda and Bonaire
Command and Data Handling	
On-board computer	Based on GR712RC with two LEON3-FT cores
Data storage size	3 Gb
Propulsion	
Propulsion system	Ion thruster with xenon propellant
Thrust	5.0 mN
ΔV budget	502 m s^{-1}

11 | Geolocation

The primary objective of this mission is the location of relevant signal sources. As discussed in Chapter 6, the differences in nature between GPS jammer and radar signals impose the design of signal-specific geolocation methods. The first step is to state the requirements imposed on the geolocation performance of the mission. The method that will be used to locate the two types of signals is then selected according to the criteria described in Chapter 8. The geolocation of radars and GPS jammers is then described separately. The descriptions include the inputs used in the models, a mathematical description of the model, the numerical results and the sensitivity analysis of the performance. Finally, a brief overview of the overall geolocation performance is provided.

11.1 Requirements

The following top level requirements were used to define the geolocation aspects of the mission:

PAY-01 The constellation shall detect RF signals in the 1-4 GHz and 8-12 GHz bands.

PAY-03 RF signal sources shall be located with an accuracy better than 5000 m.

PAY-05 GPS jammer positions shall be determined with an accuracy better than 200 m.

As can be seen, the list only contains accuracy and frequency requirements since all location algorithms assume 100% probability of detection. This major assumption will be further refined in Chapter 13, where the emitted power, signal losses and aperture angles will be taken into account. Furthermore, requirement **PAY-03** was altered with consent of the customer from 1200 m to 5000 m after difficulties in the design, due to size and budget restrictions, were reported (see Section A.13).

11.2 Method Selection

As discussed in the MTR, the TDOA-FDOA method is the most accurate location technique [5]. The drawback of this method is the large required separation between the spacecraft and the need for multiple measurements of the same signal. From an analysis of the required accuracy for GPS jammer localisation and the omnidirectional wave pattern of the signal (ensuring multiple observations of the same waveform), TDOA-FDOA was deemed to be the most appropriate option.

The radar systems, on the other hand, sweep through the airspace with varying frequencies, as detailed in Chapter 6. This decreases the likelihood that multiple spacecraft detect the same pulse, rendering Time Difference of Arrival (TDOA) and Frequency Difference of Arrival (FDOA) both highly unlikely to succeed. The only remaining option is the bearing method (Angle of Arrival). This method is capable of direction-finding with a single observation. The downside of this method is the limited accuracy and its need for large and expensive antennas. The sections below explains algorithms of the two mentioned methods.

11.3 Radars

In this section, the Angle of Arrival (AOA) geolocation method is modelled and sized. The design process is organised as follows. First, the requirements are transformed into inputs. The AOA geolocation algorithm is then explained. This is followed by an analysis of the performance of said geolocation method. Finally, a sensitivity study is performed and the requirements derived from this section are stated, to be used by other subsystems.

11.3.1 Inputs

For the estimation of the accuracy of geolocation, the following inputs are used:

- Position of the observer relative to the emitting beacon
- Standard deviation of the angular discrimination
- Standard deviation of the position of the spacecraft

The standard deviation of the angular discrimination consists of a measure of both the pointing accuracy of the receiving antenna and the angular uncertainty in the direction of position resulting from the antenna performance (more details can be found in Chapter 13). The standard deviation of the position of the satellite is directly dependent on the accuracy of the navigation system explored in Chapter 17.

11.3.2 Algorithm Description

For the purpose of this mission, the two dimensional model described by Richard G. Wiley [16], was adapted to accomodate a three dimensional angular input. The original model uses the directional knowledge of two different observers to create an intersection between the lines of bearing. These lines form an area with possible locations in two dimensions. The adapted model uses only one observer with two angle estimates (azimuth and elevation). The following assumptions have been made:

- Flat Earth
- Constant emitter altitude ($z_{em} = 0$)
- Observation uncertainties are uncorrelated
- Standard deviations per observation type are identical

Since the height of the satellite is known and the emitter is assumed to be on on ground level, the two angles measured by the observer give a possible location area in the xy-plane (ground). The angles can be calculated by (where θ is the azimuth and α is the elevation):

$$\theta = \tan^{-1}\left(\frac{y_i - y_{em}}{x_i - x_{em}}\right) \tag{11.1}$$

$$\alpha = \tan^{-1}\left(\frac{z_i - z_{em}}{\sqrt{(x_i - x_{em})^2 + (y_i - y_{em})^2}}\right) \tag{11.2}$$

These angles can be substituted in each other to isolate for x_{em} and y_{em} that correspond to the on-gorund coordinates of the emitter. With these equations known, the Jacobian of the emitter location estimate with respect to observer position and AOA can be calculated using (where x_i, y_i and z_i are the coordinates of the observer):

$$J_{x_{em},y_{em}|x_i,y_i} = \begin{bmatrix} \frac{\partial x_{em}}{\partial x_i} & \frac{\partial x_{em}}{\partial y_i} & \frac{\partial x_{em}}{\partial z_i} \\ \frac{\partial y_{em}}{\partial x_i} & \frac{\partial y_{em}}{\partial y_i} & \frac{\partial y_{em}}{\partial z_i} \end{bmatrix} \tag{11.3}$$

$$J_{x_{em},y_{em}|\alpha,\theta} = \begin{bmatrix} \frac{\partial x_{em}}{\partial \alpha} & \frac{\partial x_{em}}{\partial \theta} \\ \frac{\partial y_{em}}{\partial \alpha} & \frac{\partial y_{em}}{\partial \theta} \end{bmatrix} \tag{11.4}$$

The inputs in position and angle uncertainties are then written as the following covariance matrices. It is assumed, as is stated in the previous subsection, that the observations are uncorrelated and that the standard deviations (σ) for a specific type of observation are identical for all observers.

$$Cov(x_i, y_i, z_i) = \begin{bmatrix} \sigma_{x_i}^2 & 0 & 0 \\ 0 & \sigma_{y_i}^2 & 0 \\ 0 & 0 & \sigma_{z_i}^2 \end{bmatrix} \tag{11.5}$$

$$Cov(\alpha, \theta) = \begin{bmatrix} \sigma_\alpha^2 & 0 \\ 0 & \sigma_\theta^2 \end{bmatrix} \tag{11.6}$$

The emitter position covariance matrix $Cov(x_{em}, y_{em})$ can now be calculated using Equation 11.7. Note that the position component of the covariance matrix (first product of Equation 11.7) is five orders of magnitude smaller than the angle component of the error and is therefore, for errors in position determination lower than 20 meters, negligible.

$$Cov(x_{em}, y_{em}) = J_{x_{em},y_{em}|x_1,y_1} Cov(x_n, y_n) J^T_{x_{em},y_{em}|x_1,y_1} + J_{x_{em},y_{em}|\alpha,\beta} Cov(\alpha, \beta) J^T_{x_{em},y_{em}|\alpha,\beta} \tag{11.7}$$

The square root of the eigenvalues of the covariance matrix of the emitter position provides the semi-major and minor axes of the ellipse that encompasses 68% of the possible locations for the emitter. This percentage is obtained from the amount of possible solutions a standard deviation contains.

11.3.3 Performance

The performance of the formation is modelled as a single observation of bearing since multiple observations do not necessarily improve the accuracy. However, for the case where two observations are obtained where the observer-beacon vectors are perpendicular in the xy-plane (ground), the following results shall be improved significantly (orthogonality of the semi-major axes of the error ellipses). Since the actual improvement relies on the occurrence of a very specific and highly unlikely scenario, and depends highly on the elevation angle of the emitted signal when detected, the accuracy of only one observation has been computed. The numerical results, and the inputs used to obtain them, are tabulated in Table 11.1. A visual representation of the performance of the AOA method for the geolocation of an emitting radar in the L-, S-, and X-bands is also shown in Figure 11.1. Note that the errors in position determination are neglected (see Equation 11.7) and the elevation angle range is limited to [30°, 90°] since the function is exponential (see Figure 11.1) and below this elevation the error in localisation is too large to be considered. Furthermore, as stated in Chapters 13 and 17, the aperture angle of the antenna is ±30° and the slew angle is ±20°. The minimum elevation angle is therefore 40°.

Table 11.1: Geolocation accuracy of radars.

Inputs			**Outputs**	
Frequency band	**Orbital altitude**	σ_{AOA}	**Max. error**	**Min. error**
L	500 km	0.24°	5.98 km	2.13 km
S	500 km	0.16°	3.96 km	1.40 km
X	500 km	0.21°	5.19 km	1.85 km

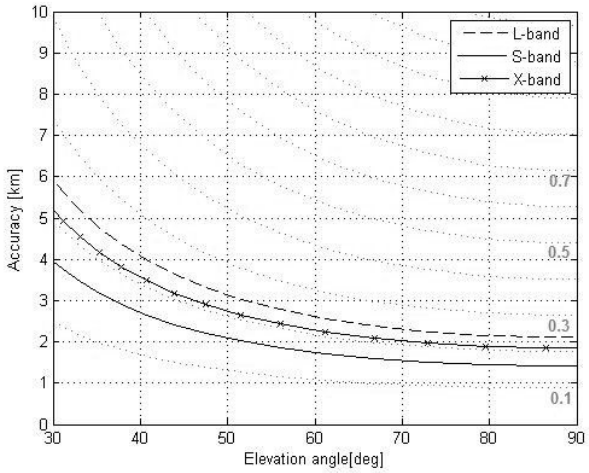

Figure 11.1: Geolocation accuracy of L-, S-, and X-band radars in km as a function of the elevation angle of the emitted signal. The faded exponential lines represent the distribution of accuracies as a function of the angular accuracy of the receiver array.

11.3.4 Sensitivity

A sensitivity analysis of the geolocation accuracy of radars can be carried out for two parameters, the altitude of the observer, and the angular accuracy of the receiver antenna.

The first parameter to be considered is the orbital altitude. As can be seen from Figure 11.2, as the altitude increases by 50 km, the geolocation error increases by 8% (6 km to 6.5 km) at 30° elevation angle (worst case considered). To obtain an increase of 50% in the error, an increase in altitude of 290 km is required. The main reason for a change in orbital altitude is orbital decay. However, since this would decrease the orbit altitude and therefore, cause an increase in geolocation accuracy, shifts in orbital altitude shall not hinder the performance of the AOA geolocation of radars.

The second parameter is the angular accuracy of the receiver antenna. From Figure 11.1 it can be determined that until an angular accuracy of 0.46° a minimum error of 5 km is achieved for the best case scenario (90° elevation angle). This represents a deterioration in angular accuracy, in the worst case (L-band), of 92%.

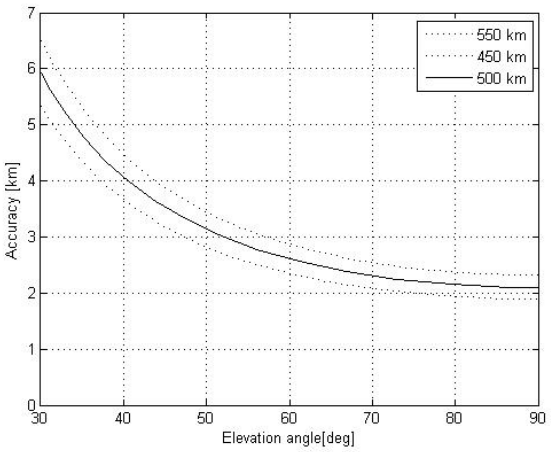

Figure 11.2: Sensitivity of the geolocation accuracy of L-band radars to orbital altitude.

11.3.5 Derived Requirements

From the sensitivity analysis above and the used inputs, the following requirements were derived. Below are the requirement codes and the thought behind their discovery.
PAY-06 From Figure 11.1, it is derived that to achieve 5 km geolocation accuracy for the radars, assuming the elevation angle is larger than 60° (aperture angle = ±30°, see Chapter 13), the angular accuracy shall be better or equal to 0.4°, regardless of the frequency band in which they operate.

AOC-11 In Equation 11.7, it was explained that within a standard deviation of determined position of 20 m, the accuracy of the AOA method remained constant.

CON-01 Finally, from 11.2, it can be seen that the orbital altitude is directly proportional to the error in geolocation. It shall therefore, be kept at a minimum, 500 km.

11.4 GPS jammers

In this section, the geolocation of GPS jammers using TDOA-FDOA is investigated. First, the inputs required for the calculation of the accuracy of localisation are stated. This is followed by an explanation of the model used. From the model, a performance analysis is carried out, including a sensitivity study. Finally, requirements for other subsystems are derived from the inputs of the model.

11.4.1 Inputs

The TDOA-FDOA method requires the following inputs for the estimation of the localisation accuracy of the system:

- Positions of the observers relative to the emitting beacon
- Velocities of the observers relative to the velocity of the emitting beacon
- Frequency of the signal
- Standard deviation of the time of arrival observation accuracy
- Standard deviation of the frequency of arrival observation accuracy

The standard deviation of the time of arrival is in meters and consists of the uncertainty in position of the observer (explored in Chapter 17), the uncertainty in propagation delay estimations, the uncertainty in the reference time (dependent on accuracy of the synchronisation of the clocks between the observers) and the bit error in the digitisation of the received signal in the time domain. The standard deviation of the frequency of arrival is in m s^{-1} and accounts for the uncertainty in velocity of the observer (refer to Chapter 17), the uncertainty in velocity of the emitter (if the emitter is not completely stationary) and the errors in determination of the frequency spectrum of the received signal.

11.4.2 Algorithm Description

The algorithm described in this subsection is a horizontal dilution of precision algorithm using differences of arrival as inputs. The two observation types considered are time and frequency. A more thorough description of the algorithm can be can be found in the JDOP Definition for Meosar Handbook [17]. Throughout the algorithm, the following assumptions have been made:

- Flat Earth
- Constant emitter altitude ($z_{em} = 0$)
- Observation uncertainties are uncorrelated
- Standard deviations per observation type are identical
- Beacon is stationary
- Same signal detected by all four observers

The first step is to define the instantaneous positions of both the observers and the beacon emitting a jamming signal. For a chosen number N of simultaneous observers, their positions and velocities are:

$$[x_i, y_i, z_i]^T \text{ with i} \in [1, N] \tag{11.8}$$

$$[\dot{x}_i, \dot{y}_i, \dot{z}_i]^T \text{ with i} \in [1, N] \tag{11.9}$$

The same can be said for the position and velocity of the emitting beacon.

$$[x_{em}, y_{em}, z_{em}]^T \tag{11.10}$$

$$[\dot{x}_{em}, \dot{y}_{em}, \dot{z}_{em}]^T \tag{11.11}$$

We can then write the observation equations with α, β, and γ (three orthogonal planes, respectively xy, yz and xz)[18]. Since the formulas are similar for each angle, due to their orthogonality, only the x-axis is portrayed. The time derivative of α is therefore defined in Equation 11.14. The reference observer is the observer that provides the reference against which all the differences of arrival are measured. The algorithm has to be run for each observer acting as reference. The selected reference is the one that provides the best performance, and therefore, the smallest position uncertainty.

$$\begin{bmatrix} \triangle R_i \\ \triangle \dot{R}_i \end{bmatrix} = \begin{bmatrix} H_{TDOA} \\ H_{FDOA} \end{bmatrix} \begin{bmatrix} \triangle x \\ \triangle y \\ \triangle z \end{bmatrix} = \begin{bmatrix} \alpha_i - \alpha_{ref} & \beta_i - \beta_{ref} & \gamma_i - \gamma_{ref} \\ \dot{\alpha}_i - \dot{\alpha}_{ref} & \dot{\beta}_i - \dot{\beta}_{ref} & \dot{\gamma}_i - \dot{\gamma}_{ref} \end{bmatrix} \begin{bmatrix} \triangle x \\ \triangle y \\ \triangle z \end{bmatrix} \tag{11.12}$$

$$\alpha_i = \frac{\partial R_i}{\partial x_{em}} = -x_{em|i} \tag{11.13}$$

$$\dot{\alpha_i} = \frac{\partial \dot{R}_i}{\partial x_{em}} = x_{em|i}[x_{em|i}\dot{x}_{em|i} + y_{em|i}\dot{y}_{em|i} + z_{em|i}\dot{z}_{em|i}] - \dot{x}_{em|i} \tag{11.14}$$

$$x_{em|i} = \frac{x_i - x_{em}}{R_i} \tag{11.15}$$

$$\dot{x}_{em|i} = \frac{\dot{x}_i - \dot{x}_{em}}{R_i} \tag{11.16}$$

The magnitude of the position of the reference observer relative to the beacon, R_i, is defined in Equation 11.17

$$R_i = \sqrt{(x_i - x_{em})^2 + (y_i - y_{em})^2 + (z_i - z_{em})^2} \tag{11.17}$$

The time of arrival and frequency of arrival observations can then be converted from seconds to meters and Hz to meters, respectively. In the equations below, f_b is the transmission frequency of the beacon in Hz and c is the speed of light in m s^{-1}.

$$\triangle R_i = (TOA_i - TOA_{ref})c \tag{11.18}$$

$$\triangle \dot{R}_i = (FOA_i - FOA_{ref})\frac{c}{f_b} \tag{11.19}$$

As was stated in the previous subsection, all the observations are assumed to be uncorrelated (Cov(TOA,FOA)=0) and the standard deviations of a certain observation type are constant for all observers ($(\sigma_{TDOA})_i = (\sigma_{TDOA})_{i+1}$). With these assumptions, the following covariance matrix for the linearised observations can be derived:

$$Cov(DOA) = \begin{bmatrix} Cov(TDOA) & Cov(TDOA, FDOA) \\ Cov(TDOA, FDOA) & Cov(FDOA) \end{bmatrix} = \begin{bmatrix} \sigma^2_{TDOA} & 0 \\ 0 & \sigma^2_{FDOA} \end{bmatrix} = \begin{bmatrix} 2\sigma^2_{TOA} & 0 \\ 0 & 2\sigma^2_{FOA} \end{bmatrix} \tag{11.20}$$

Giving the covariance matrix G of the unknowns [18] in Equation 11.21. In the following equation, the Time of Arrival (TOA) variance has to be given in m and the Frequency of Arrival (FOA) variance in m s^{-1}.

$$G = \left(0.5\sigma_{TOA}^{-2} H_{TDOA}^{T} H_{TDOA} + 0.5\sigma_{FOA}^{-2} H_{FDOA}^{T} H_{FDOA}\right)^{-1} \tag{11.21}$$

The standard deviation can then be calculated from the traces of the covariance matrix G:

$$\sigma_{HorPos} = \sqrt{2(G_{11} + G_{22})\sigma_{TOA}} \tag{11.22}$$

The location accuracy with a 95% confidence level can be obtained with $2.4477\sigma_{HorPos}$.

11.4.3 Performance

The following performance analysis of the formation in the ambit of geolocation of a GPS jammer relies on the assumption that the beacon is visible by all four spacecraft. The performance can be analysed in two ways. The first being an analysis of a 1000 km by 1000 km square region, and the second being a global analysis of the Earth.

For the first analysis, the numerical results are displayed in Figure 11.3 and tabulated in Table 11.2 . For this analysis, the optimal separation of 500 km between two spacecraft of the same side of the square is used. It can be noted that the accuracy distribution is homogeneous (to the nearest 10 m) and equal to 70 m until it reaches the central region of the plot where the error in geolocation increases rapidly to reach a maximum of 23.2 km.

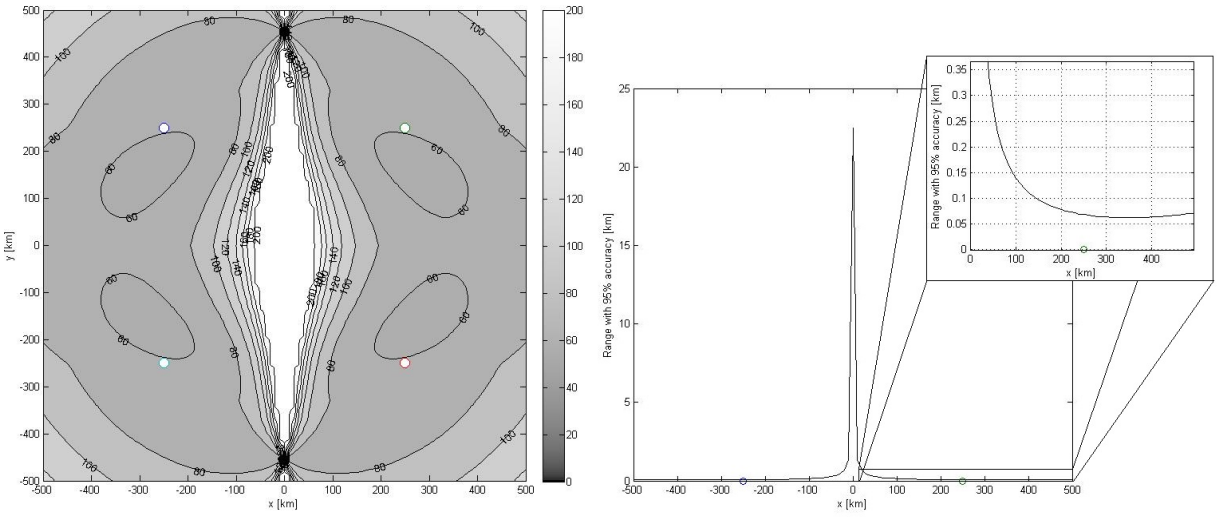

Figure 11.3: Geolocation accuracy distribution of GPS jammers in a 1000 km by 1000 km square region using a 500 km by 500 km square formation (left) and a cut-out at $y = 0$ (right). The white markers represent the observing spacecraft and the gray-scale bar represents the accuracy in m (the white region is above 200 m accuracy).

Table 11.2: Geolocation accuracy of radars. The region covered represents the percentage of the 1000 km by 1000 km square region which complies with 200 m geolocation accuracy.

Inputs			**Outputs**		
Orbital altitude	σ_{TDOA}	σ_{FDOA}	**Max. error**	**Min. error**	**Region covered**
500 km	2.5 μs	0.25 Hz	23.2 km	0.06 km	95.6%

For the global analysis, the Earth is modelled as a sphere and both the shift in length over width ratio of the formation and the change in angles between the orbital planes as the latitude changes is taken into account. The in-plane separation between the spacecraft is constant and equal to the previously stated optimal of 500 km. The results are displayed in Figure 11.3 for different separations between the two orbital planes as a measure of ΔRAAN. The chosen separation is ΔRAAN 6° (730 km at the equator) since it is the smallest separation that achieves a constant performance from the equator until 70° latitude. The size of the separation is important with respect to the required viewing angle of the receiver antenna, and the constant accuracy affects the consistency of the formation to carry-out

its function. The minimum required viewing angle to be able to locate a signal within the formation (500 km by 730 km rectangle) is 56°.

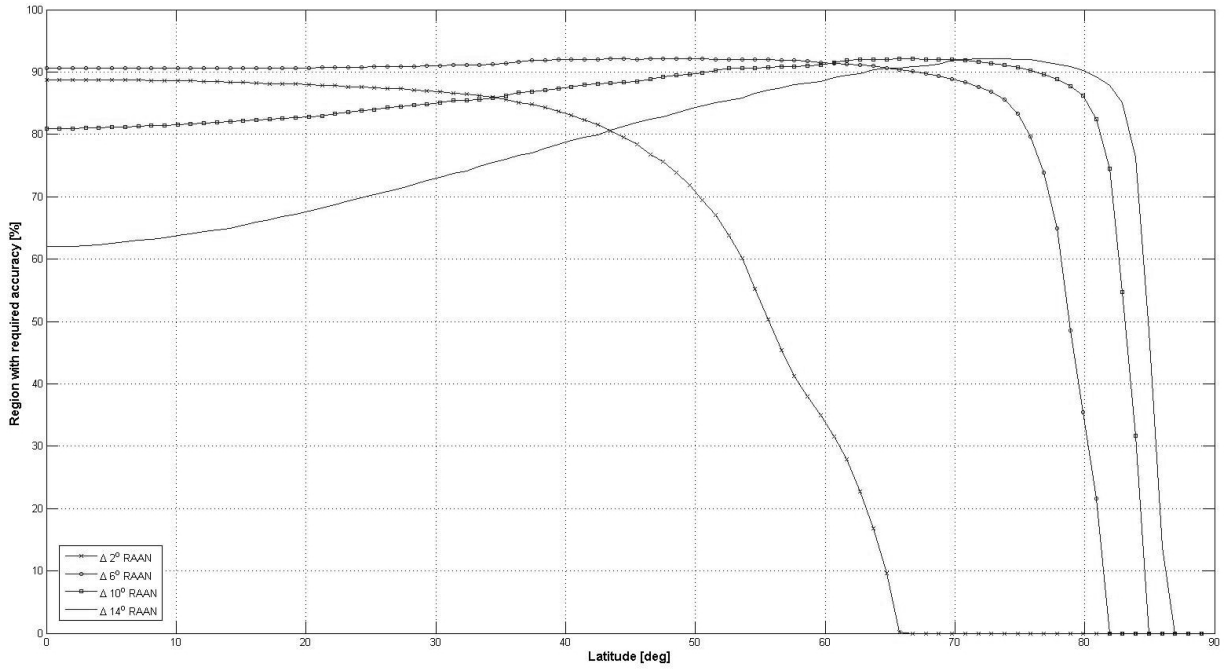

Figure 11.4: Distributions of the geolocation accuracy of GPS jammers on a spherical Earth depending on the difference in right angle of ascending node of the two circular polar planes (Orbital altitude = 500 km, in-plane separation = 500 km, inclination = 100°).

11.4.4 Sensitivity

From the inputs subsection it is deduced that a sensitivity of the geolocation of GPS jammers to five parameters can be conducted: the standard deviation of time of arrival, the standard deviation of frequency of arrival, the altitude, the shape of the formation and the loss of a spacecraft.

The standard deviation of time of arrival and the standard deviation of frequency of arrival is, as stated in the inputs subsection, a measure of, respectively, the observer position and velocity uncertainties. Since, in the TDOA-FDOA algorithm, the two standard deviations have the same weight they will affect the accuracy to the same extent. The geolocation accuracy is linearly correlated to the standard deviations of time of arrival and frequency of arrival with a conjoined gradient of 8 m per μs. The average geolocation accuracy in the 1000 km by 1000 km region (portrayed in Figure 11.3) is 94 m , excluding the central region which does not comply with the requirements. Using this value as a benchmark, it is deduced that the uncertainties in the observer's position and velocity determination shall not exceed standard deviations of 3.8 μs and 0.38 Hz. These can be converted into position and velocity root mean square errors of 11.4 m and 57 cm s^{-1}, assuming that 1% of the time of arrival uncertainty and 100% of the frequency of arrival uncertainty can be related back to state uncertainties [18].

The third parameter to be analysed is the altitude. A change of 50 km in the altitude of the formation (which could be attributed to inaccurate orbit injection or excessive decay of the formation) results in a difference in geolocation accuracy of GPS jammers of 10%. The relationship between the altitude and the geolocation accuracy is found to be quasi-linear.

The fourth parameter considered is the shape of the formation as a measure of the length:width ratio of the quadrilateral. As can be seen in Figure 11.5, the maximum geolocation accuracy occurs at a factor of 1. As the shape elongates the performance of the formation decreases steeply to reach a minimum at a factor of 2 and increases again to achieve a local maximum at a factor of 2.5. After a factor of 4.5, the performance of the formation is null. Looking back at Figure 11.4, the dip at the equator that occurs for the formation with two orbital planes separated by ΔRAAN 14° can be attributed to the length:width ratio lower than 0.5. The accuracy then increases to a maximum when the shape factor is 1 and decreases steeply at higher latitudes. The more consistent formation is the 6° ΔRAAN since the shape factor remains above 0.5 and below the unity for the longest.

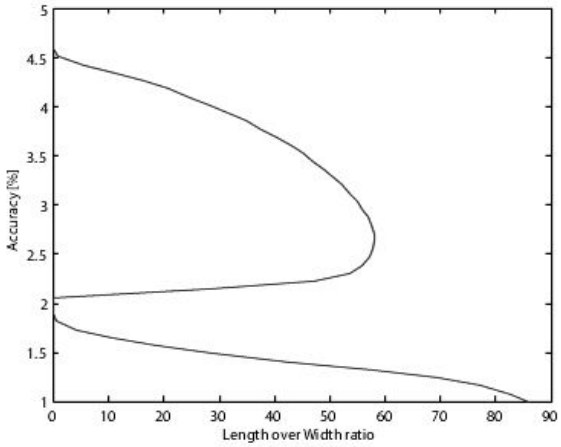

Figure 11.5: Sensitivity of the geolocation accuracy of GPS jammers to the shape ratio of the quadrilateral formation with respect to a reference, arbitrary separation.

The final parameter analysed is the loss of a spacecraft. The results of such an event are shown in Figure 11.6. The spacecraft that fails is chosen to be the top left, and since the formation is symmetrical in observer positions as well as observer velocities, the same results are expected for the loss of any of the other spacecraft. It can be seen that as soon as the spacecraft is lost, the performance of the formation drops by a mean of 8800% from 246 m to 21.86 km. If the spacecraft are rearranged into a triangular formation (see right graphs of Figure 11.6), the mean error in positioning is 22.16 km. This is 1.3% higher than for the initial formation of three. Furthermore, as can be seen in the contour map, the region with geolocation errors lower than 20 km is 2% smaller than for the initial formation. As a result, the rearranged formation does not improve the performance. This can be explained by the lack of velocity and position symmetry in the initial formation that allows a more accurate discrimination between the isodoppler and isochrone lines [19]. It needs to be stated however, that in the initial formation the largest distance between two spacecraft is 21% larger than for the rearranged formation. As a result, for the initial formation, a 9% larger viewing angle of the receiver antenna is required (61°).

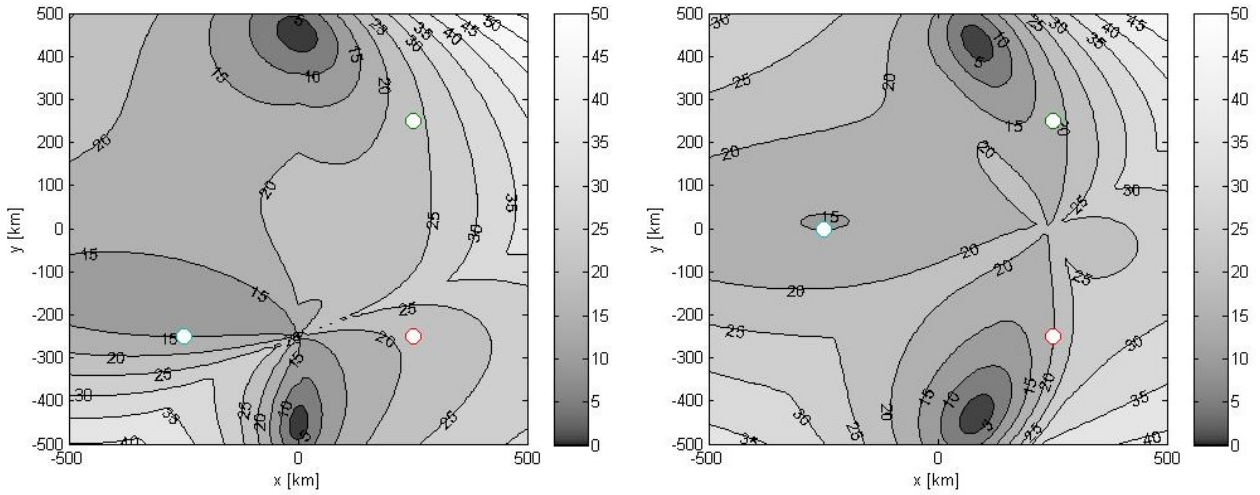

Figure 11.6: Geolocation accuracy distribution of GPS jammers in a 1000 km by 1000 km square region. Left: accuracy after the failure of one spacecraft. Right: accuracy after the in-plane shift of the lone spacecraft to achieve a triangular formation. The gray-scale bar represents the accuracy in km.

11.4.5 Derived Requirements

In the sensitivity analysis four requirements were derived. Written below are not the actual requirements (see Appendix A), but the thought behind the requirements identified with the following codes.

AOC-11/31 As explained in the sensitivity section, the error in knowledge of position of the satellite shall be less than 11.4 m and the error in velocity determination shall be less than 57 cm s^{-1}.

AOC-32/PAY-15 Also from the sensitivity section, the time synchronisation between the satellites shall be accurate to 3.8 μs and the error in frequency detection shall be less than 0.38 Hz to comply with the maximum standard deviation of time of arrival and frequency of arrival.

CON-05/06 Since the optimum formation is found to be a square with separations of 500 km, the spacecraft in-plane separation shall be 500 km. However, since the out-of plane separation varies with latitude, the separation between the two orbital planes shall be 6° ΔRAAN to achieve the best coverage (refer back to Figure 11.4).

PAY-08 Finally, in order to validate the assumption that the signals are detected by all four spacecraft, the L-band antenna viewing angle shall be larger than 56°.

11.5 Overview

The performance of the geolocation function of the formation is summarised in Table 11.3. Note that the applicability displayed in the table is the range in which the accuracy is achieved.

Table 11.3: Summary of the geolocation performance of the formation.

Source	Method	Accuracy	Applicability
L-band radar	AOA	2.13 − 5.00 km	34° − 90° elevation
S-band radar	AOA	1.40 − 5.00 km	26° − 90° elevation
X-band radar	AOA	1.85 − 5.00 km	31° − 90° elevation
GPS jammer	TDOA-FDOA	60 − 200 m	0° − 70° latitude

12 | Constellation Geometry Design

This chapter describes the detailed design of the mission's orbit geometry. First, the requirements that are imposed upon the constellation are given. After that, the model used during the constellation design iterations is discussed. Then, design considerations for the constellation parameters is given. Finally, the result of the design process is summarised.

12.1 Requirements

For the constellation design, the following requirements are applicable (these can also be found in the requirements overview in Section A.3:

CON-01 The orbit altitude shall be 500 km.

CON-02 The orbit geometry shall enable the S/C formation to be in view of a ground station on Dutch soil at least once every 6.5 hours.

CON-03 The orbit geometry shall provide global coverage for the GPS jammer localisation.

CON-04 The orbit geometry shall provide global coverage for the radar signal localisation.

CON-05 The orbit geometry shall be such that the minimum in-plane distance between S/C is 500 km.

CON-06 The orbit geometry shall be such that two orbital planes are at least 6° apart at the equator.

CON-07 The orbit geometry shall be such that the S/C nominal orbits do not collide.

12.2 Model

To study the possible design options for the constellation an analysis tool has been written in MATLAB. The main goal of this tool is to give the designer a quick indication of the behaviour of the constellation based on a user-specified set of parameters. The model is a basic tool, which gives a simplified representation of the constellation behaviour. The main assumptions and limitations of the MATLAB model are listed below:

- The orbits are modelled as Kepler orbits [20].
- Earth is assumed to be a perfect sphere with radius 6378 km.
- No third-body perturbations such as the Moon, Sun or any other forces than Earth's central force are taken into account.
- No perturbing forces such as atmospheric drag or solar radiation are taken into account.
- A time resolution of ten seconds is used.

In the model two reference frames are used: an Earth-Centred, Inertial (ECI) frame and a rotating Earth-Centred, Earth-Fixed (ECEF) frame. The two frames have the same origin, but the ECEF frame rotates about the z-axis of the ECI frame with period of 86164 seconds.

A number of inputs are required by the user, these are listed below. The model is set up in such a way that it is easy to be use in an iterative manner, where the designer is able to tweak values and study the consequences.
The inputs that are required from the user are (multiple S/C and ground stations are supported):

- **Orbit parameters per S/C:** Semi-major axis, eccentricity, inclination, RAAN, argument of perigee. The argument of perigee is undefined for orbits with zero eccentricity but in this model is used as the S/C angle above or below the equatiorial plane at $t = 0$, to specify the initial position of the S/C.
- **Parameters per ground station:** Latitude and longitude of the ground station.
- **For coverage estimation:** Choice between dense, medium or coarse grid of radar stations that is laid over Earth for computations. The dense grid has a radar station at every 1° of latitude and longitude, for the medium and coarse grid this is at every 5° and 10° respectively.

The default timespan of the simulation is set to 86400 seconds, but can be changed if the user wishes. Using the inputs the position of the S/C in a two dimensional orbit with the given semi-major axis and eccentricity is computed for all points in the specified time range. The values of the true anomaly for all positions in the Kepler orbit are computed using the iterative method in Equation 12.1 given in Space Mission Engineering [15].

$$E_{n+1} = E_n \frac{M + e\sin(E_n) - E_n}{1 - e\cos(E_n)} \tag{12.1}$$

Where E is the true anomaly, n is the number of iterations, M is the mean anomaly and e is the eccentricity. The iteration stops when the new value of E differs less than 0.1% from the previous value. The resulting two-dimensional orbit is then transformed to three dimensions by sequential application of several three dimensional coordinate transforms as seen in Equation 12.2:

$$\mathbf{r}^I_{s/c} = \mathbf{T}_z(\Omega)\,\mathbf{T}_x(-i)\,\mathbf{T}_z(-\omega)\begin{bmatrix} x_{2d} \\ y_{2d} \\ 0 \end{bmatrix} \tag{12.2}$$

Where for each S/C $\mathbf{r}^I_{s/c}$ is the position with respect to the ECI frame, Ω is the RAAN, i is the inclination, ω is the argument of perigee, x_{2d} and y_{2d} are the respective x- and y coordinates of the S/C in the two-dimensional orbital plane. The **T**'s are transformation matrices with in the subscripts their respective axis of rotation.

The positions of the ground stations are also computed by transforming their latitude and longitude to Cartesian coordinates in the ECEF frame. These are then transformed to the ECI frame for all points in the specified time range. The visibility of a ground station from a S/C is determined by the magnitude of the angle between the line connecting the S/C to the ground station and the line from the centre of Earth to the ground station as seen in Figure 12.1. The angle α is the minimum elevation above the horizon that might be required for receiving or transmitting signals between S/C and ground station.

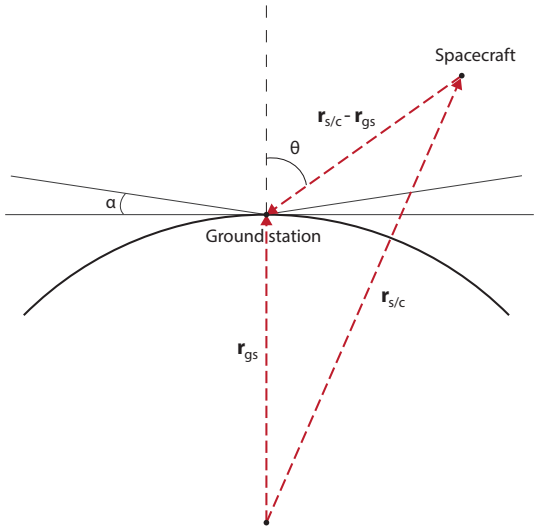

Figure 12.1: Geometry of the S/C, ground station, and local horizontal of a ground station.

The magnitude of the angle θ can be found using Equation 12.3:

$$\theta = \cos^{-1}\left(\frac{\mathbf{r}_{gs}\left(\mathbf{r}_{s/c} - \mathbf{r}_{gs}\right)}{|\mathbf{r}_{gs}|\,|\mathbf{r}_{s/c} - \mathbf{r}_{gs}|}\right) \tag{12.3}$$

Where θ is the angle as seen in Figure 12.1, $\mathbf{r}_{s/c}$ is the S/C position and $\mathbf{r}_{gs}$ is the ground station position. If the absolute value of angle θ is smaller than 90°, the S/C is above the horizon as seen from the ground station. This equation is also used for determining the visibility of the S/C from a radar station.

The results that are obtained from the simulation using the equations above return the following outputs to the user:

- A 3D rendering of the S/C orbit geometry.
- A 2D rendering of the S/C ground tracks.
- A plot per ground station showing when the ground station is visible to which satellite.
- A series of 2D plots showing the amount of time for which points on Earth are visible to different numbers of S/C over the simulated period.

12.3 Design

The constellation geometry design is driven by the requirements following from the geolocation methods. Below, the design choices for the different constellation parameters are explained.

Orbit Altitude and Eccentricity
From the AOA method for localisation of the radar sources in Section 11.3.5 it follows that the orbit altitude should not exceed 500 km. This altitude is low enough to prevent the S/C from entering the inner Van Allen belts with the exception of the South Atlantic anomaly[1]. The eccentricity is chosen to be zero, because for a non-zero value the argument of perigee shifts (see equation in time and this does not offer any advantage to the mission.

Relative Positions of S/C
From the discussion of the accuracy of the geolocation in Chapter 11 it follows that the preferred shape of the constellation is a square. The in-plane separation between S/C in the same orbital plane is 500 km. To get as close to a square as possible two orbital planes are used at an angle of 6° with respect to each other. This means that a square formation is not possible, since the planes will cross at some latitude depending on the inclinations. To prevent satellites from colliding with each other a phase shift is applied such that the two leading and the two trailing S/C are 100 km apart near the point where the two orbits cross.

Inclination
Because of the low altitude of the orbit the visibility of points near the equator is limited. To increase this coverage the choice was made to set the inclination for all orbits to 100°. This gives a better coverage at the equator than inclinations that are either 90° or 80°. Another factor in the inclination choice is the fact that the accuracy of GPS localisation decreases with decreasing distance between satellites. This means that a higher inclination decreases the accuracy of the GPS localisation at higher latitudes. The inclinations have to be the same because orbits with different inclinations have different precessions of the RAAN due to the J_2 effect [21].

Ground Stations
The RNLAF headquarters in Breda, The Netherlands is used as a ground station. It is assumed that the S/C need to be at least 5° above the horizon ($\alpha = 5°$) to allow communication. There will be five to six downlink opportunities per 24 hours for this station. To increase the downlink opportunities a second ground station on the Dutch island of Bonaire is proposed. Nearer to the equator the groundtracks are spaced further apart and have less overlap due to the Earth's rotation. Due to its geographical location the Bonaire station allows for three to four extra downlink opportunities per day. The Svalbard Satellite Station (SvalSat) ground station in Svalbard, Norway has also been considered as an option but this facility is legally prohibited from being used for military purposes[2].

12.4 Results

In this section the performance of the final constellation design is given and the sensitivity to changes in the parameters is discussed.

12.4.1 Performance

The final design is a constellation of four satellites in two orbital planes. As ground stations the RNLAF headquarters in Breda and the proposed second station on Bonaire are used. The constellation parameters and ground station positions are given in Table 12.1.

For the given orbits the orbital period is 94.6 minutes (5677 seconds). The maximum eclipse time, which occurs when the Sun lies in the orbital plane, is approximately 35.8 minutes (2145 seconds).

[1] http://image.gsfc.nasa.gov/poetry/tour/AAvan.html [Accessed 10/06/2015]
[2] http://www.jus.uio.no/english/services/library/treaties/01/1-11/svalbard-treaty.xml [Accessed on 10/06/2015]

Table 12.1: Parameters of the constellation design.

Constellation Orbital parameters				
Parameter / Name	**S/C 1**	**S/C 2**	**S/C 3**	**S/C 4**
Semi-major axis	6878 km	6878 km	6878 km	6878 km
Eccentricity	0	0	0	0
Inclination	100°	100°	100°	100°
RAAN	-3°	-3°	3°	3°
Ground stations				
Parameter / Name	**Breda**		**Bonaire**	
Latitude	51.607°		12.132°	
Longitude	4.722°		-68.267°	

An overview of the downlink opportunities for the two ground stations over a period of 24 hours is given in Figure 12.2. The longest downlink opportunity in the figure is approximately 10 minutes long, and the shortest 1.5 minutes.

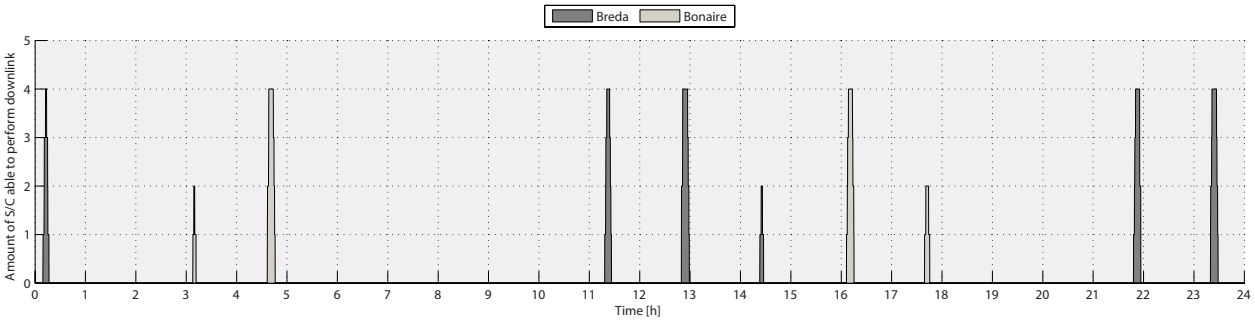

Figure 12.2: Plot of downlink opportunities over a 24h period for the Breda and Bonaire ground stations. $a = 5°$ and the time-step is 10 s, at $t = 0$ the S/C are in their perigees as defined in Table 12.1.

With the given parameters the constellation design is complaint with all requirements except for **CON-03** with which it is only partially compliant. The reason for this is the decreasing distance between S/C at higher latitudes on GPS localisation and is explained in Section 11.4.3.

12.4.2 Sensitivity

The parameter that has the largest influence on the constellation performance is the semi-major axis. A slight change in the value for one S/C means that its orbital period changes and thus the S/C will no longer orbit synchronised with the rest of the formation. With only three spacecraft flying in formation the accuracy of the GPS-jammer localisation will be as seen in Figure 11.6. To prevent this the S/C propulsion systems shall be able to keep all S/C on the same altitude during the entire mission.

The inclinations of both orbits need to be the same to ensure that their planes do not rotate relative to each other due to the difference in rate of procession of their RAAN caused by the J_2 effect [15]. To prevent this from happening the S/C propulsion systems shall be able to correct the launcher injection error for the inclination.

12.4.3 Derived Requirements

From the sensitivity analysis in Section 12.4.2 some requirements for other subsystems can be derived. These are given below:

PRO-01 The propulsion subsystem shall provide the capability to maintain orbit at an altitude of 500 km.

PRO-02 The propulsion subsystem shall be able to correct any errors in orbit injection.

TTC-07 The TT&C subsystem shall provide the telemetry capabilities at an elevation of at least 5° above the horizon, in any weather conditions.

AOC-11-F02 During normal mission mode, the absolute position knowledge error of the satellite shall not exceed 10 m.

TTC-15 The TT&C subsystem shall be able to perform all uplink- and downlink communication during the up- and downlink opportunities provided by the constellation geometry.

13 | Payload Design

In this chapter, the payload design is described. The payload consists of two main parts, the Electronic Support Measures module and the antenna array, which are both described below. The antenna array should be able to receive the signals of interest, which will be analysed by the Electronic Support Measures (ESM) module.

13.1 Requirements

The design and workings of ELINT instrumentation is of high value and mostly classified by governments and companies that produce such instrumentation. In many cases application of ELINT techniques is not difficult. Devising the methods and understanding and analysis of the intercepted signals are the most challenging aspects of ELINT. Understanding how a radar is detected by an adversary is the first step in devising countermeasures for that method or ELINT station. These restrictions confine the sections about the ELINT payload to a primarily qualitative discussion. The requirements are listed in full in Section A.2.

PAY-01 The constellation shall detect RF signals in the 1-4 GHz and 8-12 GHz bands.

PAY-03 RF signal sources shall be located with an accuracy better than 5000 m.

PAY-04 The constellation shall detect GPS jammers with an Equivalent Isotropically Radiated Power (EIRP) of 40 mW.

PAY-05 GPS jammer positions shall be determined with an accuracy better than 200 m.

13.2 Signal Processing

Target signals shall be detectable using the antenna array, but identifying target signals and performing the localisation shall depend on the performance of the signal processing payload and the quality of the signal library. The basic functions of the ESM payload are explained for the interception of radar and GPS jammer emissions. A simplified block diagram of the process is drawn in Figure 13.1.

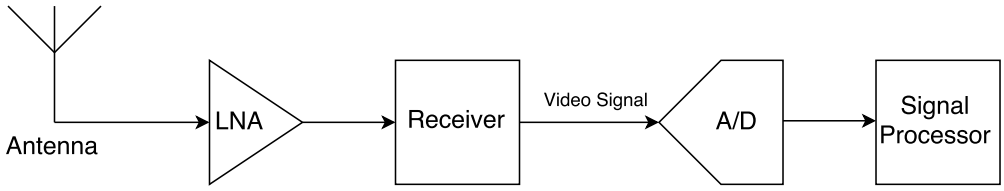

Figure 13.1: Block diagram of the main components of the payload.

The signal intercepted by the antenna is first amplified before further processing. The signal is analogue at this point and needs to be pre-processed by a receiver. Although some modern receivers are partly digital, a fully analogue receiver is common. The receiver produces a video signal as an output. This video signal is an analogue signal where threshold detection has been applied to the intercepted signal. The video signal can then be digitised by the analog-to-digital converter for signal analysis.

The amount of data generated by a single antenna is estimated. It is assumed that the video signal is digitised for the full L-, S- and X-bands. The total frequency bandwidth is 7 GHz and requires a multichannel receiver. The calculation is based on typical values of a superheterodyne receiver. The calculation is shown in Table 13.1.

Table 13.1: Estimation of digitised video channel data rate output.

Property		
Total intercepted bandwidth	7	GHz
Channel bandwidth	0.5	GHz
Digitisation resolution	14	bits
Total data rate	3.92	Gbps

Digitisation and storage of such data is difficult and expensive. Continuous monitoring of 7 GHz of bandwidth using separate channels is not easily done. Detection and analysis of target signals need to be addressed separately for radar emissions. GPS jammers on the other hand operate on a known, relatively narrow, frequency band. In this case continuous monitoring and scanning processing is possible.

A consecutive set of pulses emitted in one direction, or trigger, lasts between 1 and 200 ms [16]. During this time, the signal has to be detected, analysed and identified. In modern ELINT systems wide crystal video receivers are used as an initial detector. When a signal of interest is detected, a more accurate superheterodyne receiver is tuned to the corresponding frequency bandwidth to allow a detailed analysis of the signal. Each antenna requires a receiver, so the ELINT payload must be equipped with enough receivers to meet the antenna array output lines.

13.2.1 Signal Analysis

The task of an ELINT mission is to intercept, isolate and identify target signals of interest. Radar systems can be identified by some parameters that are characteristic to a radar. An advanced ELINT operation could have the goal to intercept signals of new unknown radar systems. These signals are analysed to produce a signal library. This is a database containing values for parameters that can be used to identify a system. A signal library can also include information that cannot be obtained by ELINT alone [16].

A modern radar system can only be identified by combining several characteristic parameters. When a radar emission is intercepted by an ESM system, these parameters are determined and compared to a signal library of known systems to identify the radar system. This is also the strategy employed by a Radar Warning Receiver (RWR) that most military aircraft are equipped with. Below is a list of the main parameters used to identify a radar system [16].

- Direction of arrival
- Peak amplitude
- Antenna patterns (beam width, side lobe levels)
- Pulse shape (duration, rise and fall time)
- Pulse intervals (interval variations, average PRI)
- Radio frequency (centre frequency, pulse-to-pulse and on-pulse RF variations)
- Associated signals

Many of the parameters listed above are determined using the video frequency of the receiver. In modern ESM systems the Intermediate Frequency (IF) signal or the video signal is digitised and processed by a computer. The process is digitised at an early stage, so that algorithms can be used to perform the analysis. When a signal is digitised at an earlier state, more information is preserved. This however will come at the expense of more data generation. A trade-off needs to be made when digitisation of the signal is considered. Primarily the goal of the ESM mission is to be considered.

13.3 Electronic Support Measures Payload Design

Identification and localisation of target signals and their source is done by the ESM payload. RF signals are intercepted by the antenna array and must be processed. This processing transforms the intercepted emission to parameters listed in the signal library. The ESM payload must be capable of performing this operation under the expected conditions on board the S/C. First the inputs are defined, then the operations are described and lastly the outputs of the payload are listed.

Inputs

- RF signals from the antenna array
- Time and GPS position
- Track data of other S/C
- Ground commands

GPS jammers are located by FDOA and TDOA triangulation of multiple interceptions of the same transmission simultaneously. The ISL will be the primary input to perform this triangulation. The ground link is required to calibrate the array, re-program the ESM algorithms and update the signal library.

The ESM payload must be matched to the antenna array. The GPS jammer antennas shall intercept CW signals and the signal processing shall be different from the radar emission analysis. The CW signal must be 'timestamped' so that the TDOA can be applied. A suitable method must be found to do so. Also simulations signals coming from multiple GPS jammers must be identified. The merging of the antenna array and the ESM payload is more critical because of the AOA computation. The phase difference on arrival of the signal must be measured accurately to compute the AOA. This is done by ensuring the length of the line from the receiver to the antenna must be exactly the same.

When a GPS jammer is detected, the emitted signal must be timestamped and tracked. Using the ISL track data from other S/C containing signal characteristic parameters and TOA, the track can be updated. When three or four S/C in the constellation also intercept the jammer emission the triangulation will be performed. A decision is then made which S/C will down-link the coordinates of the jammer.

Modern radars employ several techniques to reduce interception of their emission and to resist jamming. Methods like frequency hopping, complicated waveforms and electronic scanning are examples of such measures. Interception of such signals is difficult without any knowledge about the emission characteristics, thus requiring the use of a signal library. The ESM payload must be capable of measuring the parameters listed in 13.2.1 for every intercepted signal. When a radar is identified, the type, time and location must be determined. The radar is then tracked for the period it is in sight of the S/C to generate a more accurate localisation. The track is then stored and made ready for down-link.

The technology to perform the ELINT operations is present and available for governments. Three challenges are identified in fielding a ESM module in space. The instrumentation needs to be suitable for surviving the radiation and temperature in space, the distance to the emitter source is much greater than ground, air- and ship-borne ELINT operations and the higher noise levels in space. The radiation is discussed in section 13.3.1 and is focused on modifying existing instrumentation to enable space applications. The large distances and added noise will require the use of sensitive instrumentation. The general specifications and lower level requirements for the ESM payload are discussed in 13.3.2. The outputs of the ESM module are listed below:

Outputs

- Radar identification number / jammer identification parameters
- Time of detection radar/jammer
- Angle of arrival w.r.t S/C (radar)
- Centre frequency (radar)
- Location of radar/jammer
- Track data of radar/jammer

Track data can produce large amounts of data, especially when gathered over a dense theatre with many assets. Tracking of emitters can however provide information about moving emitters, increasing the value of the detection and localisation.

13.3.1 Radiation Mitigation

Costs and development time can be reduced by using existing instruments for signal processing. Besides the mechanical loads experienced during launch the instruments must be able to withstand the harsh extraterrestrial environment. Radiation and ionised particles degrade electronic components and can cause errors and failures. Shielding can be used to reduce damage to electronic components caused by ionised particles. Radiation and high energy particles are not stopped easily by shields and require a different approach to cope with the radiation.

The total radiation dose, measured in rad, that an electronic component endures during operation is the measure for the radiation tolerance of a part. The total dose is a function of the time in orbit, the specific orbit and the behaviour of the Sun. In LEO, the inner Van Allen belt is present, which contains protons, electrons and radiating particles. Impact of high energy particles from the Sun or cosmic radiation with electronics can cause secondary radiation and

the creation of ionised particles despite the presence of shielding. Long term exposure of electronics to radiation can cause an increased power consumption, speed reduction and a variability between identical components[1].

High energy particles can also cause Single Event Effects (SEE) that impact the functioning of electronic components at a microscopic level. Radiation can cause a bit flip in a data storage device, called a Single Event Upset (SEU) or disrupt a processing unit. These events are classified as soft errors, because no permanent damage is caused to the circuit. An Error Detection and Correction (EDAC) algorithm can be applied to memory devices to detect and correct bit flips caused by SEU. Another class of SEE are hard errors such as Single Event Latchup (SEL), Single Event Burnout (SEB) and Single Event Gate Rupture (SEGR) that can be destructive for a circuit. These events are types of short circuits that cause an immediate increase in power consumption. If the device is not turned off, destructive failure might occur [22].

Electronic components can be designed to better withstand SEE at a circuit level or at system level or both. Radiation hardened components are protected at circuit level and components have been extensively tested to identify the risks and behaviour of the components after extended periods of exposure [23]. Radiation tolerance can also be achieved by using COTS components in combination with a SEE mitigating system architecture. Protection mechanisms like EDAC and voltage monitoring can be implemented to prevent failure of the system. Other methods are implementation of duplex or triple architecture. In such cases redundancy is used to add protection. Inactive components are less sensitive to SEE. In the event of failure of one components, the other is switched on. In triple modular redundancy, three identical components are operated in parallel and a vote takes place. In case of an error one component will produce a different output and is reset [23].

Using COTS electronic components will require extensive testing to determine radiation effects and to predict the behaviour of components. One such method requires the acquisition of components originating from the same production batch [23]. Complicated systems such as an ESM module will require extensive testing and possibly alteration of the system architecture to ensure a lifetime of five years. Such modification will require destructive testing of at least one unit and extensive testing at component level. The required time for such testing should also be accounted for in the mission planning.

13.3.2 ESM Specification and Lower Level Requirements

The ESM module is regarded as a black box in the design and inputs, outputs, and operations are defined in Section 13.2.

Table 13.2: Specifications of ESM module [2], [16].

Mechanical Specifications	
Mass of module	8 kg
Dimensions of module	200 mm x 200 mm x 400 mm
Power consumption	150 W
Operational temperature	$-40°C$ to $55°C$
Performance Specifications	
Analysis range for radars	1-4 and 8-12 GHz (L-, S-, and X-band)
Analysis range for GPS jammers	L1 band
AOA measurement accuracy	L-band: 0.24°, S-band: 0.16°, X-band: 0.21°
Carrier frequency accuracy	0.25 Hz
Time stamp accuracy	25 μs
Operational life time of module	Seven years

The specifications listed in Table 13.2 are general and are necessary to meet the localisation algorithm, antenna array requirements and spacecraft bus constraints. The power consumption, dimensions and mass are based on an airborne RWR. Due to the similar functions, it is reasonable to assume similar specifications. The specifications listed in Table 13.2 impose requirements on the ESM module. These are listed on the next page.

[1] https://nepp.nasa.gov/workshops/etw2012/talks/Tuesday/T14_LaBel_COTS_Radiation_Effects.pdf [Accessed on 10/06/2015]
[2] Information from Terma A/S of Denmark

PAY-01 The constellation shall detect RF signals in the 1-4 GHz and 8-12 GHz bands.

PAY-01-F01: The intercepted signal shall be analysed with at least 500 MHz channel width.

PAY-01-F02: The intercepted signal shall be identifiable for a 40 dB dynamic range per channel.

PAY-01-F03: The signal needs to be transformed to a video signal with an output frequency of 10 MHz.

PAY-01-F04: Identification of target signals shall be done using comparison with an on-board signal library.

PAY-01-F05: The signal library shall be up-dateable.

PAY-01-C01: The signal library shall be accessible by the spacecraft on-board computer.

PAY-01-C02: The ESM module shall not be affected by the TT&C S-band downlink transmission.

PAY-04 The constellation shall detect GPS jammers with an EIRP of 40 mW.

PAY-04-C01: The receiver shall have a sensitivity better than −170 dBW.

13.4 Antenna Array

To provide information about the AOA of the signal of interest, which is needed for the localisation, an array of antennas is needed. The signals they receive are compared to each other, and an algorithm comes up with the estimate for the AOA. These techniques can be divided into two categories, which are amplitude comparison methods and phase comparison methods. The first can achieve a $3° - 10°$ accuracy, and the latter $0.1° - 1°$ [24]. Because an accuracy better than 3° is needed for the geolocation algorithm, the phase comparison method will be used, and the array will be designed to match the needed accuracy.

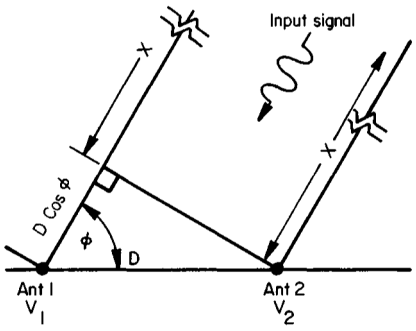

Figure 13.2: Principle phase interferometry [25].

The method which uses the comparison of phases is also called phase interferometry. It uses the phase difference of a signal impinging on the array to compute the AOA [26]. Because one antenna is located further away from the source, a delay in arrival, so a phase shift, occurs. This is illustrated in Figure 13.2.

13.4.1 Initial Requirements

For the geolocation, an accuracy of better than 0.4° is required, for one standard deviation, stated in **PAY-06**. This is the value for which the array will be designed, using the model presented later.

13.4.2 Model Description

Accuracy of the AOA calculation is limited by two factors. One is the phase error, $\Delta\phi$, due to errors in the electronics. The accuracy error, $\Delta\theta$, due to this is given in Equation 13.1 [27].

$$\Delta\theta = \frac{\lambda}{2\pi D\cos\theta}\Delta\phi \tag{13.1}$$

The other is the phase error due to noise, depicted in Figure 13.3. The corresponding equation is Equation 13.2 [25], where the phase error, γ, is a function of the Signal-to-Noise Ratio (SNR) of a single receiving antenna.

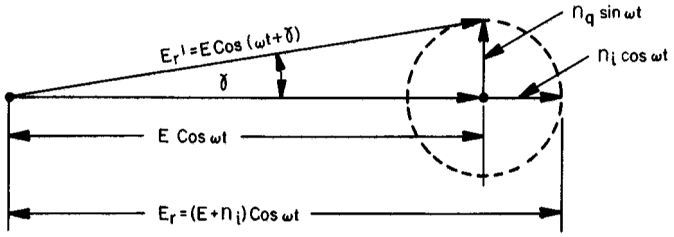

Figure 13.3: Noise effect on phase [25].

$$\gamma = \frac{1}{\sqrt{SNR}} \tag{13.2}$$

This noise error leads to an AOA inaccuracy, of which the Root Mean Square (RMS) error is given by Equation 13.3 [27], [25].

$$\sigma_\theta = \frac{\lambda}{D\ \cos\theta\ \pi\ \sqrt{SNR}} \tag{13.3}$$

To calculate the received power at each antenna element, a link budget is set up. In this, the atmospheric losses are neglected, since they are in the order of magnitude of 0.3 dB [28]. The power emitted from the radar is multiplied by the combined gain factor (main and sidelobe). This power is divided by the free space path loss, L_{FS}, given by Equation 13.4 [29].

$$L_{FS} = \frac{4\pi\ R}{\lambda} \tag{13.4}$$

The power of the noise, N, is given by Equation 13.5 [30].

$$N = \mathrm{k}\ T_S\ B \tag{13.5}$$

13.4.3 Design

To use the model described before, different inputs to the model are needed. The values used during the design are explained in this section.

The quantisation error, $\Delta\phi$, is the error in the phase measurements by the electronics. This error is estimated at 10° [27]. The maximum off-boresight angle, θ, should be half of the viewing angle. Therefore, a value of 30° is used in the model. The frequency, f, is also required as an input. The highest frequencies of each band have been used, since these are most critical for the accuracy. This means that 2 GHz, 4 GHz, and 12 GHz have been used for the L-, S-, and X-band, respectively.

To estimate the SNR, some other parameters need to be specified as well. The transmitted power during a pulse of a radar, P_{TX}, is estimated at 150 kW, 200 kW, and 100 kW for L-, S-, and X-band radars, respectively[3]. The gain of the main lobe, G_{TX}, of these types of radar systems ranges between 30 dBi and 40 dBi[4]. Therefore, a conservative value of 30 dBi is used in the model. Since it is unlikely that the main lobe will be detected by the spacecraft, it is necessary to estimate the power in the side lobes of the radars. Typical side lobe power levels are about 23 dB below the power of the main lobe [3]. Therefore, they are estimated to have a gain of 7 dBi. Due to the polarisation of the radar antenna and the polarisation of the antennas used to detect the signals on the spacecraft, a loss can occur due to a mismatch in the polarisations. However, this loss will be minimised by using orthogonally placed Vivaldi antennas, so the loss is estimated as 0 dB. As discussed in the previous section, the distance, R, from the transmitter to the receiver plays a large role in the free space path loss. As a worst case, the distance is taken as the maximum distance between a spacecraft in the constellation and a point on the viewed area ($R = \sqrt{2 \cdot 500^2 + 730^2} = 1016$ km). To estimate the noise power, the system noise temperature, T_S, and the bandwidth, B, are needed. They are estimated to be 290 K and 200 MHz, respectively.

[3] ausairpower.net [Accessed on 09/06/2015] and customer correspondence
[4] radartutorial.eu [Accessed on 10/06/2015] and customer correspondence

Using the model, the distance, d, between the first and last element is varied to achieve the needed accuracy. However, to avoid ambiguities, the antenna elements need a binary spacing, so at $\frac{\lambda}{2}, \lambda, 2\lambda, ...$ [25]. This is illustrated in Figure 13.4. This also implies that the value of d should be rounded up to the next binary value. The value of the wavelength is derived from the highest frequency from each band [31].

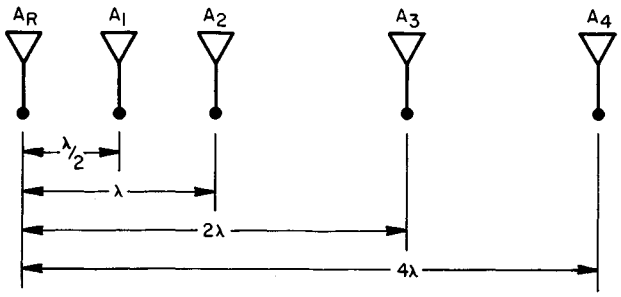

Figure 13.4: Binary spacing of array elements [25].

.

As antenna type, a Vivaldi antenna is selected for the L- and S-band, since they can have a 5:1 bandwidth [32]. Placing two Vivaldi antennas orthogonally w.r.t. each other also avoids polarisation mismatch losses. For the X-band, patch antennas are chosen. They are of simple construction, small and provide the needed minimum of 1 dBi gain over the whole frequency band [33]. They should also be placed orthogonally to ensure no polarisation mismatch. To reduce signal attenuation from the antenna elements to the signal processing ESM module, every antenna shall be equipped with a Low Noise Amplifier (LNA).

The antennas are designed using the MATLAB Antenna toolbox [34]. The requirements for the antenna are that every element has at least -1 dBi gain in the L-band, 0 dBi gain in the S-band and 1 dBi gain in the X-band, over a viewing angle of 60°. A simulation tool has been developed which calculates the minimum gain in the viewing angle. Using this tool and iterating with it, a Vivaldi element with dimensions of 12 cm x 5 cm is found to be matching the requirements for the L- and S-band. This minimum required gain over the ±30° is plotted versus the frequency in Figure 13.5. From this figure can be derived that the antenna meets the requirements. In Figure 13.6, the simulated patterns for 1 GHz, 2.5 GHz, and 4 GHz are shown.
For the X-band, a patch antenna is chosen, because the bandwidth ratio of the X-band is much lower (1.5:1), so there is no need to use antennas with very large bandwidth. An advantage of those patch antennas is their size, they are extremely small (< 1 cm) in one direction. With the MATLAB Antenna toolbox [34], a design is done as well for the patch antenna. This resulted in a patch antenna with dimensions 1.25 cm x 2.5 cm x 1 mm. The radiation pattern of it is showed in Figure 13.8, and the maximum and minimum gains over the viewing angle are displayed in Figure 13.7. These graphs are made using MATLAB [34] as well.
For the GPS jammer localisation, a specific patch antenna is designed. This results in more gain than using the Vivaldi antenna. A patch antenna is designed in MATLAB [34] as well. The design is done for the frequency of the GPS carrier, which is 1.57542 GHz. It measures 20 cm x 10 cm, and has a maximum gain of 8.45 dBi, and a gain of 5 dBi at the edge of the viewing angle (± 30°). This is illustrated in Figure 13.9.

13.4.4 Results

For the L- and S-band, a minimum distance of 2.4 m is found. The inaccuracy due to phase error is 0.11° and 0.06 °, for the L- and S-bands respectively. The RMS noise phase errors are 0.13° and 0.10°. Together, they sum up to 0.24° and 0.16° inaccuracy. For the X-band, the minimum distance is 1.6 m, which gives a phase error inaccuracy of 0.03° and a RMS noise phase error of 0.19°, which sums up to 0.21°. Using the binary spacing, this results in a seven-element array for L- and S-band, and a nine-element array for the X-band. To save space and weight, two linear arrays have been chosen, instead of a rectangular array. However, they need deployment, because the two arrays need to be under an angle w.r.t. each other, preferably orthogonal. The GPS patch antenna is designed, such that it provides at least a 5 dBi gain over the needed beam-width, with a maximum of 8.45 dBi. A sensitivity analysis is performed on this results. From this resulted that the design is sensitive to analysis bandwidth, because this greatly influences the noise power. The powers of the radar are also very important to the design of the array. However, there is some margin left, both for the array and the antenna elements, so the design will not likely change a lot when these parameters change. Another important parameter is the accuracy. When an accuracy of 0.1° is needed, the antenna array should be 9.6 m.

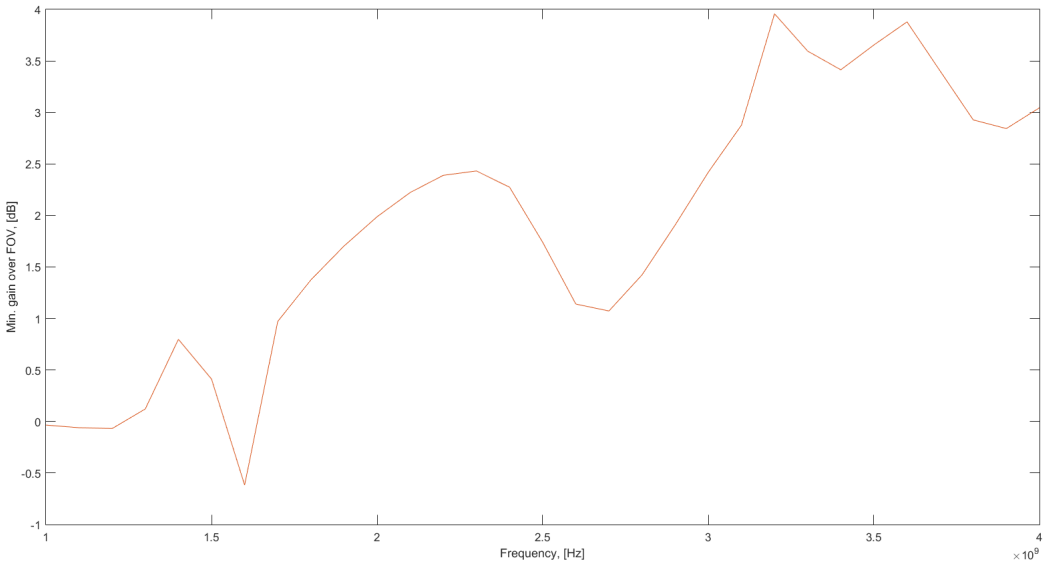

Figure 13.5: Minimum gain versus frequency from MATLAB simulation.

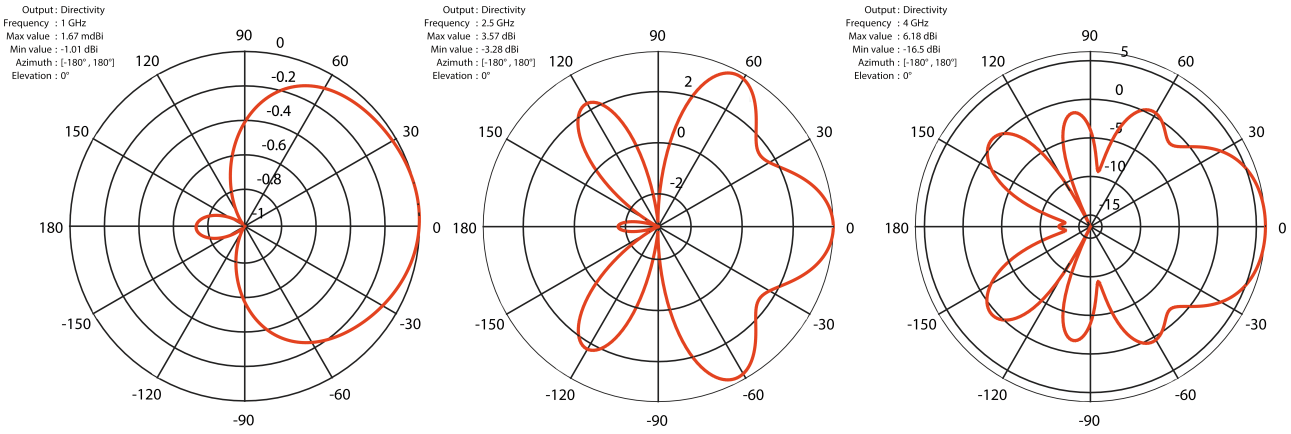

Figure 13.6: Vivaldi radiation pattern of 1 GHz, 2.5 GHz, and 4 GHz respectively.

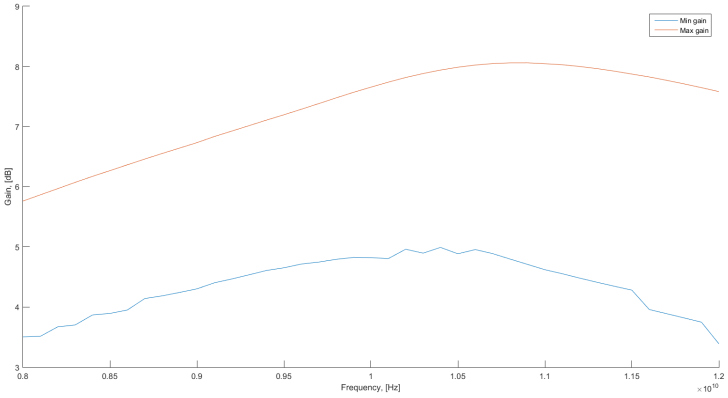

Figure 13.7: Minimum and maximum gains versus frequency.

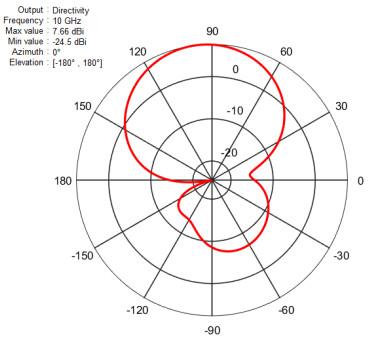

Figure 13.8: Radiation pattern of centre frequency of 10 GHz.

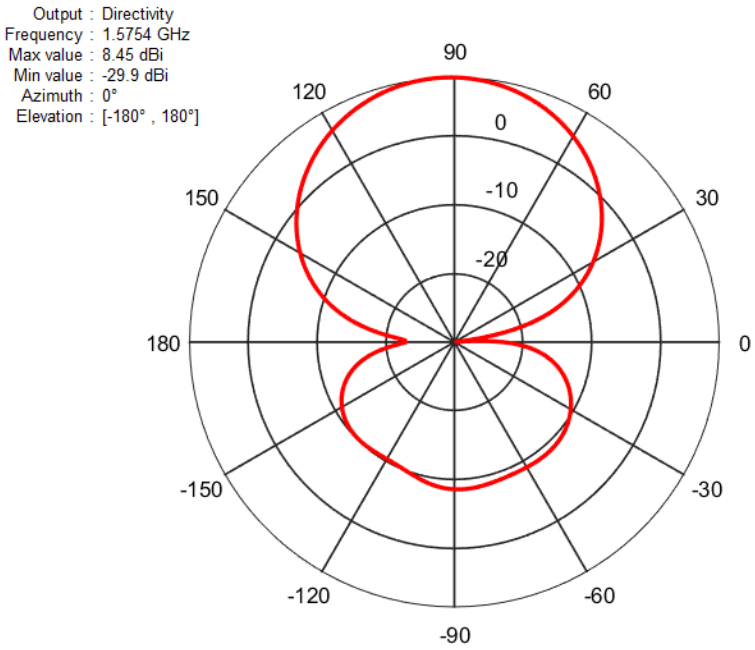

Figure 13.9: Radiation pattern of the GPS antenna.

The deployment of the arrays can cause some errors, as well as production errors and boom displacement due to thermal stresses. This has not been incorporated in the model, but there is still some margin left. The array should be tested attached to the spacecraft bus in anechoic chamber. This way, there can be checked if the spacecraft bus interferes with the antenna. Using data from this test, the array should be calibrated as well. The computation of the AOA is to be done by the ESM module. To do so, the Multiple Signal Classification algorithm is preferred over the Estimation of Signal Parameters via Rotation Invariance Techniques algorithm. Reasons for this are that the first is more accurate than the latter, and also more stable [35]. However, this comes at the cost of more computing power.

13.4.5 Derived Requirements

The antenna array needs to be accurate, but the accurate AOA information will be worthless when the attitude knowledge is bad. Therefore, as a rule of thumb, the pointing knowledge should be ten times better than the AOA accuracy. Therefore, a 0.04° (1σ) pointing knowledge accuracy is required from the AOCS. To point the array to the area of interest, the whole spacecraft should be slewed 20° to the direction between the spacecraft. Because the spacecraft switch left-right position w.r.t. each other when crossing the poles, they should be slewed 40° to the other side when the latitude is larger than 80°. To avoid interference, the payload should not work when the communications are active. To avoid phase errors, the antenna element placing should not deviate more than 1 mm. This is a requirement for the structure on which the antennas are placed. The two arrays should be placed orthogonal as well, with an accuracy of within 1°. These requirements are summarised below.

AOC-29 The absolute pointing knowledge error of the L & S-band antenna during ELINT gathering shall not exceed 0.04° half cone angle.

AOC-12-F01 The AOCS shall be capable of slewing the payload's line of sight, over 40° while above 80° latitude.

PAY-12 The antenna element placement shall be precise within 1 mm.

PAY-13 The antenna boom placement shall be 90°, with an accuracy of 1°.

PAY-14 The antenna array shall not be influenced by the TT&C.

14 | Electrical Power Subsystem Design

This chapter describes the detailed design of the Electric Power System (EPS). Firstly, the requirements for the subsystem are given. Consequently, the models used for the detailed design and the detailed design itself are presented. Afterwards, a sensitivity analysis is performed on the EPS.

14.1 Requirements

This section contains the the requirements for the power subsystems. The main purpose of the EPS is to provide all power required by the subsystems of the satellite (the "loads"). It was determined through a trade-off that the best option to fulfil this purpose was to use solar panels in combination with batteries. To achieve the goal of providing the satellite with the required power, the EPS has to perform four main tasks:

- Condition electrical power (voltage regulation)
- Control electrical power
- Store electrical power
- Distribute electrical power

The requirements that follow from these functions and other requirements for the EPS are listed below:

PWR-01 The power subsystem shall provide all power required by the satellite during all mission phases and for all operation modes through the entire duration of the mission.

PWR-02 The power shall be provided by means of both solar cell array and batteries.

PWR-03 The solar cell array shall be sized with 5% margin for the worst case power situation and provide power up to the end of mission.

PWR-04 The power subsystem shall condition, control, store and distribute electrical power on the spacecraft.

PWR-05 The subsystem shall provide adequate status monitoring and telecommand interfaces necessary to operate the subsystem and permit evaluation of its performance.

PWR-06 The subsystem shall provide adequate failure tolerance and protection circuitry to avoid failure propagation and to ensure recovery from any malfunction within the subsystem and/or load failure.

PWR-07 The power subsystem shall contain all necessary electronics.

PWR-07-F01: The power subsystem shall contain all electronics necessary to provide electrical power from the solar cell generator and/or batteries to all users.

PWR-07-F02: The power subsystem shall contain all electronics necessary to charge, discharge and recondition all batteries.

PWR-07-F03: The power subsystem shall contain all electronics necessary to give the capability for automatic and commanded control of the operation of the subsystem.

PWR-07-F04: The power subsystem shall include all power switching and protection electronics for all spacecraft subsystem users.

PWR-08 The power subsystem shall meet the requirements for average and peak power electrical loads.

PWR-14 A maximum Depth-of-Discharge (DOD) of 45% in nominal cases shall not be exceeded.

The complete set of requirements for the EPS can be found in Section A.11

14.2 Model

In this section, the models to determine the required solar array power and the required battery storage capacity are established and explained. A general overview of the flow of power through the system is derived. It is shown in Figure 14.1.

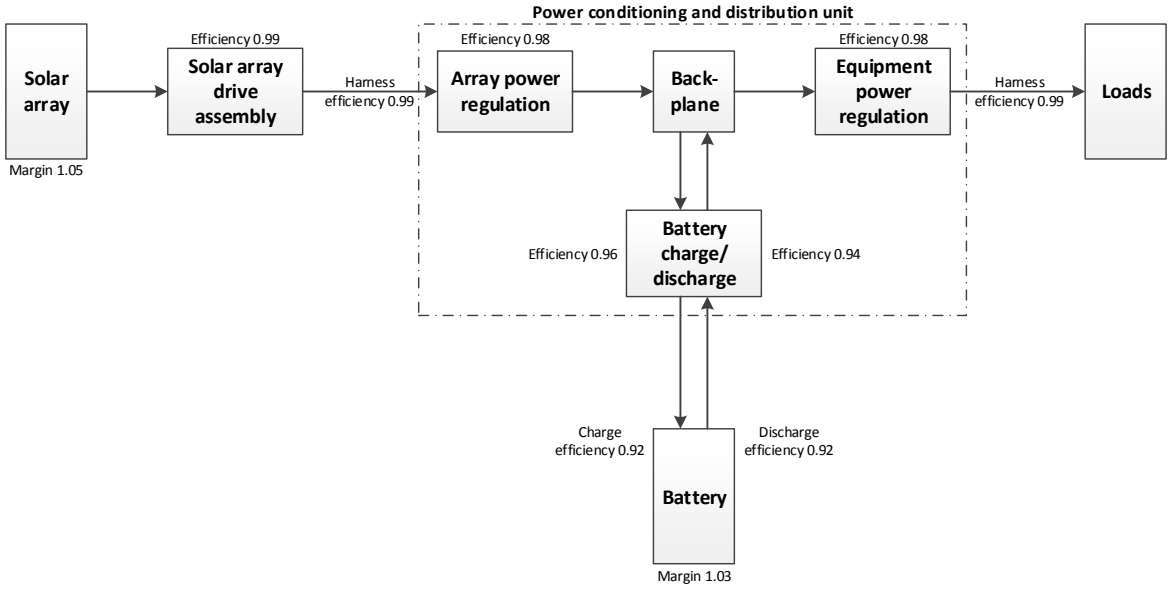

Figure 14.1: Power flow diagram.

With the general overview of the EPS the power rates in various parts of the system, the solar array EOL power generation capability and battery storage capacity can be calculated. The results of these calculations are given in Section 14.3. The efficiencies in various sections of the EPS are given in Figure 14.1. At first, estimates from literature were used in the power flow diagram. After the hardware of the Power Conditioning and Distribution Unit (PCDU) was selected, the efficiencies were updated to estimate the final solar array power capability and battery storage capacity. The final efficiencies are shown in Figure 14.1.

The required solar array EOL power capability and battery energy storage size are determined with the average power demand from the loads. This figure is determined in Chapter 24. The power in the system is modelled back to the solar arrays with a basic equation for efficiencies, given in Equation 14.1.

$$P_{in} = \frac{P_{out}}{\eta} \tag{14.1}$$

Here P_{in} and P_{out} are the powers going in and coming out of a component respectively, and η is the efficiency. To incorporate a margin for the solar arrays, Equation 14.2 is used

$$P_{in} = P_{out} \text{ margin} \tag{14.2}$$

The energy storage capacity of the batteries is calculated using Equation 14.3

$$\text{Wh}_b = \frac{P_e T_e}{\eta \text{ DOD}} \text{ margin} \tag{14.3}$$

where Wh_b is the energy storage capacity of the battery, P_e is the required power during eclipse, T_e is the eclipse time, η is the efficiency of the system between the battery and the loads, and DOD is the maximum depth of discharge of the batteries.

14.3 Design

With the model set to determine the power through the system, the inputs need to be set to calculate the required Photovoltaic (PV) array area and battery storage capacity. The inputs for the model are listed in Table 14.1.

Table 14.1: Inputs for power analysis of the system.

System requirement and constraints		
Loads during sunlight	345.46	W
Loads during eclipse	345.46	W
Orbit period	5681	s
Eclipse time	2147	s
Sun time	3534	s
System efficiencies and margins		
Array margin	1.05 [36]	-
Charge time margin	1.03 [36]	-
Solar Array Drive Assembly (SADA) efficiency	0.99 [36]	-
Harness efficiency	0.99 [36]	-
Array Power Regulation (APR) efficiency	0.95[1]	-
Battery Charge Regulation (BCR) efficiency	0.96[2]	-
Battery Discharge Regulation (BDR) efficiency	0.94[2]	-
Equipment Power Distribution (EPD) efficiency	0.98[3]	-
Battery efficiency	0.85 [36]	-
Battery characteristics		
DOD	0.45 [37]	-

The loads during sunlight and eclipse are the average power demands derived in the power budget analysis in Chapter 24. Using these figures for the power demand of the system will ensure that enough power will be collected during sunlight to provide enough power for one orbit. The orbit period, sunlight time and eclipse time result from the orbit determined in Chapter 12. The 45% DOD follows from the number of cycles during the mission and the type of battery cell selected. The selection of the type of battery cell is explained in the hardware selection. The same holds for the APR, Battery Charge/Discharge Regulation (BCDR) and EPD, since there efficiencies follow from the selected hardware.

The outputs of the model are listed in Table 14.2. The EOL capability of the solar arrays was calculated to be 736 W. This means that the solar arrays must be capable of providing at least 736 W at the end of the mission to ensure all the loads can function properly. The calculated battery energy storage capacity is 566 W h. With the efficiency of the system between the battery and the loads, and a DOD of 45% this amount is sufficient to supply the loads with enough power during eclipse.

Solar arrays

Now that the model has been run, the hardware selection can be started. For the solar arrays, triple junction solar cell technology is selected due to its high area power density ($W\,m^{-2}$), low specific weight ($W\,kg^{-1}$) at panel level and low normalised cost ($€\,W^{-1}$) at panel level [38]. The search for COTS solar arrays has led to the selection of Modular Solar Arrays with Integrated Construction (MOSAIC). These pre-qualified and plug-and-play modular panels shorten design development and simplify spacecraft integration, testing and ground maintenance functions. One solar panel delivers approximately 100 W[4] power at EOL. Therefore, eight panels are required to satisfy the 730 W EOL power capability for the solar arrays. The resulting solar array size, considering two equally sized wings, is 0.61 m by 2.98 m per wing including hinges. Each solar array will be mounted to a SADA which can rotate the solar arrays around one axis. Since rotation around the spacecraft's yaw axis is not restricted, the solar arrays can be rotated around two axes. This means that the spacecraft will be capable of pointing the solar arrays with 1° accuracy to the Sun [36].

[1] http://terma.com/media/177686/array_power_regulation_module.pdf [Accessed on 12/06/2015]
[2] http://terma.com/media/177689/battery_cd_regulation_module.pdf [Accessed on 12/06/2015]
[3] http://terma.com/media/177695/equipment_power_distribution_module.pdf [Accessed on 12/06/2015]
[4] http://vst-inc.com/satellite-components/solar-power-systems/modular-solar-panels/ [Accessed on 12/06/2015]

Table 14.2: Power analysis through the complete system.

Power analysis during sunlight		
PV array EOL power capability including margin	730.46	W
Load at PV array during sunlight (including charge)	695.67	W
APR module rating (input)	681.83	W
APR module rating (output)	647.74	W
BCR module rating (input)	291.67	W
BCR module rating (output)	280.00	W
Charge power in battery	257.60	W
EPD module (input)	356.07	W
EPD module (output)	348.95	W
Power analysis during eclipse		
Discharge power out of battery	378.80	W
BDR Module rating (output)	356.07	W
EPD module (input)	356.07	W
EPD module (output)	346.95	W
Energy analysis in battery		
Battery Wh energy storage rating	561.58	Wh
Energy discharged from storage during eclipse	225.72	Wh

Power Conditioning and Distribution Unit
To condition and distribute electrical power throughout the EPS, a PCDU is needed. Hardware from Terma is selected, because the PCDU is built up of different modules. In this way the PCDU can be tailored specifically for this mission. The following modules are selected for the PCDU:

- **Array Power Regulation Module**: this module consists of a power regulator supported by a Maximum Power Point Tracking (MPPT) capability to maximise power output. The design is targeted at any type of solar array technology. The power output capability per module is 250 W [1].
- **Battery Charge/Discharge Regulation Module**: this module consists of two power regulators, a BCR and a BDR. The design is targeted at Li-Ion battery systems. The power output per module is 300 W [2].
- **Equipment Power Distribution Module**: this module is available for distribution of bus power to the spacecraft equipments. In case of overload or short circuit, the output current is instantly limited to protect the upstream main power bus. Each EPD module consists of sixteen Latching Current Limiter blocks, which can be operate in parallel for increased load current classes[3].
- **MIL-STD-1553 Interface Module**: this module interfaces to the unit power modules, can set remote commandable functions, and read the telemetry of system power modules[5].

To be able to regulate sufficient solar array power for the system, at least three APR modules are required. For redundancy, one extra APR module is installed. Since the output capability of the BCDR module is 300 W and the power discharged from the batteries during eclipse is 381 W, two BCDR modules are integrated into the PCDU. Typically, one equipment is used per output to prevent failure propagation. With 26 loads in the system that require power directly from the EPD modules (derived from Appendix C), two EPD modules are needed to provide enough outputs for the loads. For a redundant interface between the EPS and the C&DH system, two MIL-STD-1553 interface modules are added to the PCDU. The resulting PCDU has a mass of 8.6 kg and dimensions of 19.3 cm x 15.0 cm x 26.4 cm.

Batteries
The last part of the EPS to be sized is the battery. The required energy storage of the batteries was determined to be 562 W h. Due to the relatively high energy density of Li-ion batteries in comparison to other batteries used in space such as NiCd and NiH_2, Li-ion batteries are selected for this mission [39]. Average figures suggest the energy density of Li-ion batteries lies between 70 and 100 W h kg^{-1} [39]. To make a safe estimate, an energy density of 70 W h kg^{-1} is used at this stage to estimate the battery mass. Using this value results in an estimated battery mass of 8.0 kg. The complete overview of the EPS with the loads is illustrated in the electrical block diagram in Appendix B.

[5] http://terma.com/media/177704/mil-std-1553_interface_module.pdf [Accessed on 12/06/2015]

14.4 Results

In this section the performance of the final EPS design is discussed and the sensitivity of the design to changing parameters is discussed.

14.4.1 Performance

In Table 14.3, the characteristics of the EPS design are listed.

Table 14.3: Characteristics of EPS design.

Component	Value	Unit
Solar array EOL power	800	W
Battery storage capacity	562	W h
EPS mass	33.0	kg

As indicated in Section 17.4, estimations show that the batteries have sufficient power stored for the system until the solar panels have been deployed after separation.

14.4.2 Sensitivity

A change in the mission lifetime has two main effects on the EPS design. Due to degradation effects, the solar array area needs to be increased to be able to provide sufficient power at EOL to the system. Also, when the mission lifetime increases, the number of cycles of the battery increases. This will mean that an increased lifetime will require a larger battery since the DOD of the battery goes down [37].

If the power required by the loads increases, the system will need to provide more power. This will have an effect on the size of the solar arrays, the battery size and the PCDU. An increased amount of required power will increase the size of the solar arrays and batteries. This will also increase the required power throughput of the PCDU, which will yield an increased mass of this unit as well.

The effects on the EPS due to an increased mission lifetime and increased power demand might not have an effect immediately. Since margins have been incorporated in the power budget, the possibility exists that the change of one of the two variables will not require resizing of the EPS.

15 | Telemetry, Tracking, and Command Subsystem Design

This chapter contains the design of the Telemetry, Tracking, and Command subsystem. First, the requirements for this subsystem are given. Then, the models and assumptions used during the design process are explained and justified. Finally, the design process is performed and the results are given.

15.1 Requirements

For the Telemetry, Tracking, and Command subsystem, the following requirements have been used during the design:

TTC-01 The TT&C subsystem shall receive and demodulate telecommands, modulate and transmit telemetry data, and transpond the ranging signal.

TTC-02 The TT&C subsystem shall interface exclusively with ground stations on Dutch soil.

TTC-03 The TT&C subsystem shall interface with the other S/C in the constellation.

TTC-05 The TT&C subsystem shall have no requirements for telemetry operation during the launch phase.

TTC-06 The TT&C subsystem shall provide the telecommand capabilities in any of the S/C attitudes, at an elevation of at least 5° above the horizon, in any weather conditions.

TTC-07 The TT&C subsystem shall provide the telemetry capabilities at an elevation of at least 5° above the horizon, in any weather conditions.

TTC-12 The TT&C subsystem shall have a link margin of at least 10 dB to account for any unexpected attenuations in any of the telecommunications links.

TTC-13 The TT&C subsystem shall be redundant.

TTC-15 The TT&C subsystem shall be able to perform all uplink- and downlink communication during the up- and downlink opportunities provided by the constellation geometry.

15.2 Model

This section describes the important equations and assumptions used in the models created to help design the TT&C subsystem.

15.2.1 Transmission Analysis

To get an estimate of the received power, Equation 15.1 was used. It includes the various powers, gains, and losses that are relevant to making a propagation analysis

$$P_{RX} = P_{TX} - L_{TT} + G_{TX} - L_{P,TX} - L_{PM} - L_{FS} - L_{AT} - L_{IO} - L_{RA} - L_{P,RX} + G_{RX} - L_{TR} - L_M \tag{15.1}$$

where P_{RX} is the receiver input power in dBm, P_{TX} is the transmitter output power in dBm, L_{TT} are the total transmitter losses in dB, G_{TX} is the transmitting antenna gain in dBi, $L_{P,TX}$ is the transmitting antenna pointing loss in dB, L_{PM} is the polarisation mismatch loss in dB, L_{FS} is the free space path loss in dB, L_{AT} is the atmospheric absorption loss in dB, L_{IO} is the ionospheric loss in dB, L_{RA} is the rain loss in dB, $L_{P,RX}$ is the receiving antenna pointing loss in dB, G_{RX} is the receiving antenna gain in dBi, L_{TR} are the total receiver losses in dB, and L_M are miscellaneous losses in dB.

The losses and gains in the transmitter and receiver are usually presented by the manufacturer in the product documentation. The other losses need to be calculated or estimated.

Antenna Pointing Loss

The antenna pointing loss is caused by a misalignment between the transmitting and receiving antennas. In practice, there will never be perfect alignment, so this loss will always be present. The antenna pointing loss is divided in losses at the S/C antenna and losses at the ground station antenna.

Polarisation Mismatch Loss
The polarisation mismatch loss is caused by a difference in polarisation in the signal and the receiving antenna. This loss can range from 0 dB for equal polarisations, to complete loss of the signal in some combinations of signal polarisation and antenna polarisation[1]. To minimise the losses due to polarisation mismatch, a circular polarisation will be used for the telecommunications in this mission. The transmitting and receiving antenna need to have the same type of circular polarisation (either left-handed or right-handed).

Free Space Loss
The free space path loss can be calculated using Equation 15.2. This will be the largest contributing factor to the signal degradation in any of the telecommunications links.

$$L_{FS} = 20\log_{10}(d) + 20\log_{10}(f) - 147.55 \tag{15.2}$$

where d is the distance from the transmitter to the receiver in m, and f is the frequency of the signal in Hz. The larger the distance or frequency, the higher the free space path loss. It is therefore beneficial to use lower frequencies, as long as the data rates allow this.

Atmospheric Absorption Loss
The atmospheric absorption loss is strongly dependent on the frequency used for the links. The higher the frequency, the larger the atmospheric absorption loss. There are several resonance peaks at 22.3 GHz and 60 GHz, but these will not influence the design of the TT&C for this mission.

The first 10 km of the atmosphere measured from the surface are most influential for the atmospheric absorption loss. At an elevation of 10°, the path length to reach an altitude of 10 km is about 60 km. It was found that the atmospheric absorption would not exceed 0.6 dB in this case [40]. As a conservative estimate, a 1 dB loss due to atmospheric absorption will be used for the links with the ground station.

Ionospheric Loss
The ionospheric loss occurs when the electromagnetic waves of the radio signal and the free electrons in the ionosphere interact. Higher frequencies tend to be less susceptible to ionospheric losses [41]. Since the ionospheric loss is a complex random process, values from documentation of similar links[2] [3] [29] are used to make a reasonable estimate. It is estimated the ionospheric loss will be between 0.4 dB and 0.8 dB for frequencies between 135 MHz and 2.5 GHz. A conservative value of 1 dB will be used in the link budgets for all links.

Rain Loss
The rain loss is negligible at frequencies below 2 GHz. Above 2 GHz, the rain attenuation becomes significant [42]. The higher the frequency, the higher the rain loss. At a frequency around 2.5 GHz, the rain loss is about 1 dB. A conservative value of 1 dB will be used in the link budgets for all links.

15.2.2 E_b/N_0 Calculation
Now the received power is known, the E_b/N_0 can be calculated, which is a normalised SNR.

Energy Per Bit
The signal power at the receiver needs to be converted into the received energy per bit, E_b, by using Equation 15.3.

$$E_b = P_{RX} - 10\log_{10}(R) - 30 \tag{15.3}$$

where E_b is the energy per bit in dBJ, and R is the bit rate of the transmission.

Receiver Noise Power Spectral Density
The energy per bit at the receiver alone is not enough to determine if the data transfer will be successful. Equation 15.4 gives the noise power spectral density, N_0, expressed in dBm s.

$$N_0 = 10 \cdot \log_{10}(\mathrm{k}T_S) \tag{15.4}$$

where k is the Boltzmann constant and T_S is the system noise temperature in K.

[1] http://paginas.fe.up.pt/ ee97054/Link%20Budget.pdf [Accessed on 09/06/2015]
[2] http://www.oit.ac.jp/elc/ satellite/image/Linkbudget.pdf [Accessed on 09/06/2015]
[3] http://gomspace.com/documents/gs-ds-nanocom-ax100-1.5.pdf [Accessed on 09/06/2015]

Energy Per Bit To Noise Power Spectral Density Ratio
Calculating E_b/N_0 is now a straightforward process, as can be seen in Equation 15.5

$$\frac{E_b}{N_0} = E_b - N_0 \tag{15.5}$$

where E_b/N_0 is the energy per bit to noise power spectral density ratio in dB.

15.2.3 Link Margin
The calculated value for E_b/N_0 will be compared to a required E_b/N_0 value to achieve a certain Bit Error Rate (BER) using a certain modulation scheme. The difference between the two is called the link margin and needs to be positive for successful data transfer.

15.3 Design
This section is dedicated to describing the design process of the TT&C subsystem.

15.3.1 Data Generation Rate
First, the data generation rates have to be estimated. This results in a data generation rate of about 1 kbps for the housekeeping data[4] and a few bps (on average) for the payload data as discussed in Chapter 13. A conservative estimate for the generated data in one hour is 4 Mb. Because the payload data is relatively small compared to the housekeeping data, they will be transmitted over the same link.

15.3.2 Ground Station Location
The payload data needs to be downlinked as soon as possible, so the Svalbard Satellite Station would be the ideal candidate as a ground station, because a downlink opportunity occurs every orbit (± 98 minutes) when the inclination is near 90°. However, Article 9 of the 1920 Svalbard Treaty[5] states that Svalbard may never be used for warlike purposes. This treaty puts the use of SvalSat for the downlink of this mission in a legal grey area. Therefore, a different solution will be proposed.

If a single ground station in Breda is used for the downlink, there would be periods of about eleven hours without a downlink opportunity for the constellation. These periods could be reduced to about six and a half hours by using a second ground station in one of the Caribbean special municipalities of the Netherlands, as can be seen in Figure 12.2. This way, the information will reach the RNLAF headquarters faster on average, while maintaining ground stations exclusively on Dutch soil.

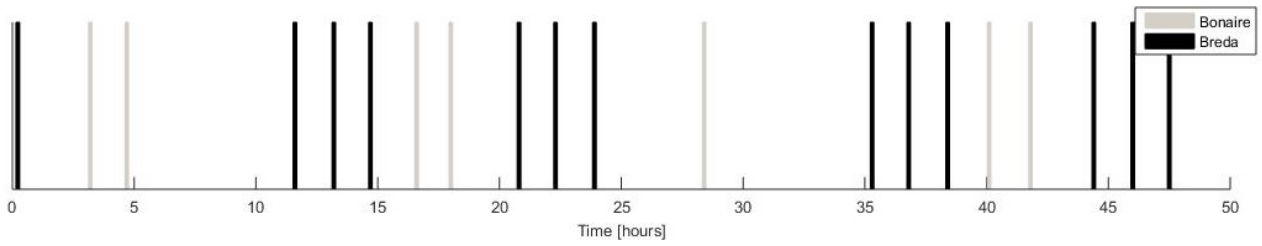

Figure 15.1: Downlink opportunities over a 48 hour period using ground stations in Breda and Bonaire.

15.3.3 Data Rates
Assuming two ground stations will be used as discussed above, the S/C shall have to send down data, which was generated over a period of six and a half hours in the worst case. To take into account one or two missed downlinks, a maximum time without downlink of eleven hours is found by inspecting Figure 15.1. Eleven hours of payload and housekeeping data amounts to about 44 Mb of generated data. This is the maximum amount of data that needs to be sent down in one downlink. Assuming about seven minutes per downlink opportunity as found in Chapter 12, that gives a maximum required downlink rate of about 105 kbps. The uplink data rate required for telecommands will most likely not exceed a few kbps. The S/C only need to exchange payload data when a GPS jammer has been detected to perform the localisation. The amount of data they need to exchange is a few kbits per detection at maximum.

[4] http://www.lr.tudelft.nl/?id=26198&L=1 [Accessed on 12/06/2015]
[5] http://www.jus.uio.no/english/services/library/treaties/01/1-11/svalbard-treaty.xml [Accessed on 12/06/2015]

15.3.4 Frequency Selection

Common Very High Frequency (VHF) and Ultra High Frequency (UHF) transmitters can provide data rates of up to 9.6 kbps. These will not be enough for the downlink, but will be enough for the uplink of telecommands. Furthermore, the UHF band (approximately 437 MHz) will be used for both the uplink and inter-satellite communications, due to the low data rate requirements for those communications links, and low cost of components. The S-band (approximately 2.25 GHz) will be used to downlink data to the ground stations. Using this band gives a good balance of bandwidth and cost of the components. The free space loss is limited by using relatively low frequencies.

15.3.5 Modulation Scheme and E_b/N_0

In digital communications, modulation is used to transfer a bit stream over an analogue channel. This is achieved by varying one or more properties of the carrier signal, in this case the radio frequency signal. The choice of modulation scheme has a direct impact on the energy per bit, E_b, required for successful communications with a certain allowed BER and a certain noise power spectral density, N_0. A BER of 10^{-6} has been chosen for all communication links to minimise the amount of data that has to be retransmitted due to a corrupted message.

Commonly used modulation schemes for satellite communication are Binary Phase-Shift Keying (BPSK), Quadrature Phase-Shift Keying (QPSK), Frequency-Shift Keying (FSK), and Minimum-Shift Keying (MSK). Figure 15.2 shows the required values of E_b/N_0 of these modulation schemes. As can be seen from this figure, the FSK scheme requires a significantly higher E_b/N_0 to achieve a certain BER. The BPSK and QPSK schemes have identical E_b/N_0 requirements (10.5 dB) to achieve a BER of 10^{-6}. MSK schemes have a slightly higher required E_b/N_0.

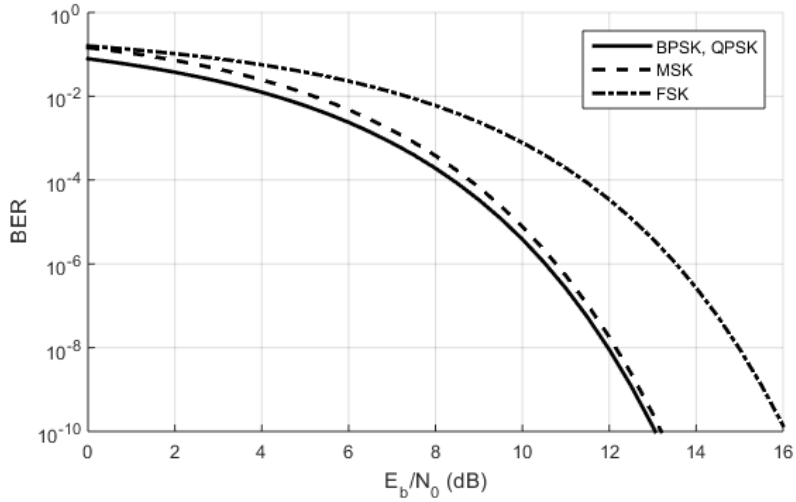

Figure 15.2: BER curves of BPSK, QPSK, MSK, and FSK modulation schemes.

15.3.6 Hardware Selection

Due to the overall time and cost constraints, it will not be possible to design the transmitters, receivers, and antennas specifically for this mission. Therefore, COTS components have been investigated. Due to the limitations imposed by International Traffic in Arms Regulations (ITAR), only components from non-US manufacturers have been looked into. The COTS equipment looked into for the links is from ISIS[6], SSTL[7], GomSpace[8] and Clyde Space[9]. Although some of these companies specialise in CubeSat products, their products can be used in larger satellites as well. The selected components are discussed below.

[6] http://www.isispace.nl/cms/ [Accessed on 12/06/2015]
[7] http://www.sstl.co.uk/Products/Subsystems/Communication [Accessed on 12/06/2015]
[8] http://gomspace.com/ [Accessed on 12/06/2015]
[9] http://www.clyde-space.com/cubesat_shop/communication_systems [Accessed on 12/06/2015]

S-band Downlink
It was decided to use an ISIS S-band ground station kit[10] for the downlink, because of its high performance (maximum data rate of 115.2 kbps and a 35.4 dBi gain) and relatively low price. It is recommended to put one of these in Breda, and another in one of the Caribbean special municipalities of the Netherlands to maximise the amount of downlink opportunities and increase redundancy. The SSTL S-band Transmitter has been selected for the space segment of the mission, because of its performance, design lifetime (more than seven years), and extensive flight heritage. The SSTL S-band Patch Antenna has been selected for the downlink, because of its wide beamwidth (6 dBi on boresight, 0 dBi at 60° off-boresight), small dimensions, and extensive flight heritage.

UHF Uplink
An ISIS VHF/UHF ground station kit[11] has been selected for the uplink of this mission. It offers a very high RF output power (up to 100 W) and a high gain. This means less strain will be put on the receiving equipment on the S/C. It is suggested to put this element of the ground segment in Breda. The GomSpace U482C UHF transceiver[12] has been selected to handle the incoming uplink signals. It is a half-duplex transceiver capable of receiving uplink signals at a rate of 4800 bps. The antenna to be used with this transceiver is a GomSpace ANT430 turnstile antenna[13]. It has a near-omnidirectional radiation pattern, so does not need to be pointed very precisely. Its gain ranges from 1.5 dBi to −1 dBi.

UHF Crosslink
The same UHF equipment will be used on the S/C for the crosslinks, because the requirements on the data rates for the inter-satellite communications are low as well. The free space loss of UHF signals is lower than that of higher frequencies, so less radiated power is needed. The near-omnidirectional antenna allows crosslinks without moving then antenna to point it. Since the uplink and crosslinks are chosen to operate at the same frequency and the GomSpace transceiver is a half-duplex system, they need some kind of Time Division Multiple Access (TDMA). This way, the satellites will not try to communicate with each other when in contact with the ground station to maximise the amount of data that can be uplinked. By using TDMA, the satellites can all receive and transmit on the same frequency, without interfering with each other. The effective achievable data rate will be lower when using TDMA methods. Since some of the selected equipment is designed for CubeSat missions, it might require some additional radiation shielding to extend the expected lifetime of the components, as well as adding extra redundancies in the system.

15.3.7 Redundancy
To ensure a redundant design for the TT&C subsystem, single points of failure are to be avoided whenever possible. Figure 15.3 shows the redundant design of the S-band downlink chain. There will be two S-band transmitters, as well as two S-band antennas. These will be switched using an electromechanical switch. The downlink chain will feature cold redundancy, meaning the second transmitter will not be powered on until the first unit suffers a failure. There will be some downtime when this happens, but the data can be transmitted to the ground station again during a next downlink opportunity.

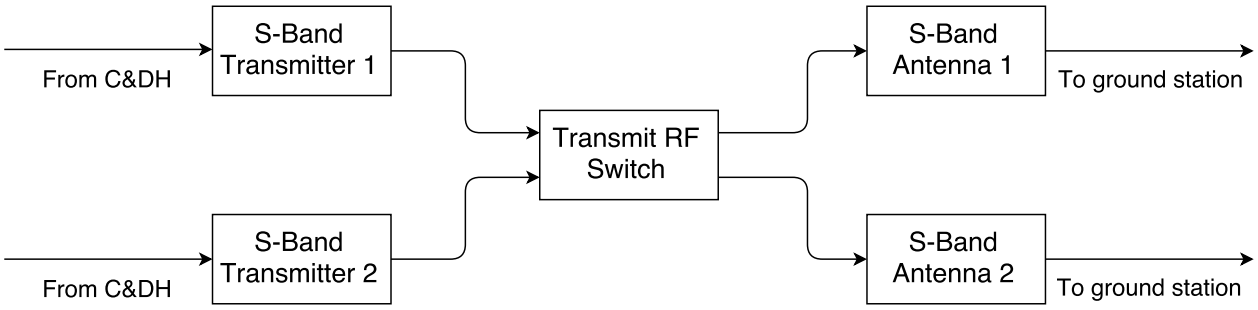

Figure 15.3: Layout of the S-band downlink chain.

[10] http://www.cubesatshop.com/index.php?page=shop.product_details&flypage=flypage.tpl&product_id=117&category_id=3&option=com_virtuemart&Itemid=
[Accessed on 12/06/2015]
[11] http://www.isispace.nl/brochures/ISIS.GS.DS.v13.7%20Data%20Sheet%20Gound%20Station-1.pdf [Accessed on 12/06/2015]
[12] http://gomspace.com/index.php?p=products-u482c [Accessed on 12/06/2015]
[13] http://gomspace.com/index.php?p=products-ant430 [Accessed on 12/06/2015]

Figure 15.4 shows the redundant design of the UHF crosslink and uplink chains. The transceivers will be switched on by electromechanical switches. This design will be implemented twice (once at the front and once at the rear of each S/C) to ensure uplink communications with the ground station, no matter the orientation of the S/C. The uplink chain will feature hot redundancy during the parts of the orbit when one of the ground stations is in view. This means that during most of the orbit, one of the transceivers is turned on. However, when the ground station is in view, a second unit will be powered on as a hot standby. This way, the reception of telecommands is not interrupted in case of a failure of one of the transceivers.

In case of a failure of the S-band downlink chain, the UHF components could be used as a low data rate backup downlink. However, this would severely limit the amount of data that can be transmitted to the ground station.

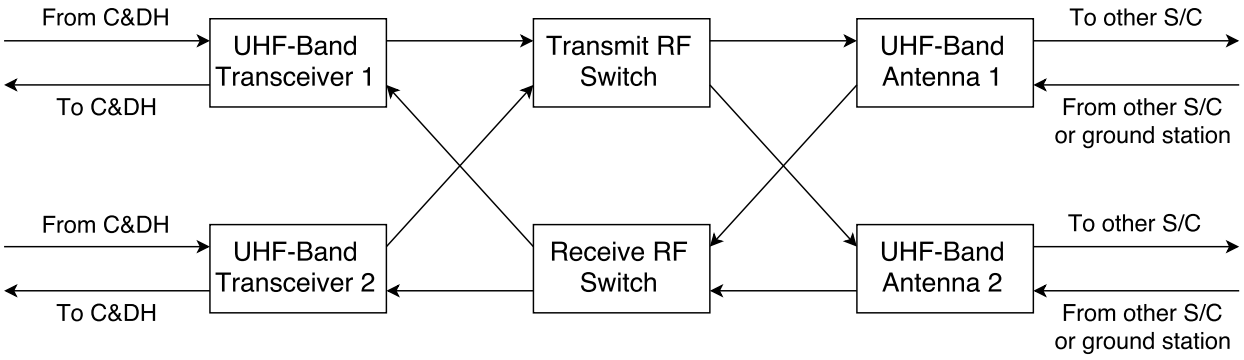

Figure 15.4: Layout of the UHF crosslink and uplink chains.

The RF switches that are required to switch between different antennas and transmitters/transceivers have been selected based on the frequencies and amount of power they can handle. The amount of insertion loss and space qualification were also looked at. The Radiall Low Power Coaxial Double-Pole, Double-Throw (DPDT) Switch[14] was chosen, because of its performance and low weight. Since Radiall is a French company, the ITAR restrictions do not apply.

Table 15.1: List of space segment components.

Component	Type	Mass	Power	Unit Cost	Quantity
S-Band Transmitter	SSTL S-Band Transmitter (High Rate)	1.8 kg	38 W	€ 200000	2
S-Band Antenna	SSTL S-Band Patch Antenna	0.080 kg	–	€ 36000	2
UHF Transceiver	GomSpace U482C	0.070 kg	5.5 W	€ 8000	4
UHF Antenna	GomSpace ANT430	0.030 kg	–	€ 5500	4
RF Switch	Radiall Low Power Coaxial DPDT Switch	0.080 kg	–	€ 2000	3

Table 15.2: List of ground segment components.

Component	Type	Mass	Power	Unit Cost	Quantity
S-Band Ground Station	ISIS Full Ground Station Kit for S-band	N/A	N/A	€ 31000	2
UHF-band Ground Station	ISIS Full Ground Station Kit for VHF/UHF	234 kg	700 W	€ 32500	1

[14] http://www.radiall.com/media/files/Switches%20D73500CE%20Space.pdf [Accessed on 19/06/2015]

15.4 Results

This section gives the results of the design process for the TT&C subsystem.

15.4.1 Performance

Now all equipment is selected, it is possible to make the link budgets for all links. These will represent worst-case scenarios. If the link margins are adequate in these situations, it is safe to assume they will be in all other situations as well.
For the downlink and uplink a distance of 2078 km is used, which corresponds to an altitude of 500 km with an elevation of 5° above the horizon at the ground station. A distance of 885 km is used for the crosslink, since that would be the maximum diagonal distance in a rectangular formation of 730 km by 500 km at the equator.
As can be seen from Table 15.3, all links have a positive link margin and should therefore provide reliable data transmissions.

Table 15.3: Link budgets for the downlink, uplink, and crosslink.

Downlink		
Inputs		
BER	10^{-6}	–
Frequency	2250	MHz
Distance	2078	km
Data Rate	115200	bps
Modulation	BPSK	–
Spacecraft		
P_{TX}	33	dBm
L_{TT}	1.0	dB
G_{TX}	6.0	dBi
S/C EIRP	38	dBm
Downlink Path		
$L_{P,TX}$	6.0	dB
L_{PM}	0.5	dB
L_{FS}	165.8	dB
L_{AT}	1.0	dB
L_{IO}	1.0	dB
L_{RA}	1.0	dB
Power at G/S	−137.3	dBm
Ground Station		
$L_{P,RX}$	3.0	dB
G_{RX}	35.4	dBi
L_{TR}	1.0	dB
T_S	67	K
Received Power	−105.9	dBm
E_b/N_0	23.8	dB
Required E_b/N_0	10.5	dB
Link Margin	**13.2**	**dB**

Uplink		
Inputs		
BER	10^{-6}	–
Frequency	437	MHz
Distance	2078	km
Data Rate	1200	bps
Modulation	MSK	–
Ground Station		
P_{TX}	50	dBm
L_{TT}	1.0	dB
G_{TX}	15.5	dBi
G/S EIRP	64.5	dBm
Uplink Path		
$L_{P,TX}$	1.0	dB
L_{PM}	0.5	dB
L_{FS}	151.6	dB
L_{AT}	1.0	dB
L_{IO}	1.0	dB
L_{RA}	1.0	dB
Power at S/C	−91.6	dBm
Spacecraft		
$L_{P,RX}$	1.5	dB
G_{RX}	1.5	dBi
L_{TR}	1.0	dB
T_S	120	K
Received Power	−92.6	dBm
E_b/N_0	54.4	dB
Required E_b/N_0	10.8	dB
Link Margin	**43.6**	**dB**

Crosslink		
Inputs		
BER	10^{-6}	–
Frequency	437	MHz
Distance	885	km
Data Rate	4800	bps
Modulation	MSK	–
Transmitting Spacecraft		
P_{TX}	33	dBm
L_{TT}	1.0	dB
G_{TX}	1.5	dBi
TX S/C EIRP	33.5	dBm
Crosslink Path		
$L_{P,TX}$	1.5	dB
L_{PM}	0.5	dB
L_{FS}	144.2	dB
L_{AT}	0	dB
L_{IO}	1.0	dB
L_{RA}	0	dB
Power at RX S/C	−113.7	dBm
Receiving Spacecraft		
$L_{P,RX}$	1.5	dB
G_{RX}	1.5	dBi
L_{TR}	1.0	dB
T_S	120	K
Received Power	−114.7	dBm
E_b/N_0	26.3	dB
Required E_b/N_0	10.8	dB
Link Margin	**15.5**	**dB**

15.4.2 Sensitivity

The large link margins in Table 15.3 indicate that the links are not sensitive to a slight change in one of the variables.

15.4.3 Derived Requirements

This system imposes the following requirements on some of the other subsystems.

CON-02 The TT&C requires that the constellation geometry allows for a communication opportunity with a ground station on Dutch soil at least every 6.5 hours.
PAY-01-C02 The ESM should filter out the TT&C signal, since it uses the S-band as well.
CDH-01/02 The C&DH subsystem needs to prepare data to be transmitted and process the received data.

16 | Command and Data Handling Subsystem Design

This chapter contains the design of the Command and Data Handling subsystem. First, the requirements for this subsystem are given. Then, the models and assumptions used during the design process are explained and justified. Finally, the design process is performed and the results are given.

16.1 Requirements

For the Command and Data Handling subsystem, the following requirements have been used during the design:

CDH-01 The C&DH subsystem shall decode, validate, and distribute telecommands acquired from the TT&C subsystem.

CDH-02 The C&DH subsystem shall acquire telemetry data and format it for transmission by the TT&C subsystem.

CDH-03 The C&DH subsystem shall distribute commands to other subsystems.

CDH-04 The C&DH subsystem shall be able to store software, payload data and housekeeping data.

CDH-05 The C&DH subsystem shall supervise the on-board autonomy.

CDH-06 The C&DH subsystem shall be capable of compressing data.

CDH-07 The C&DH subsystem shall be able to encrypt telemetry data and decrypt telecommands.

CDH-08 The C&DH subsystem shall manage and distribute a time signal.

CDH-09 The C&DH subsystem shall accommodate all interfaces required by the various subsystems.

The radar and GPS signal processing is part of the payload subsystem, so the C&DH does not need to be able to perform the computations needed for the identification and localisation of the signal sources.

16.2 Model

As a start for the design of the C&DH subsystem, an inventory has been made of all the subsystems and equipment that need to communicate with the On-Board Computer (OBC). A visualisation of how the various subsystems relate to the OBC has been made and can be seen in Figure 16.1. A list of the data flows as seen in Figure 16.1 is provided in Table 16.2 with descriptions of the types of data that need to be exchanged between the various subsystems. It is important that the C&DH subsystem can interface with the various subsystems.

16.3 Design

Due to the overall time and cost constraints, it will not be possible to design a C&DH unit specifically for this mission. Therefore, COTS components have been investigated. Due to the limitations imposed by ITAR, only components from non-US manufacturers have been looked into. Systems from SSTL[1], SSBV[2], and DSI[3] have been compared. The criteria looked at for the OBC during the comparison are listed below.

- **Performance:** The amount of operations or instructions a processor can perform per second
- **Data storage:** The amount of storage available to the OBC
- **Available interfaces:** The amount and type of available interfaces
- **Power consumption:** The maximum and typical power consumption of the C&DH subsystem

[1] http://www.sstl.co.uk/ [Accessed on 19/06/2015]
[2] http://www.ssbv.com/ [Accessed on 19/06/2015]
[3] http://www.dsi-it.de/ [Accessed on 19/06/2015]

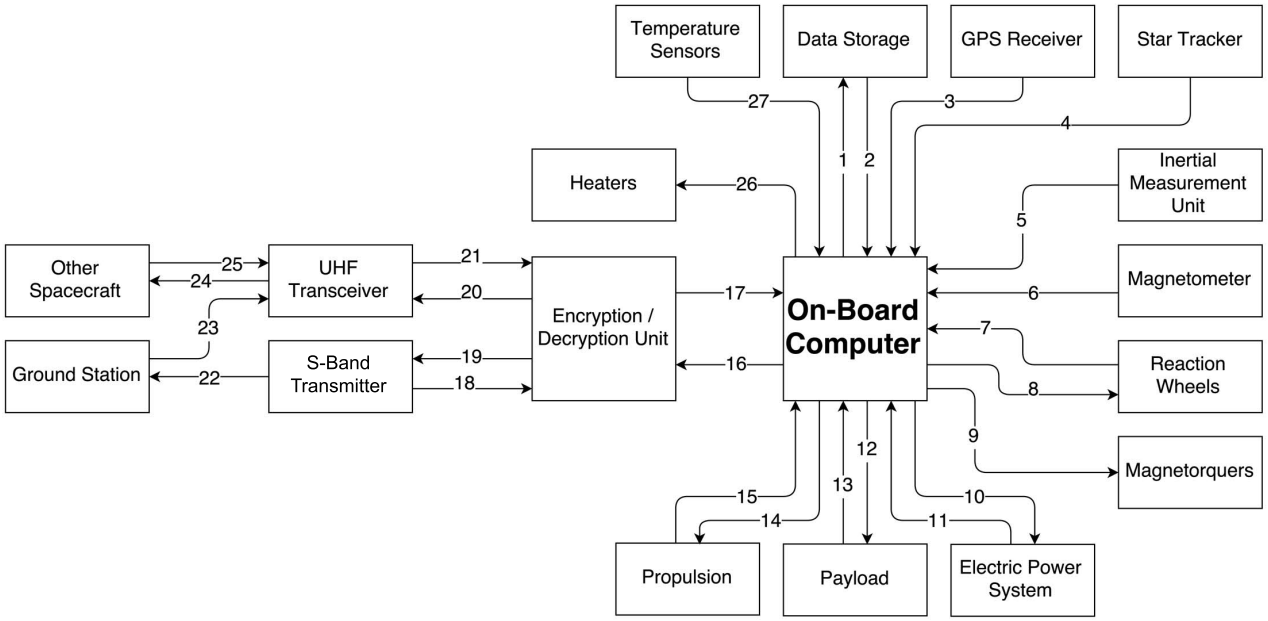

Figure 16.1: Communication flow diagram.

Table 16.1 shows a list of interfaces and the equipment that uses these interfaces to communicate with the C&DH subsystem. At this point it is unknown what interface will be used to connect the payload to the rest of the system.

Table 16.1: List of interfaces required by selected equipment.

Interface	Equipment
RS-422	Reaction wheels, magnetometer, GPS receiver, magnetorquers, IMU
LVDS	S-band transmitter
I^2C	UHF transceiver
CAN bus	GPS receiver, reaction wheels, S-band transmitter
MIL-STD-1553	Electric power system, star tracker

Some of the investigated OBC units do not provide the interfaces required by the selected subsystem equipment. However, they can usually be supplemented by adding expansion cards to the system. This does complicate the design and might cause some compatibility issues, so it should be avoided if possible. Since most of the OBC designs are based on a Field Programmable Gate Array, their functions are flexible and easily changed by a firmware update.

The telecommands the C&DH subsystem receives from the TT&C subsystem are encrypted, so a decryption module is required to decrypt the messages. The same goes the other way around. An encryption module is needed to encrypt the data the S/C sends to the ground station and the other S/C. However, there is not much detailed information publicly available about these components. One of the available encryption/decryption units is from DSI[4]. It is not possible to make a proper trade-off when not many options can be compared.

[4]http://www.dsi-it.de/en/product/authentication-and-en—decryption-unit,20.htm [Accessed on 20/06/2015]

Table 16.2: List of data flows and descriptions of types of data.

#	Source	Target	Type of data
1	OBC	Data Storage	Data to be stored
2	Data Storage	OBC	Stored data
3	GPS Receiver	OBC	Location and time
4	Star Tracker	OBC	Attitude
5	IMU	OBC	Accelerations and angular rates with respect to inertial space
6	Magnetometer	OBC	Magnitude and direction of local magnetic field
7	Reaction Wheels	OBC	Rotation speed
8	OBC	Reaction Wheels	Required rotation speed
9	OBC	Magnetorquers	
10	OBC	EPS	Required voltages to actuators and heaters
11	EPS	OBC	Voltages
12	OBC	Payload	Update of signal library, time signal
13	Payload	OBC	Geolocation result with metadata
14	OBC	Propulsion	Required firing duration
15	Propulsion	OBC	Propellant level
16	OBC	Encryption Unit	Data to be downlinked, time signal, telecommands acknowledgements
17	Decryption Unit	OBC	Decrypted, demodulated telecommands and incoming transmissions from other S/C
18	S-Band TX	Decryption Unit	Encrypted, demodulated telecommands
19	Encryption Unit	S-Band TX	Encrypted data to be downlinked, time signal, telecommands acknowledgements
20	Encryption Unit	UHF TRX	Encrypted data to be sent to other S/C
21	UHF TRX	Decryption Unit	Demodulated telecommands and incoming transmissions from other S/C
22	S-Band Transmitter	Ground Station	Encrypted, modulated downlink signal
23	Ground Station	UHF TRX	Encrypted, modulated telecommands
24	UHF TRX	Other S/C	Encrypted, modulated outgoing transmissions for other S/C
25	Other S/C	UHF TRX	Encrypted, modulated incoming transmissions from other S/C
26	OBC	Heaters	Required heating duration
27	Temperature Sensors	OBC	Temperature data

16.4 Results

This section gives the results of the design process for the C&DH subsystem.

16.4.1 Hardware Selection

At this point, the Integrated On-Board Computer[5] (iOBC) from SSBV [43] and the Satellite Computer Board (SCB) from DSI [44] are considered as options for the OBC. These two systems are both based on the Gaisler GR712RC processor. This processor uses LEON3-FT cores, which are capable of detecting and correcting SEUs. As discussed in Section 13.3, these upsets flip a bit of data and corrupt the data.
Both of these OBCs would be an appropriate choice, but the SSBV iOBC has been chosen, due to its larger internal data storage, as well as increased internal redundancies.

[5] http://www.ssbv.com/ProductDatasheets/page42/page30/index.html [Accessed on 19/06/2015]

16.4.2 Performance
The GR712RC provides a performance of 300 DMIPS at the maximum system frequency of 125 MHz. At this point it is not possible to give any figures on the performance of the encryption/decryption module required to encrypt and decrypt the data going in and out of the spacecraft.

16.4.3 Sensitivity
The iOBC has a fully redundant configuration, so failure of any of its components should not mean failure of the entire On-Board Computer.

16.4.4 Derived Requirements
This system imposes the following requirements on some of the other subsystems.

TTC-01 The TT&C subsystem shall demodulate the telecommands, and modulate the telemetry data.

17 | Attitude and Orbital Control Subsystem Design

This chapter contains the detailed design of the AOCS. Firstly, the requirements are derived by analysing the customer requirements, mission requirements, mission control modes, and requirements from other subsystems. Consequently, any models used in this chapter are described after which the design of the AOCS is performed. At the end, the final design of the AOCS is presented and any requirements/constraints it will put on any other subsystem are derived.

17.1 Requirements

In this section, the requirements for the AOCS are presented. Firstly, the attitude control modes are examined. The requirements derived from the identified attitude control modes can be found in Section A.9.2. The control modes are listed below:

Acquisition mode: during this control mode the initial determination of the attitude and the stabilisation of the vehicle just after separation from the launcher. Hereby it enables the spacecraft to communicate with the ground and generate power using its solar panels. In addition this mode is used to damp high rotation rates of the S/C, and to recover from power upsets or emergencies.

Orbit manoeuvre mode: the attitude of the spacecraft must be controlled during orbit manoeuvres, since large disturbance torques will probably be induced by the rocket motors during firing. This mode may drive the AOCS design to larger actuators, since motors for orbit manoeuvres can create large disturbances.

Normal mission mode: this mode is used for the vast majority of the mission and therefore drives the design of the AOCS. The attitude must be controlled to such an extent that the payload antennas are able to acquire the data for the mission. Pointing and stabilisation requirements defined by the payload drive the sizing for this AOCS mode.

Slew mode: it might be required during certain parts of the mission to reorient the attitude of the spacecraft. This could impose new requirements on the AOCS.

Safe mode: this mode is used when during emergencies a regular mode fails or is disabled. Generally, the AOCS can not utilise its components to their maximum extent, since less power is available. Through this mode the minimum power and thermal needs of the S/C are met.

In addition to the requirements derived from the attitude control modes, some general and design requirements for the AOCS are derived. These requirements concern aspects such as lifetime, redundancy, and autonomy. Furthermore, pointing requirements from different subsystems are derived. The (ELINT payload, TT&C, up-/downlink, and ISL) antennas require certain pointing accuracies. The power subsystem and orbit control system (propulsion) do as well. Concerning determination of the position of the satellites, a positioning requirement is derived. A list of the most significant requirements is given below:

AOC-02 The AOCS shall provide hardware and associated on-board software to acquire, control and measure the required spacecraft attitude during all phases of the mission.

AOC-09 The AOCS shall provide the required attitude determination and control during acquisition mode.

AOC-09-F01: Upon separation from the launcher interface the AOCS shall damp out the residual angular rates and acquire the Sun along a specific spacecraft axis before the batteries are depleted.

AOC-09-F02: After Sun acquisition, the AOCS shall provide stable 3-axis attitude control before and after solar array deployment and during the deployment of the antennas.

AOC-09-F03: The AOCS shall be able to reacquire Sun pointing attitude and realign solar arrays to the Sun from any initial orientation after initial Sun acquisition, solar array deployment and other acquisition mode activities.

AOC-10 The AOCS shall provide the required attitude determination and control during orbit insertion mode.

AOC-11 The AOCS shall provide the required attitude determination and control during normal mission mode.

AOC-11-F01: During normal mission mode, the AOCS shall be compliant with the pointing requirements specified in Section A.9.4.

AOC-11-F02: During normal mission mode, the absolute position knowledge error of the satellite shall not exceed 10 m.

AOC-12 The AOCS shall provide the required attitude determination and control during slew mode.

AOC-12-F01: The AOCS shall be capable of slewing the payload's line of sight, over 40° while above 80° latitude.

AOC-13 The AOCS shall provide the required attitude determination and control during safe mode.

AOC-13-F01: Spacecraft shall autonomously manoeuvre into a predefined safe mode on determination of an unsafe situation on-board. This autonomous functionality may be disabled by ground command during certain critical manoeuvres.

AOC-21 The absolute pointing error of the thrust vector during orbital manoeuvres shall be sufficiently small.

AOC-24 The absolute pointing error of the X-band antenna during ELINT gathering shall not exceed 1° half cone angle.

AOC-25 The absolute pointing error of the L- and S-band antenna during ELINT gathering shall not exceed 1° half cone angle.

AOC-26 The absolute pointing error of the S-band antenna during downlink communications shall not exceed 60° half cone angle.

AOC-27 The absolute pointing error of the L-band antenna during GPS jammer detection and localisation shall not exceed 1° half cone angle.

AOC-28 The absolute pointing error of the UHF-band antenna during uplink and inter-satellite communications shall not exceed 90° half cone angle.

AOC-29 The absolute pointing knowledge error of the L- and S-band antenna during ELINT gathering shall not exceed 0.04° half cone angle.

AOC-30 The AOCS will provide stability and momentum control for orbit maintenance during 720 s per orbit.

AOC-31 The GPS will provide the velocity with an accuracy of 0.57 m s^{-1}

AOC-32 The GPS will provide the time with an accuracy better than 38 μs.

The complete set of requirements for the AOCS can be found in Section A.9.

17.2 Model

In order to size the AOCS system the internal and external disturbance torques were estimated. To allow for iterations, the calculations were programmed in MATLAB. The equations used in the model were taken from Space Mission Analysis and Design (SMAD) [15]. Before explaining them it is necessary to state the additional assumptions and conventions that were adopted to develop the model for the disturbance torques:

- **Reference frame:** The model uses a body fixed reference frame with the z-axis pointing zenith. The satellite will thus always have the same orientation with respect to the local horizontal. This is convenient as the payload needs to be nadir pointing at all times. Its in orbit position will be specified in 2D using polar coordinates as can be seen in Figure 17.1.
- **Eclipse duration:** The eclipse period was calculated using the Earth Cylindrical Shadow Model [45]. It was assumed that the penumbra period in LEO is negligible in duration.
- **Solar array orientation:** It is assumed that during eclipse the solar panels will be rotated into the xy-plane to minimise aerodynamic drag. It is assumed that in this configuration the solar arrays generate no drag. It is assumed that at any other time the solar panels will be oriented perpendicular to the Sun by means of rotating them around their longitudinal axis combined with yawing the S/C (See Figure 17.1).
- **Spherical Earth:** The Earth is assumed to be a sphere so that its gravity field is uniform over an orbit.

- **Symmetric magnetic field:** The magnetic field is assumed to be symmetric around the rotation axis of the Earth. Furthermore for simplicity the magnetic and true north are assumed to coincide. Besides that it is assumed that the magnetic latitude λ, which ranges between 1 at the equator and 2 at the poles, can be represented by an average of 1.5.
- **S/C model:** The S/C is assumed to have a cuboid bus (0.9 m x 0.7 m x 0.55 m in x-, y-, and z-direction) with an homogeneous mass of 136.7 kg. 16.1 kg is divided over the two solar arrays that are located at 2.5 cm above the centroid of the sides of the spacecraft. They are 0.61 m x 2.98 m with the longitudinal axis along the y-axis. For the moment the connecting boom is neglected. The thruster is located at the centroid of the aft panel. Besides that two 4.6 kg booms with antennas are located at 5 cm before the centroid of the nadir side forming a 'V' shape with an inner angle of 90°.

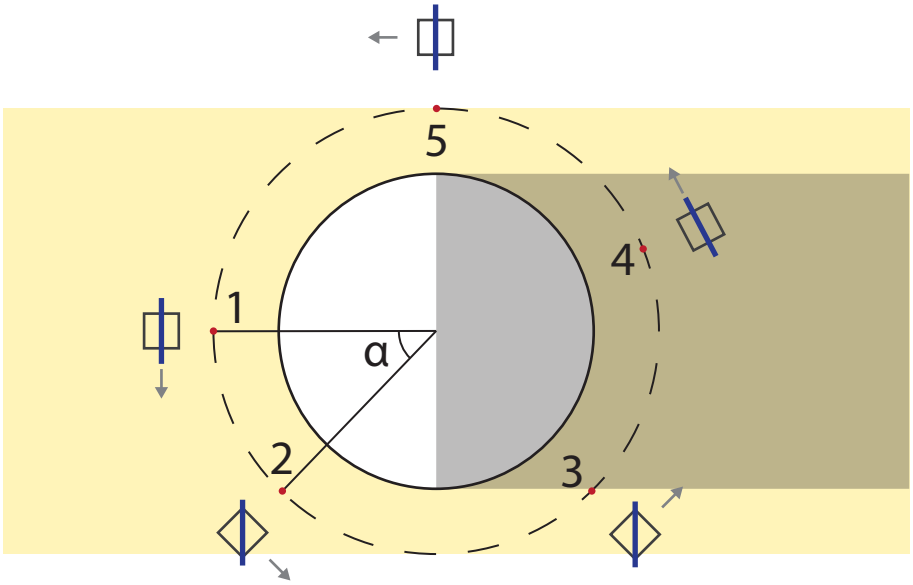

Figure 17.1: Graphical representation of the orbit considered in calculating the torques and momentum acting on the spacecraft. Besides that the figure shows the orientation of the solar arrays at various positions in the orbit.

It is assumed that the deviation in disturbance torques between the polar and real orbit are small, and that the estimate obtained is conservative. The polar orbit presented in Figure 17.1 was chosen because it presents the worst case scenario for the orbiting S/C. During a polar orbit the highest magnetic disturbance torque will be experienced, giving a conservative estimate for orbits with lower inclination. The estimate is conservative for aerodynamic and solar radiation pressure torques as well. The orbit shown in the figure will give the maximum values for both the area exposed to the free stream air and to sunlight. Other orbits, varying in inclination or longitude of ascending node will experience lower torques, as the combination of rotating the solar arrays and yawing the S/C, required for solar array pointing, will decrease the exposed area for both torques. The external disturbance torques are given by Equations 17.1−17.4.

$$T_a = \frac{1}{2}\rho C_D A_r V^2 (cp_a - cm) \tag{17.1}$$

$$T_s = \frac{\Phi}{c} A_s (1+q)(cp_s - cm)\cos\phi \tag{17.2}$$

$$T_m = DB = D\left(\frac{M}{R^3}\lambda\right) \tag{17.3}$$

$$T_{g,x} = \frac{3\mu}{2R}\left|I_z - I_y\right|\sin 2\theta \tag{17.4}$$

Where T_a, T_s, T_m and T_g are the aerodynamic, solar radiation pressure, magnetic, and gravity gradient disturbance torques, respectively. ρ is the atmospheric density while C_D represents the drag coefficient of the S/C. A_r and A_s represent the frontal and sunlit area, respectively. V is the orbital velocity and cp_a and cp_s are the centres of aerodynamic and solar radiation pressure. The centre of mass is denoted by cm. The solar radiation pressure torque depends on

Φ, the solar radiation flux, c, the speed of light, q, the reflectivity of the S/C, and ϕ, the incidence angle of the Sun. The factor D in Equation 17.3 represents the residual magnetic dipole of the S/C while B represents the strength of the magnetic field, which can be split up in M, the magnetic field strength of the Earth, R, the orbital radius, and λ, the magnetic latitude. Finally the gravity gradient torque depends on μ, the gravitational constant of the Earth, I, the mass moment of inertia, and θ, the angle between the local vertical and the principle axis of the S/C. To obtain T_g around other axes, the subscripts should be changed.
To find values such as the torques due to thruster misalignment and the slew time, standard dynamics was applied.

Finding I, cm, A_r, A_s, cp_a, and cp_s
To find some of the S/C characteristics, a simplified model of the S/C was developed. All parts of the spacecraft were modelled as cuboids or cylinders with a homogeneous mass distribution. Only the antenna booms were modelled as a distribution of point masses. I was found by adding all the individual contributions of the modelled parts. cm was found using the average of the positions of the subsystems weighed with respect to their respective masses. A_r and A_s were determined by calculating the exposed area at multiple instances in the orbit. Then the values for cp_a and cp_s were determined averaging positions of the areas exposed to the free stream velocity or sunlight taking into account a weighing function related to the magnitude of their exposed areas. The momentum accumulation calculations utilised a discrete simulation of the orbit and at each step a new value for cp_a and cp_s was calculated.

Finding the Momentum Accumulation in Body Axis Components
To size the actuators it is important to know the total momentum generated over an orbit with respect to the body axes system. The solar radiation pressure torque has a cyclic behaviour as the S/C will first move towards, and then away from the Sun. The more symmetric the S/C is, the more cyclic the solar radiation pressure torque will be. The aerodynamic torque is easily modelled, as the drag will always be pointed towards the negative x-direction. However as the cp_a varies position, the momentum change may reverse sign, giving a more complex accumulation pattern. The magnetic torque will alternately act on different axes of the S/C, but it will cover all of them in an entire orbit because the selected orbit is highly inclined. As modelling the magnetic field is beyond the scope of this report, the average magnetic torque over a quarter orbit is added to all axes to obtain the total momentum around all axes. The same is done for the gravity gradient torque. Finally, the thruster torques act around all axes. The direction of its contributions can be found by considering the position of the thruster and decomposing the thrust force along the vector describing the alignment error.

17.3 Design
This section presents the estimates of the torques as found by applying the models and equations presented in the previous section.

Table 17.1 shows the inputs that were used to estimate the disturbance torques. The left column shows the inputs that were determined from the chosen design solutions. R, V and ρ were determined by the orbit chosen in Chapter 12 while F_{th} and t_{burn} were determined by the propulsion system in Chapter 18. The other values were calculated by the program. Naturally inputs like the solar array area and the system layout had to be known as well. The variables showing three separate numbers, show the values defined with respect to the x-, y-, and z-axis, respectively.

Table 17.1: Inputs to the disturbance torque estimation model.

Variable						**Variable**		
R			$6.878 \cdot 10^9$	m		M	$7.96 \cdot 10^{15}$	T m^3
V			$7.613 \cdot 10^3$	m s^{-1}		Φ	$1.366 \cdot 10^3$	W m^{-2}
ρ			$6.15 \cdot 10^{-13}$	kg m^{-3}		c	$3.0 \cdot 10^8$	m s^{-1}
F_{th}			$5 \cdot 10^{-3}$	N		μ	$3.986 \cdot 10^{14}$	m^3 s^{-2}
t_{burn}			720	s		λ	1-2	–
cm	0.05	0.0	0.26	m		C_D	4.0	–
I	80.7	20.5	92.6	kg m^2		D	1	A m^2
cp_a	0.05	0.0	0.30	m		q	0.6	–
cp_s	0.02	0.0	0.33	m		θ	0.35	rad
c_{th}	-0.45	0.0	0.28	m		ϵ_{err}	0.01	rad
A_r			0.39 – 4.02	m^2		ω_{res}	0.026	rad s^{-1}
A_s			0 – 4.37	m^2				

The right hand side of the table shows the values that have been taken from SMAD [15]. The values are either given as estimates, or chosen from an range of possible values that best corresponds to a smallsat. M, Φ, c, μ and λ are constants. The value for C_D corresponds to a spacecraft with a cuboid shape, which is a reasonable approximation for the S/C bus and the solar arrays. The value for D corresponds to small, uncompensated S/C. By using a carefully designed wire harness and by operating magnetorquers this value can be influenced. The value for q is an estimate for S/C that do not feature large reflective surfaces like solar sails. θ is based on the maximum off nadir pointing angle that is required for the operation of the antennas. ϵ_{err} is based on typical values. Finally, ω_{res} has been taken from the Vega launcher manual [46].
In Table 17.2 the outputs of the model are listed. It can be clearly seen that the magnetic torques are the dominant torques, followed by the thruster torques. Note that the momentum H shown in the table results from integrating the disturbance torques over an entire orbit, except for the H_m, as the maximum momentum due to the magnetic torque will accumulate in a quarter orbit. The three values shown for the momentum corresponds to the momentum around the x-, y-, and z-axis, respectively. It is important to realise that T_{cont}, the control torque required for attitude control, is the sum off all absolute torque contributions multiplied with a safety factor of 1.15. The total momentum is determined slightly less straightforward. H_a and H_s have clearly defined orientations, however the other momentum contributions might have an opposite orientation. The total momentum is thus found by adding up H_a, and H_s followed by adding and subtracting the other contributions in such a way as to find the largest possible momentum accumulation. The values shown for H_{tot} are absolute values. The last value that is shown corresponds to the momentum due to the angular velocity after orbit insertion.

Table 17.2: Outputs of the disturbance torque estimation model.

Variable				**Variable** [x, y, z]				
T_a	$10.2 \cdot 10^{-6}$	N m		H_a	0.0	-0.027	0.0	N m s
T_s	$2.0 \cdot 10^{-6}$	N m		H_s	0.0	-0.002	0.0	N m s
T_m	$48.9 \cdot 10^{-6}$	N m		H_m	0.050	0.050	0.050	N m s
T_g	$85.4 \cdot 10^{-6}$	N m		H_g	0.485	0.080	0.405	N m s
T_{th}	$93.2 \cdot 10^{-6}$	N m		H_{th}	-0.001	0.067	-0.020	N m s
T_{cont}	$275.7 \cdot 10^{-6}$	N m		H_{tot}	0.537	0.227	0.477	N m s
t_{slew}	154	s		H_{res}	2.11	0.54	2.42	N m s

The following part of this section addresses the proposed solution for the AOCS subsystem. Table 17.3 gives an overview of the selected sensors and actuators.

Table 17.3: Overview of the selected hardware for the AOCS subsystem.

Sensors	**Quantity**	**Mass**	**Power**	**Specifications**	**Type**
GPS Antenna	2	0.05 kg	–	Position accuracy 10 m	SGR-10[1]
GPS Receiver	1	0.95 kg	5.5 W		
Magnetometer	3	0.06 kg	0.3 W	Attitude accuracy 1°	FGM-A-75[2]
IMU	2	0.055 kg	1.5 W	Random drift <0.15° min^{-1}	STIM300[3] [4]
Star Tracker OH	3	1.41 kg	1.0 W	Attitude accuracy 0.004°	Hydra CMOS Star Tracker[5]
Star Tracker EU	2	1.9 kg	9.8 W		
Actuators	**Quantity**	**Mass**	**Power**	**Specifications**	
Magnetorquers	3	0.35 kg	1.0 W	Dipole moment 10 A m^2	SMTR-R010 [47]
Reaction Wheels	4	0.96 kg	2.8 W ([6])	Momentum storage 0.42 N m s Maximum torque 11 mN	10SP-M[7]

The entire AOCS system is redundant, either by internal redundancy or by taking redundant parts. With these sensors and actuators, all AOCS modes can be constructed.

[1] http://www.sstl.co.uk/getattachment/cda26002-f017-4d5a-9920-2174e9c8c907/SGR-10-Space-GPS-Receiver [Accessed on 18/06/2015]
[2] http://www.zarm-technik.de/downloadfiles/ZARMTechnikAG_Magnetomers_web2010.pdf [Accessed on 18/06/2015]
[3] http://www.sensonor.com/media/99614/ts1524.r19%20datasheet%20stim300.pdf [Accessed on 18/06/2015]
[4] http://www.sensonor.com/media/84604/2014-11-12-product-brief-stim300-a4-web.pdf [Accessed on 18/06/2015]
[5] http://www.sodern.com/sites/docs_wsw/RUB_51/2015_SODERN_HYDRA.pdf [Accessed on 18/06/2015]
[6] Power at maximum torque is 10 W
[7] http://www.sstl.co.uk/getattachment/f31aaa67-3750-4a8a-9742-c1cd800c0a5b/Microwheels-Reaction-Wheel [Accessed on 18/06/2015]

Nominal Mode
The payload requires an pointing knowledge of 0.04°. This is the most stringent requirement of all pointing requirements, and therefore leading in the design. This requirement drives the nominal mode to a design utilising star trackers, and an Inertial Measurement Unit (IMU). As the S/C needs to be able to be oriented towards the control area at any time, reaction wheels need to be used. As a rule of thumb, the attitude determination accuracy can than be one tenth of the pointing knowledge, so 0.4°. The use of reaction wheels requires momentum dumping, which is done by using magnetorquers in order to reduce propellant mass. To optimise the control over the magnetorquers, magnetometers are used in this mode as well. The position knowledge, which should be better than 10 m is provided by a GPS receiver, as this is the lightest solution giving the required accuracy. Besides that the GPS receiver also provides the required velocity and time knowledge.

Acquisition Mode
The main goal of the acquisition mode is to damp the residual angular momentum in order to allow the spacecraft systems to start before the batteries are depleted. As the absolute attitude is not important, only the angular rates are, the sensors are lightweight magnetometers. The magnetorquers will be used as actuators. The advantage of this method is the simple control loop that is required. This acquisition principle is known as the B-dot method [48]. After stabilisation the pointing requirements for downlink becomes leading.

Safe Mode
In safe mode, accurate pointing is not required. The main requirement is low power usage. Consequently this mode will use a combination of magnetometers and magnetorquers, linked by a simple algorithm. During this phase the downlink requirement is leading.

Manoeuvre Mode
In manoeuvre mode strict requirements regarding the pointing apply to make sure that the thrust is directed in the desired direction. As a consequence, the manoeuvre mode uses the same sensors and actuators as the nominal mode, only the control laws might differ. The leading requirement is the pointing accuracy of the thruster.

Slew Mode
In this mode the slew requirement is most important. The S/C needs to slew 40° wile above 80° latitude. The allowed slew time corresponds to the time required to traverse 20° in orbit, which is approximately 315 seconds.

17.4 Results

This section discusses the performance and sensitivity of the AOCS subsystem.

Performance
Using the AOCS hardware as proposed in the previous section, the following conclusions can be drawn:

- The required control torque is 0.3 mN, but the reaction wheel torque authority is 11 mN. So the AOCS performs better than required.
- The momentum accumulation per orbit is maximal 0.54 N m s. The reaction wheels provide 0.46 N m s so the magnetorquers have to be operated during each orbit. Dumping 0.54 N m s requires approximately 2190 seconds of magnetorquer operations, at the worst case of a magnetic latitude of 1. This translates to a magnetorquer duty-cycle of 40%. So the AOCS performs adequate.
- The residual momentum after orbit insertion is maximal 2.4 N m s. The minimum operating time required to dump the momentum per axis using magnetorquers is 8480, 1940, 9620 seconds for x, y, and z, respectively. With a power consumption of 1.2 W per magnetorquer and a power consumption of 0.3 W for the magnetometers that would require approximately 31.000 J. With a battery capacity of 670 W h this will not be a problem, even when computing power for running the algorithm is included.
- The available slew time is 315 s. Using the 11 mN control torque the slew time is maximal 151 s. The AOCS performs good.
- The required pointing knowledge was 0.04° or 144 arcsec. The star trackers have an accuracy of 15 arcsec (0.004°) and thus perform much better than required.

- The pointing accuracy during nominal mission conditions should be better than 1°. According to the rule of thumb, a pointing knowledge of 0.004° will lead to a pointing accuracy of 0.04°, which is better than required. During safe mode and acquisition less stringent pointing requirements exist. Using for example the B-dot algorithm a pointing accuracy better than 5° is feasible [48]. This will be sufficient to allow up- and downlink communications.
- The payload needs to know its position up to 10 m, its velocity up to 0.57 m s^{-1}, and the time up to 38 μs. The GPS receiver provides 10 m positioning accuracy, 0.15 m s^{-1} velocity knowledge and a time accuracy of 0.5 μs.

Most of the other requirements deal with software. At this stage the compliance of the AOCS with these requirements cannot be checked, but based on technical credibility and flight heritage of other satellites it is believed to be possible.

Sensitivity
The AOCS subsystem performance is influenced to a large extend by only a few parameters. The location of cp_a, cp_s and cm linearly influence the torque and momentum. Another important parameter is R, it influences the aerodynamic torque and momentum via the atmospheric density and orbital velocity. It influences the solar radiation pressure momentum via the eclipse time. The magnetic field strength and the gravity gradient strength depend on R via an inverse cubic and inverse linear relation, respectively. All other parameters linearly increase or decrease the torques and corresponding momentum. A more detailed analysis of the sensitivity of the AOCS can be found in the MTR [5]. It should be noted that if the torques increase a little more, larger actuators will be required, increasing the mass as COTS magnetorquers and reaction wheels only come at certain discrete performance levels. However, the star tracker accuracy can be lowered, allowing a lighter solution to be used if necessary.

18 | Propulsion Subsystem Design

In this chapter the propulsion subsystem is detailed. First its requirements and tasks are determined. Then a required ΔV budget is calculated, from which a propulsion system is selected. Finally a hardware sizing for the components of the subsystem is performed.

18.1 Requirements

For the propulsion subsystem sizing and selection process a number of requirements was identified. These requirements are listed in Appendix A.10. There is one top level requirement related to the propulsion:

ORB-02 The orbit shall be maintained during the lifetime of the S/C.

Requirements **PRO-01**, **PRO-02** and **PRO-03** all directly follow from this orbit requirement and the need for a satellite constellation. Requirements **PRO-05, PRO-06, PRO-08** and **PRO-11** all follow from the impact the propulsion subsystem may have on other subsystems. Requirement **PRO-07** is related to propellant storage, and requirement **PRO-12** is for de-orbiting.

PRO-01 The propulsion subsystem shall provide the capability to maintain orbit at an altitude of 500 km.

PRO-02 The propulsion subsystem shall be able to correct any errors in orbit injection.

PRO-03 The propulsion subsystem shall be able to perform its tasks for the duration of the mission and the in orbit commissioning.

PRO-03-F01: There shall be enough propellant to perform the mission for the duration of the mission and the in orbit commissioning.

PRO-03-F02: The components used in the propulsion subsystem shall have a lifetime of the duration of the mission and the in orbit commissioning.

PRO-05 The thruster(s) shall cause no electrical interference with other subsystems.

PRO-07 The propellant tank shall be sized large enough to allow for a 20% increase in volume of the propellant.

PRO-08 The thruster and propellant tank placement shall take into consideration the structural parameters of the spacecraft.

PRO-12 The propulsion subsystem shall provide the capability to actively de-orbit the S/C at EOL.

18.2 Model

For the selection and sizing of the propulsion subsystem a number of parameters had to be found in literature or calculated. The most important of these is the required ΔV budget, which is the required velocity change the propulsion subsystem needs to provide over the duration of the mission. This required ΔV budget can be divided in three parts: the ΔV required for orbit keeping, the ΔV required for de-orbiting and the ΔV required for correcting any possible errors in orbit injection. It is assumed that the orbit remains circular for the entire duration of the mission.

Orbit keeping, which is what the propulsion system will do for the majority of the mission lifetime, is needed because the orbit of the S/C decays over time. The major cause of this orbital decay is atmospheric drag, which gives a force opposite to the velocity vector of the S/C. The acceleration due to this drag is given by Equation 18.1.

$$a_D = -\frac{\rho C_D A_r V^2}{2m} \tag{18.1}$$

Where a_D is the acceleration, C_D the drag coefficient of the S/C, A_r the area of the S/C that is perpendicular to the velocity vector, m the S/C mass, V the orbital velocity, and ρ the atmospheric density. Integrating these accelerations over a year gives the required ΔV budget for a year. At an altitude of 500 km, the atmospheric density is $1.40 \cdot 10^{-13}$ kg m^{-3}, $6.15 \cdot 10^{-13}$ kg m^{-3} and $2.03 \cdot 10^{-12}$ kg m^{-3} for solar minimum, mean and maximum conditions respectively. The orbital velocity is 7613 m s^{-1} and $\frac{C_D A_r}{m}$ is assumed to be 20 for average mission conditions. Further information on how the densities and S/C parameters were found can be looked up in the MTR [5].

At an altitude of 500 km, ΔV requirements to counter aerodynamic drag, for average drag and mission conditions are listed in Table 18.1. For a mission duration of five years, and an in-orbit commissioning it is assumed that in a worst case scenario a S/C will experience one year of solar minimum conditions, three years of solar mean and two years of solar maximum.. Adding a safety factor of 1.2 for unexpected events in the solar activity and other unexpected manoeuvres gives a total ΔV requirement for orbit maintenance of 276.38 m s^{-}1 for the mission lifetime.

The ΔV required for active de-orbiting from a starting altitude of 500 km was found in SMAD to be 143.3 m s^{-1} [15]. The ΔV needed for correcting possible errors during orbit injection can vary a lot, but in a worst case scenario there is a 0.2 °error in the RAAN according to the Vega manual [46]. The effect of this difference in RAAN is calculated by Equation 18.2 [20]. Both of these ΔV values are listed in Table 18.1.

$$\frac{\Delta V}{V} = 2\sin(i)\sin\left(\frac{\Delta\Omega}{2}\right) \tag{18.2}$$

In which V is the orbital velocity, i is the inclination and $\Delta\Omega$ is the required change in RAAN. For a worst case scenario, a polar orbit with an inclination of 90° and an orbital velocity of 7613 m s^{-1}, a difference in RAAN of 0.2° requires 26.57 m s^{-1} of ΔV.

Table 18.1: ΔV required for different tasks during the mission.

Task	**ΔV**
Orbit keeping solar minimum (one year)	6.40 m s^{-1}
Orbit keeping solar mean (three years)	28.12 m s^{-1}
Orbit keeping solar max (two years)	92.81 m s^{-1}
Orbit keeping total	331.66 m s^{-1}
De-orbit	143.30 m s^{-1}
Correction of errors in orbital injection	26.57 m s^{-1}
Total	501.53 m s^{-1}

18.3 Design

With the total ΔV budget known, it is possible to do a hardware selection. In the MTR, after a preliminary trade-off, a number of types of propulsion systems were found to be feasible for this mission. These included monopropellant, bipropellant, electric and cold gas thruster systems. A number of COTS thrusters for each of these types were found, and their specifications were researched. The most important properties that were assessed for each of these systems were the required propellant mass, the mass of the rest of the system and the required electrical power.

The rest of the system mass mainly consists of tank, feed system, and thruster mass. For electrical systems the Power Processing Unit (PPU) mass belongs to the subsystems as well. The tank mass scales with propellant mass while the feed system mass is assumed to be approximately equal for most systems except for cold gas. The thruster mass is higher for electrical systems and the PPU is only present in electrical systems. The required power is very low for cold gas and chemical thrusters, in the order of 25 W, while it varies a lot for electric thrusters, between 50 W and 20 kW, for 1 mN to 1 N of thrust, respectively.

After looking at these three properties for a number of COTS propulsion systems it was found that an electrical thruster would best suit the mission, because of the low required propellant mass. The Astrium RIT 10 EVO ion thruster[1] system was selected, because of its low power requirement. Other relevant specifications of this system are listed in Table 18.2.
Another important property of the thruster is the exhaust velocity, which is the product of the specific impulse and g_0, for this thruster its value is 18639 m s^{-1}. With the thruster system known, the rest of the propulsion system can be sized. The main components of an electric propulsion system are besides the thruster, the propellant tank, the PPU and the feed system.

The propellant tank size is dictated by the density of the fuel used, the pressure under which it is stored and the amount of fuel it needs to store. To calculate the required propellant mass, the total preliminary S/C budgeted mass of 162 kg was used. For this the Tsiolkovsky rocket equation was used, which is show in Equation 18.3 [15].

[1] http://cs.astrium.eads.net/sp/spacecraft-propulsion/ion-propulsion/ [12/06/2015]

Table 18.2: Specifications of Astrium RIT 10 EVO ion thruster.

Property	
Propellant	Xenon
Nominal thrust	5 mN
Nominal power	145 W
Specific impulse	>1900 s
Divergence angle	<15°
Mass	1.8 kg
Size	186 mm x 186 mm x 134 mm

$$\Delta V = v_e \ln(\frac{m_0}{m_1}) \tag{18.3}$$

In which v_e is the exhaust velocity and $\frac{m_0}{m_1}$ is the fraction of the begin mass to the end mass of the S/C. Since the difference between the begin mass and the end mass equals the mass of the propellant, the total required propellant mass for a given amount of ΔV can be calculated using this formula. For a begin mass of 162 kg, an exhaust velocity of 18639 and a required ΔV of 501.33 m s^{-1} the required propellant mass is 4.31. Adding a safety factor of 1.25, to account for possible suboptimal performance of the thruster or other components of the propulsion subsystem, makes the total propellant mass 5.39 kg.

The optimum storage density is 1350 kg m^{-2} at a pressure of 8.3 MPa [49]. Under these conditions 5.39 kg of xenon will have a volume of 0.0040 m^3, which equals 1.8 litres. With a safety factor of 1.2 to account for any unexpected expansion of the gas this brings the total tank volume to 0.0048 m^3. A propellant tank mass estimation is given by Equation 18.4.

$$\frac{m_t}{m_p} = \frac{3p\beta\rho_t}{2\sigma_y\rho_p} \tag{18.4}$$

Where m_t/m_p is the ratio of tank to propellant mass, p is the pressure of the fuel in the tank, β the safety factor, σ_y the yield strength of the material and ρ_t and ρ_p are the densities of the tank material and the propellant respectively. For an aluminium tank with a material density of 2840 kgm^{-3}, a material yield strength of $463{\cdot}10^6$ Nm^{-2} [50] and a safety factor of 2 the tank mass fraction is 0.113. This ratio gives a total tank mass of 0.61 kg. It should be noted that a heater required to keep the propellant above 17°C, which is a supercritical condition for xenon. By comparison to a reference tank, a 15 W heater was selected [2].

The mass of the PPU was estimated using a sizing method from SMAD [15]. Its mass was estimated to be 6-10 kg per kW. This yields a PPU mass of 1.61 kg. Assuming a PPU efficiency of 90%, a 161 W input power is required. There is no clear relation between input power and system volume, so it is assumed to have double the size of a PPU system with half the mass [3]. According to this calculation its size will be 0.0014 m^3.

A propellant feed system usually weighs 5 kg to 10 kg [15]. Since the mass flow of this propulsion system is not very high, the feed system is assumed to be relatively small and lightweight, for this reason a low mass estimate of 5 kg was made. A size estimation can be made by looking at comparable feed systems[4]. The size was found to be 440 mm x 280 mm x 230 mm or 0.0283 m^3. The temperature in this component also needs to be controlled when the propellant is flowing, it is assumed that a 15 W heater like the one on the propellant tank is enough to do this. Other electric systems like pumps are not necessary since the pressure in the propellant tank is very high.

18.4 Results

The final results from the propulsion system sizing process are presented in Table 18.3. The total value in the case of the size and the power is not a sum of the other values in this table, because the propellant volume is contained within the tank, and the power used by the thruster is an output of the PPU.

[2] http://www.sstl.co.uk/getattachment/205cfce6-9b54-42bf-9141-5738e7e015ad/Xenon-Propulsion-System [Accessed on 14/06/2015]
[3] http://www.terma.com/media/177716/propulsion_power_distribution_module.pdf [Accessed on 14/06/2015]
[4] http://cs.astrium.eads.net/sp/spacecraft-propulsion/valves/pressure-regulators.html [Accessed on 14/06/2015]

Table 18.3: Properties of propulsion system components.

Component	Mass	Volume	Power
Thruster	1.80 kg	0.0046 m^3	145 W
PPU	1.61 kg	0.0014 m^3	161 W
Feed system	5.00 kg	0.0283 m^3	15 W
Propellant	5.39 kg	0.0040 m^3	0 W
Propellant tank	0.61 kg	0.0048 m^3	15 W
Total	14.41 kg	0.0391 m^3	191 W

Performance

The selected propulsion subsystem is capable of providing a thrust of 5 mN, at a specific impulse of 1900 s, with a power consumption of 161 W for the thruster. An additional 30 W is required for the thermal systems of which 15 W only needs needs to be used when the thruster is switched on. To save the total load on the power system the propulsion is only used over the poles, when the payload can be turned off temporarily. To provide enough ΔV per day it needs to operate for 720 s per orbit. The thrust force is very low, so the vibrations this induces in the S/C are also very low. The electrical interference the thruster could cause is concentrated in the divergence angle of 15 ° behind the thruster, when nothing is placed within this area minimal electrical interference with other subsystems will occur.

Sensitivity

There are some unexpected events that could happen to the S/C that may have an influence on the propulsion subsystem. These are listed below, along with ways in which their effects might be mitigated.

Firstly there may be an error in the orbital injection, as stated above there is enough propellant to make sure the mission is not jeopardised by any such error, provided this error is within the bounds given by the Vega launch manual [46]. If there is a larger error in the orbit injection, then depending on the ΔV needed it could affect the mission in a number of ways. Another reason which could change the amount of ΔV required is an unexpected increase in solar activity, which would increase the drag of the S/C.

There is a safety factor applied to the propellant mass to account for unexpected events such as these. If even more ΔV is needed than was accounted for in this safety factor, then the propellant reserved for the de-orbit may be used and a partly or fully uncontrolled de-orbit may be done at EOL instead. If the error is so large that even this amount of propellant does not suffice to correct the error, propellant reserved for the final years of the mission may be used. However this implies that the mission will last shorter. If in any case the amount of ΔV is less than accounted for, then more propellant must be dumped at the EOL operations.

19 | Structure Design

The different subsystems of the S/C are designed independently and are unified into a system inside the S/C bus. This integration process is the matter of Chapter 22. The physical merging of the various subsystems is done by the S/C structure. The structure of the S/C must comply with launcher requirements for fundamental frequencies and sustain the loads induced by the launcher. Secondary considerations are loads during ground handling and accessibility of instruments during assembly and testing.

19.1 Requirements

Requirements to meet the basic functionality of a spacecraft body structure are listed below. Requirements that are driven by the launcher are specific to the Vega launch vehicle.

STR-01 The S/C fundamental frequencies shall be different from those of the launcher.

STR-02 The S/C shall have a fundamental frequency in longitudinal direction between 20 Hz and 45 Hz or more than 60 Hz.

STR-03 The S/C shall have a fundamental frequency in lateral direction greater than 15 Hz.

STR-04 The structure of the S/C shall be capable of withstanding the loads induced by the launcher during launch.

STR-05 The S/C structure shall be capable of withstanding the loads induced during ground handling before launch.

STR-06 The S/C structure shall be capable of withstanding loads encountered during in orbit operation.

STR-07 The S/C structure shall not hinder access of ground support equipment to on-board instruments.

STR-08 All component connection contact areas shall be made of three types of material with thermal conductivities of 0.25, 55 and 105.5 $W\,m^{-1}\,K^{-1}$.

STR-09 The S/C structure shall have a thermal conductivity of at most 105.5 $W\,m^{-1}\,K^{-1}$

19.2 Structural and Vibration Analysis

The design of the S/C structure is driven by three primary considerations listed below. The requirements for these factors are formulated independently, but the most stringent ones shall define the design space. Stiffness is the most important parameter, as it governs both the stresses due to quasi-static and loading, but also the frequency response of the spacecraft.

- Mechanical loads
- Vibrational analysis
- Deformation and deflection of the structure during launch and operations

The antenna array is constrained by stringent accuracy requirements for the angle of arrival measurements. The performance of the array is greatly affected by misalignment of the elements. The array must be fastened to the S/C bus with high accuracy to prevent errors in the AOA computation.

The structural design of the of the S/C is done to a first order. Compliance with the highest load cases is performed for a simple model of the S/C. Vibrational analysis of the S/C is also limited to an eigenfrequency analysis to size the brackets to the payload adaptor.

19.2.1 Mechanical Loads

The structure is the backbone of the S/C. The loads encountered during launch are well described in the user manual of the Vega launcher [46]. The highest load during launch is 5g in compression. This is due to the acceleration during the launch. The S/C must endure a load equal to five times its own weight. The subsystems of the S/C should be designed to withstand this loading. The main structure provides a load path to the payload adaptor.

The backbone of the S/C is either a truss structure or a series of sandwich panels and rings. Such designs are usually chosen for larger S/C. Panels have a larger surface than a truss-structure that is suitable for mounting components.

For the conceptual design the primary structure of the S/C is modelled as a mass-less plate. The mass of the S/C is assumed to be centred at the geometric centre of the S/C bus. During launch the point-mass induces a moment on the primary structure. This load case is more critical than a distributed load and can be regarded as a good first order sizing method.

The moment generated by the mass lumped in one point at the centre of mass (COM) is given in Equation 19.1. This moment is modelled as a free moment that is bending the beam.

$$M_{cm} = mdg_0 g \tag{19.1}$$

In Equation 19.1 m is the mass of the S/C, d is the distance of the COM to the plate, g is the load factor induced by the launch and g_0 is the gravitational acceleration on Earth. The moment M_{cm} results in a stress in the panel. This stress is given by Equation 19.2 for a sandwich panel [51].

$$\sigma_p = \frac{M_{cm}}{h_c f t_f} \tag{19.2}$$

Where σ_p is the stress in the panel, h_c the height of the sandwich panel core and t_f the combined thickness of the face sheets of the panel. The stress inside the panel should not exceed the yield stress of the panel. Attention should be given to the size of the internal honeycomb structure to prevent inter-cell buckling of the face sheet. In the event that the thicknesses of the face sheets and the core are driven by stiffness requirements for the vibrational behaviour, the main panel will be over-designed.

19.2.2 Vibrational Analysis

The eigenfrequency or fundamental frequency of the S/C should not match that of the launcher. For any design, the frequency of the structure is a function of the stiffness, mass and dimensions of the S/C. As an initial estimate the fundamental frequencies of the S/C are made assuming a concentrated mass on the main panel. The fundamental frequencies are effected by the fasteners to the payload adaptor of the launcher. At this stage of the design the main panel can be sized with relative ease to tailor the first fundamental frequencies of the S/C. The antenna booms are slender and relatively long and can be affected by vibration easily. Slender structures show relatively large deflection, so dynamic coupling with the launcher should be avoided.

The vibrational analysis is performed by assuming a non-damped free vibration of finite point masses attached with springs. The equation of motion of a multiple degree of freedom system is given in Equation 19.3.

$$M\ddot{\mathbf{x}} + K\mathbf{x} = 0 \tag{19.3}$$

The degrees of freedom, or axes at which the masses can move are listed in the column vector $\ddot{\mathbf{x}}$ in Equation 19.3. The mass and stiffness are filled in the M and K matrices respectively. The system of equations in Equation 19.3 can be solved to compute the fundamental frequencies of the system. Using the symbolic solver Maple, the fundamental frequencies can be computed parametrically for the m's and k's. The parameters can be changed easily to tailor the fundamental frequencies to meet the launcher requirements.

19.2.3 Deformation and Deflection Analysis

At this stage of the design, the fasteners and joints are not designed yet, making an analysis of the deflections not possible. Therefore deformations and deflections are not analysed, but only mentioned. The antenna array is delicate and shall be restrained at the end to prevent damage. This makes any potential deflection less critical.

19.3 Spacecraft Main Structure Design

The size and weight of the S/C are relatively small and the S/C does not require a large internal surface area to mount components, while a full strut design requires many cross members. The cross members are required to attain sufficient rigidity is all directions. The benefits from both systems can be combined by using one sandwich panel as a basis for a strut structure of the bus. A sketch of the hybrid design is shown in Figure 19.1. The sandwich panel will consist of carbon fibre face sheets with an aluminium honeycomb.

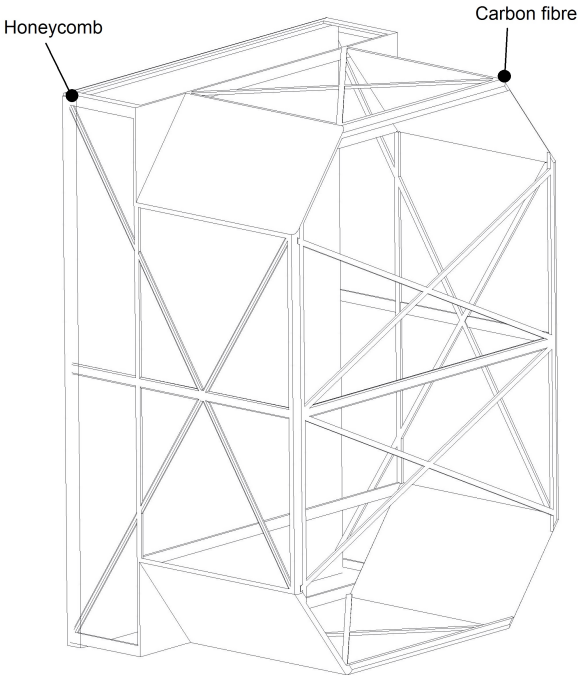

Figure 19.1: Sketch of the spacecraft main structure with a sandwich panel basis.

It is assumed that a hybrid structure shall be more weight efficient than either a full panel or truss design. A more detailed structural analysis should be conducted to verify this assumption. The hybrid design provides good access to S/C components from most sides. The bottom panel has a high stiffness and can provide an effective load path to the payload adaptor of the launcher. The antenna array can also be fitted to the panel rigidly to attain an accurate alignment.

19.4 Results

Using the methods described in the previous chapter the stresses due to quasi static loading on the main panel and the fundamental frequencies of the S/C are computed. The antenna array is built by mounting the elements on circular cross-section composite booms. The S/C bus and boom system is analysed to obtain the fundamental frequencies of the two booms. The models used for the vibrational analysis are sketched in Figure 19.2.

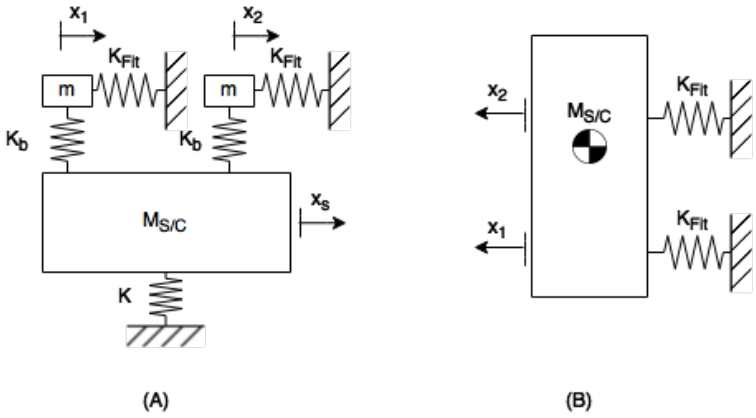

Figure 19.2: Vibration analysis model of the S/C - antenna array system (A) and the S/C fittings (B).

19.4.1 Sandwich Panel Sizing

For the main panel of the S/C an initial thickness for the face sheet and core is selected. The stress due to the bending moment M_{cm} is then computed. For a S/C mass of 110 kg and a COM located at the geometric centre of the bus, the moment M_{cm} equals kN m and the stress for 2 mm face sheets with a 28 mm core height is equal to 26.5 MPa. As expected, the stress due to bending is relatively low. Based on this initial dimension the vibrational analysis is performed.

19.4.2 Spacecraft Bus Vibration

When the main plate is assumed to have a much higher stiffness compared to the payload adaptor mounting, these mountings can be analysed as the driving factors in the fundamental frequency of the S/C. The model is shown in Figure 19.2 (B). The size of the antenna elements for the L- and S- Band are 12 cm long and require a separation of at least this distance between the S/C bus and the payload adaptor. Assuming a length of 25 cm for the fitting and a circular cross-section made out of aluminium the stiffness of the beams k_{fit} can be computed.

For the configuration shown in figure 19.2 a fundamental frequency f_0 of 95.74 Hz is found. The fittings shall have a radius of 15 cm. The radius is very large and adds much weight to the payload adaptor. During the detailed design the use of a hollow cross-section combined with a stiffer material should be investigated to reduce weight.

The behaviour of the antenna array is investigated and computed. The weight of the antenna elements is very low and the combined weight of all antennas are assumed to be 1 kg. The footprint of the L- and S- Band antennas are 5 cm by 5 cm and these values are used as an outer radius of the array booms. To obtain an optimal omnidirectional behaviour of the booms and allow the use of filament winded composites a circular cross-section is selected. The weight is automatically computed in the model when the inner diameter of the boom is selected. A reasonable wall thickness is taken to be 2 mm. With this assumption and the model from Figure 19.2 (B) the fundamental frequency of the S/C - antenna array system is computed. In Figure 19.2 the two fittings of the S/C are combined and represented by k. A fundamental frequency of 18482 Hz is found for the booms and 1287.2 Hz for the S/C. These values are well beyond the fundamental frequencies of the launcher. In the detailed design phase the use of a smaller fitting for the booms should be investigated.

20 | Thermal Subsystem Design

The thermal subsystem ensures that all the other subsystems are kept within their optimal temperature range. This guarantees that the spacecraft will perform as expected and prevents damage to critical components. For the conceptual design stage, an estimate should be made for the temperature distribution during an orbit. This chapter discusses the thermal control in more detail.

20.1 Requirements

Based on the hardware selection from the other subsystems, thermal requirements are imposed on the thermal subsystem. These are derived from the components' allowed operational temperature ranges. Note that only the most crucial components are considered in this chapter.

TML-01 The thermal subsystem shall maintain a propellant temperature of at least 17°C at all times.

TML-02 The thermal subsystem shall maintain a temperature range between −20°C and 50°C for the internal parts of the propulsion system.

TML-03 The thermal subsystem shall maintain a temperature range between −40°C and 55°C for the Payload ESM Unit.

TML-04 The thermal subsystem shall maintain a temperature range between −20°C and 65°C for the battery.

TML-05 The thermal subsystem shall maintain a temperature range between −20°C and 50°C for the transmitter.

TML-06 The thermal subsystem shall maintain a temperature range between −100°C and 150°C for the solar panels.

20.2 Model

To obtain a good estimate for the temperature distribution on the spacecraft, a multi-node thermal model has been made with the use of the SIMULINK. A lot of assumptions had to be made, since the design of the spacecraft is still in the conceptual phase. The section below gives an overview of the assumptions made and the principles behind the model.

20.2.1 Assumptions

To avoid unnecessary model complexity, some assumptions have been made. These will be explained in more detail in the model description afterwards.

- Constant solar flux, Infrared (IR) and albedo values.
- One face in direct sunlight obtaining IR, albedo and perpendicular sun flux, five other faces only obtaining IR and albedo.
- Internal components only connected to front and rear panel.
- Heat transfer only possible by conduction and radiation.
- No heat gradient in components and side panels.
- Components and side panels are modelled as uniform mass nodes absorbing or generating power.

Although the above assumptions might have a significant effect on the accuracy of the model, they still provide sufficient boundaries for a first order estimation.

20.2.2 Model Description

The supporting structure of the spacecraft is dominated by composites (see Section 19). The Earth facing side of the bus structure consists of a stiff sandwich panel with a truss structure on top. Because of the low thermal conductivity, the temperature variations can become very large. Some parts of the structure show behaviour similar to insulators. On the other hand, this effect can also be used to direct and route the heat flows.

The structure and all the internal and external components are modelled as mass nodes which, based on their nature, transmit or obtain heat. The outside of the spacecraft is modelled as three distinct nodes: the front panel, side panels and rear panel. As stated before in the assumptions, one node (front panel) obtains perpendicular sun flux, albedo and IR while the other two nodes only receive IR and albedo. These faces radiate heat to a deep space temperature sink (3 K) proportional to their absorption and emission characteristics.

The components inside the model are connected to the front and rear face by conduction and the inter-component relation is purely based on radiation. This is not only done to simplify the model, but also because conduction is significantly more dominant than radiation. In other words, radiation is only significant if there is no physical contact (or insulator) between two components.

To further simplify the analysis, not all components are modelled separately as nodes. Only the components that operate under fragile temperature range and the component that generate significant heat are represented as separate nodes:

- Propellant tank
- Propulsion system
- Payload
- Battery
- S-Band Transmitter
- Solar panels
- Side panels

The rest of the components are combined in a single mass node. Appendix E shows the full SIMULINK model including subsystems.

20.3 Design

A successful mission requires the spacecraft to perform during extreme situations. For the thermal design, two cases are considered: the hot and the cold case. During the hot case, the spacecraft encounters an orbit without eclipse, while all heat generating components are switched on. The cold case tests the spacecraft by going into the longest possible eclipse with as little internal heat generation as possible. The section below explains the inputs, the optimisation parameters and the final outputs and hardware selection.

20.3.1 Inputs

The model described above requires the following inputs to simulate the temperature variation during several orbits:

- Power fluxes (albedo, IR, solar), orbit and eclipse times
- Operational and survival temperature ranges
- Component geometry, mass, material properties and contact areas
- Duration and amount of internal heat generation

The values used are listed in Table E.1 of Appendix E.

20.3.2 Outputs

As mentioned before, the majority of the structure has been made out of composites. This gives the opportunity to regulate the temperatures by adjusting the contact area and conductivity between the components and structure. The thermal analysis will provide the following outputs:

- Contact area and conductivity between components
- External surface emissivity and absorption coefficients
- Thermal range experienced by components
- Power required for components with active thermal control

These outputs will impose requirements on the structural design and are listed in the derived requirements section below.

20.3.3 Hardware Selection

The outside surface of the spacecraft will be covered with Multilayer Insulation (MLI), which is made of layers polyimide with vapor deposited aluminium in between. This ensures proper face temperatures and good internal insulation. For the inter-component connections, three materials are selected:

- Low conductivity: 0.25 $W\,m^{-1}\,K^{-1}$ (For example: Teflon [1])
- Medium conductivity: 55 $W\,m^{-1}\,K^{-1}$ (For example: Carbon steel [2])
- High conductivity: 105.5 $W\,m^{-1}\,K^{-1}$ (for example: Carbon fibre and Honeycomb[3])

With these chosen materials, parts that need to dissipate heat can have large contact areas and high conductivity whereas other parts can be insulated using the opposite approach. Furthermore, the propellant tank needs to maintain a temperature of at least 17°C which is done by using a single 15 W patch heater attached to the tank.

20.4 Results

This section shows the performance of the thermal system design and the sensitivity analysis.

20.4.1 Performance

The graphs below show the temperature distribution over three orbits. Boundary conditions for component temperature were set at 0°C. The graphs for both the cold and hot case (Figure 20.1 and Figure 20.2) show that system temperature settles around two values which should comply with the thermal requirements discussed above (Table 20.1). The convergence is caused by the inflow of heat reaching equilibrium with the outflow.

Table 20.1: Thermal requirement compliance

Requirement	T_{min} Operational	T_{max} Operational	T_{min} Cold case	T_{max} Hot case	Compliance
TML-01	17°C	–	17.7°C	23.9°C	Full
TML-02	$-20°C$	50°C	$-0.2°C$	25.6°C	Full
TML-03	$-40°C$	55°C	$-7.1°C$	20.3°C	Full
TML-04	$-20°C$	65°C	$-0.2°C$	22.9°C	Full
TML-05	$-20°C$	50°C	$-6.9°C$	20.5°C	Full
TML-06	$-100°C$	150°C	$-0.2°C$	80.8°C	Full

[1] http://www.matweb.com/search/DataSheet.aspx?MatGUID=168993db850043b1b550e27a76e2f843&ckck=1 [Accessed on 16/06/2015]
[2] http://www.matweb.com/search/DataSheet.aspx?MatGUID=ee25302df4b34404b21ad67f8a83e858 [Accessed on 16/06/2015]
[3] http://www.hexcel.com/Resources/DataSheets/Honeycomb-Data-Sheets/CR3_us.pdf [Accessed on 16/06/2015]

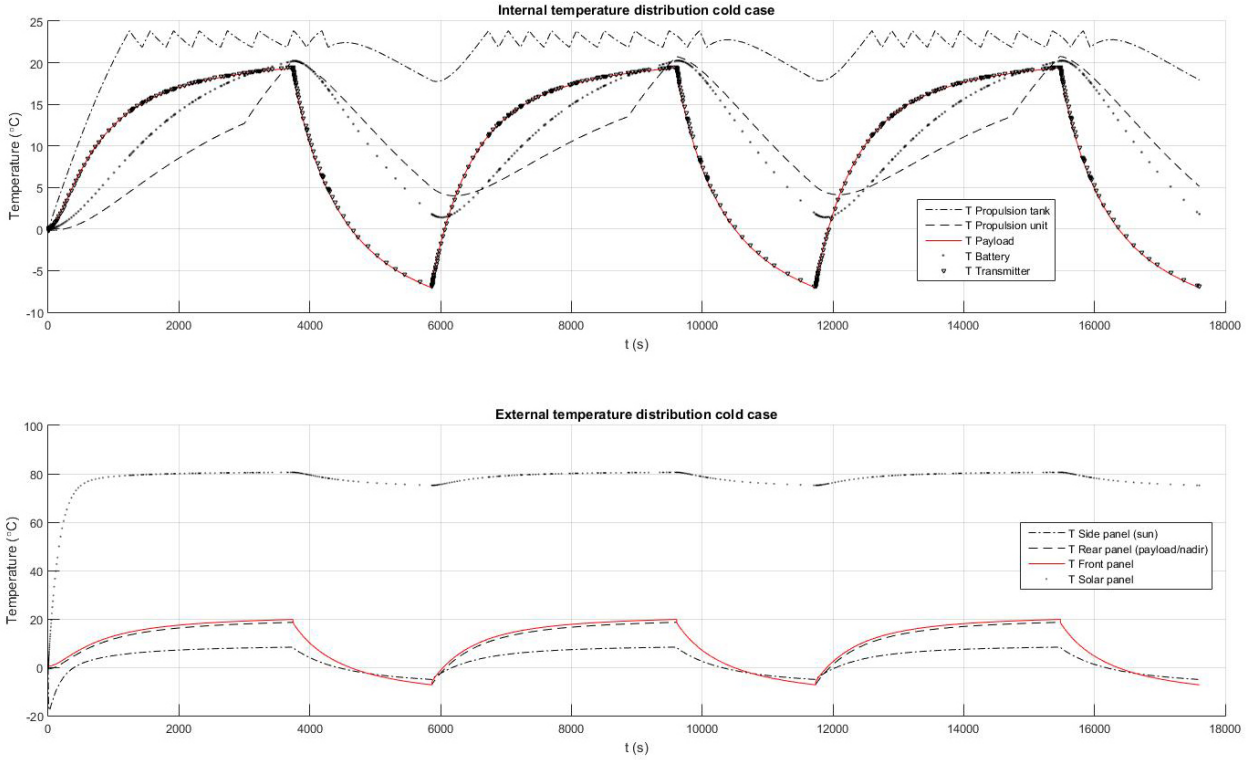

Figure 20.1: Cold case temperature variation during a three-orbit period

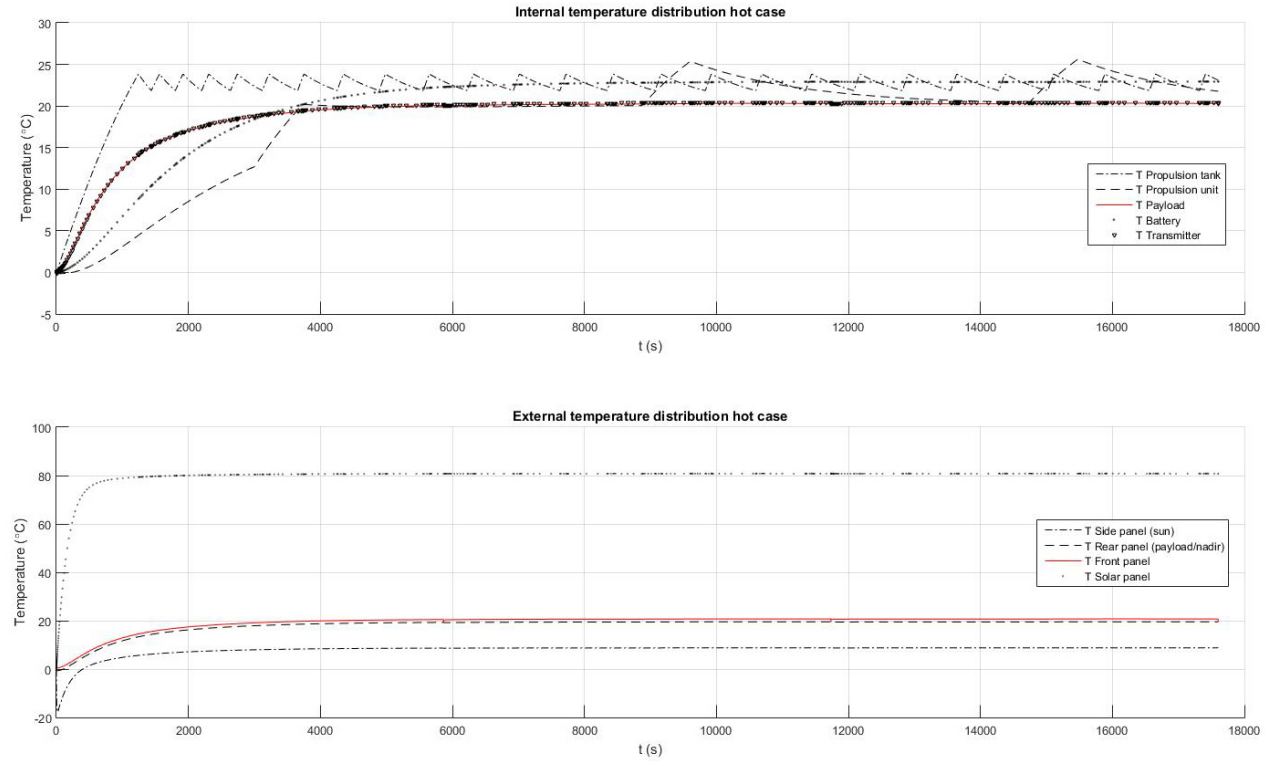

Figure 20.2: Hot case temperature variation during a three-orbit period

20.4.2 Sensitivity

For the current design phase, its very unrealistic to talk about sensitivity of the thermal subsystem. The temperature distribution in the spacecraft is a delicate interaction between all the components, attachments and orbital environment. For the current estimates, all temperature values are well in between operational limits set by each of the components. This means that changes in conditions are not likely to result in failure. Furthermore, the thermal subsystem has been designed to maintain operational conditions. Almost all components can survive more extreme temperatures.

In the current design, failure modes are not taken into account. In the occasion of full spacecraft shutdown, the internal temperature will most likely drop below the operational limit. Additional heaters and a redundant computer can solve this extreme situation.

20.5 Derived Requirements

The thermal subsystem derived the following requirements for the structural subsystem

STR-08 All component connection contact areas shall be made of three types of material with thermal conductivities of 0.25, 55 and 105.5 $W\,m^{-1}\,K^{-1}$.

STR-09 The S/C structure shall have a thermal conductivity of at most 105.5 $W\,m^{-1}\,K^{-1}$.

It can be a challenging task for the structural engineer to design the component attachments with a certain thermal conductivity. A solution for this can be to use flat contact pads, made of the required material, in between the attachment structure.

21 | Harness Subsystem Design

This chapter contains the design of the harness subsystem. First, the requirements for this subsystem are discussed. Then, the design process of the harness is explained. Finally, the results of this chapter are summarised.

21.1 Requirements

For the harness design, the following requirement is applicable:

HAR-01 The harness shall provide distribution of cabling for power, signals, and data.

21.2 Design

The harness is always designed specifically for the S/C in question. This way the mass and volume can be optimised for the specific shape and layout of the S/C. The manufacturing of harnesses is usually performed by hand, because automating the production for a small amount of harnesses would be more expensive. It can therefore be assumed that the production of the harness for this constellation will also be done by hand.

21.3 Results

Since this is a feasibility study, the harness itself will not be designed during the course of this project. However, a list of requirements has been made for the harness subsystem to be used in the further development of the S/C. The requirements for the harness subsystem have been generated from the main tasks the harness needs to perform during the mission. The list of requirements for the harness can be found in Appendix A.12.

22 | Spacecraft and System Architecture

This chapter elaborates upon the S/C architecture. Both with respect to the internal and external layout as with respect to the hardware and software configuration.

22.1 Spacecraft Architecture

The internal configuration of the components inside the S/C is shown in Figure 22.1. The solar panels, antenna booms and fairing attachments are not shown in this picture for clarity. The main ideas behind this design are:

- Central fuel tank: Mass balance.
- UHF Transceiver: Placed on corners for optimal ISL.
- Star Tracker Optical Heads: Positioned at at all axes, furthest away from thruster.
- Control and power units: Positioned in the centre for optimal thermal performance.

22.2 Software Architecture

This section describes the different software configurations that can be encountered during the mission. A visual representation can be found in Figure 22.2. As can be seen from the diagram, the software configuration is mostly determined by the mode of the AOCS. During acquisition, the OBC uses the AOCS algorithm to stabilise the S/C. Furthermore the software for the electrical power system and the thermal control system will be started to ensure safe operations. Finally the communications system is activated to make communications with the ground station possible. At this stage no encryption is needed. The same software will be used during safe mode. During the manoeuvre mode only the electrical power system, the propulsion, and the OBC are required. It is assumed that the duration of this mode is short, so power and thermal effects can be neglected.

During nominal mode the OBC and payload interact to point the payload in the required direction and to provide the payload with information on time, attitude, and position. The payload generates data, that is encrypted by the C&DH and than send by communications. The electrical power system, the thermal system, and the communication system interact with the OBC to obtain the required attitude, and in case of the communications the data to be transmitted. During this phase data is being encrypted before being send. During slew mode, the corresponding AOCS algorithm is executed by the OBC. The electrical power system takes care for providing the peak power required by the reaction wheels to provide the slew manoeuvre in minimal time.

22.3 Hardware and Interface Architecture

Apart from the software, the architecture of the hardware and interfaces is important as well. A comprehensive overview of hardware, data flow, and communication flow is shown in Figure 16.1 in Section 16.2. An overview of the electrical architecture can be found in Figure B.1 as displayed in Appendix B.

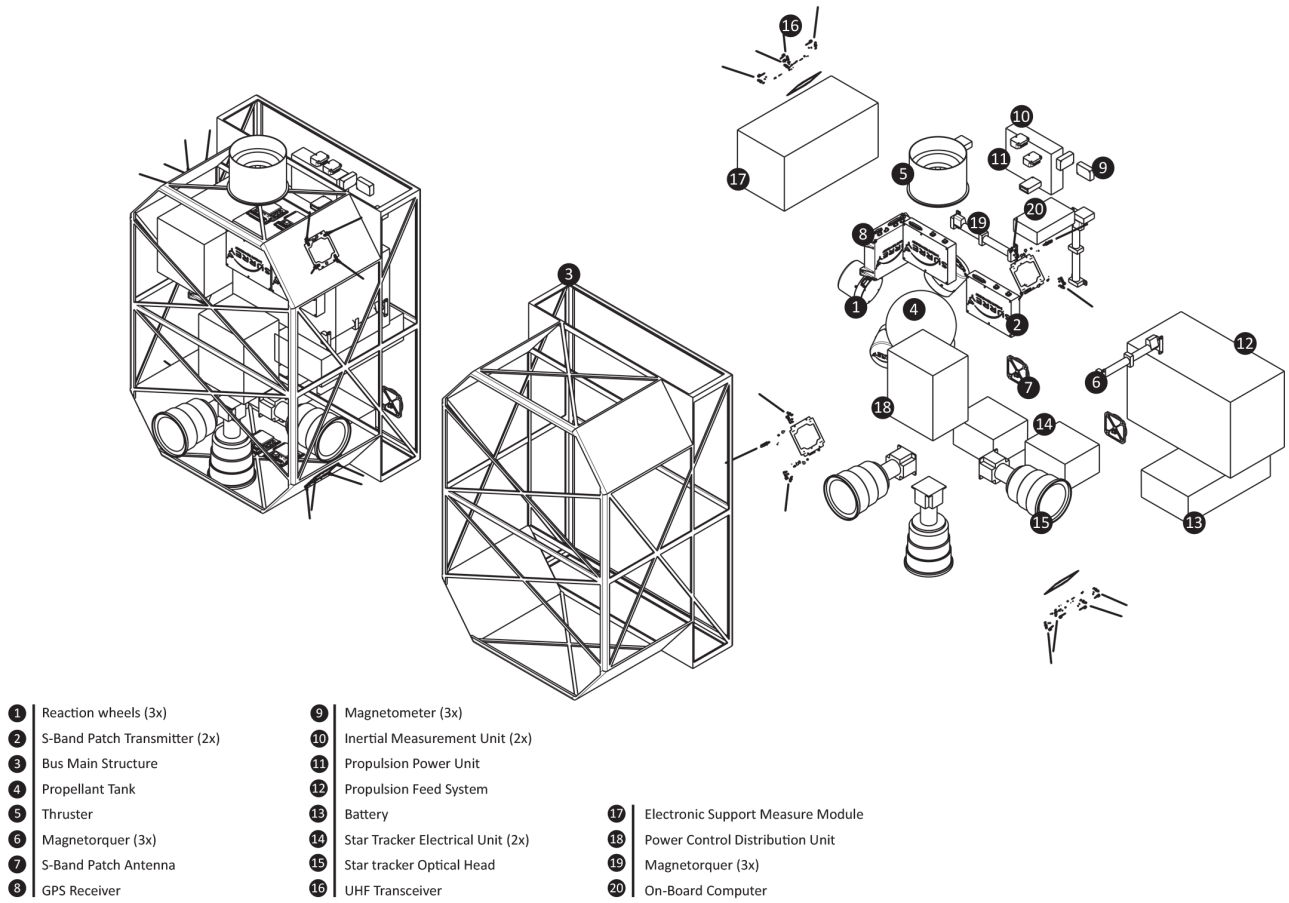

Figure 22.1: Overview of the LEOPARDSAT's internal configuration.

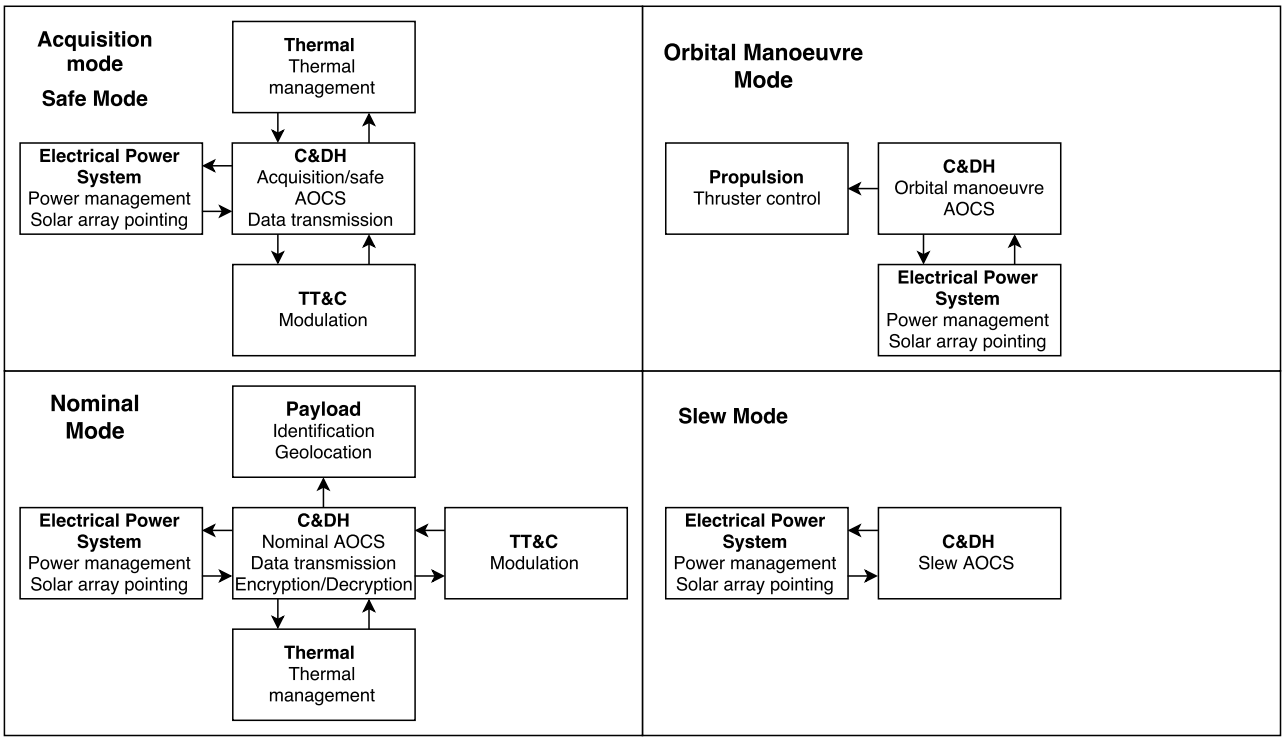

Figure 22.2: Software configuration.

23 | Operations and Logistics

This chapter provides information concerning the additional activities that come with a space mission. The chapter focuses on launch, on ground operations and logistics, and on EOL procedures.

23.1 Launch

In this section the launch phase of the mission will be discussed. First, the requirements on this phase will be stated. Then, the launcher choice will be explained briefly. Finally, a summary of the most important launcher parameters and characteristics is given.

23.1.1 Launch Requirements

In this section the requirements on the launcher are given. Because this report is focused mainly on the S/C design it is assumed that there is no requirement on the launch costs.

LCH-01: The launcher shall be able to lift 648 kg into a 500 x 500 km orbit at 100° inclination.

LCH-02: The launcher shall be able to carry four S/C in one launch.

LCH-03: The S/C shall be separated from the launcher in 3-axis stabilisation mode.

LCH-04: The launch date shall be compliant with GEN-06.

LCH-05: The launcher shall be able to perform a plane change of 6° at 500 km altitude.

23.1.2 Launcher Choice

A number of launchers have been considered for use, an overview can be found in Table 23.1. Even though cost is assumed not to be an issue, some indicative values are included. Because figures for cost are hard to find most values are taken from ESA's Launch Vehicle Catalogue (LVC) which was last updated in 2004 [52]. For the cost, the values given in Fiscal Year (FY) 2004 are taken and corrected for FY2015 by 25.9% and 27.7% inflation for US Dollar[1] and Euro[2] values respectively. This means that all cost figures presented below are meant only as a rough indication of the actual current value. These values will be used later on in Chapter 30.3 for the cost estimation of the entire mission.

The useful payload for a S/C is often only given for one or a few reference orbits. It is assumed that all launchers that have a useful payload higher than required for this mission for orbital heights higher than 500 km are able to perform the launch. For launchers with a prograde reference orbit a useful payload higher than the total constellation mass may be required, because the mission uses retrograde orbits. It is assumed that the unused payload capacity allows for the launch to be retrograde. In the payload column, the S/C reference orbit perigee and apogee, as well as inclination are given.

Table 23.1: Launchers considered for use.

Launcher	Country	Payload (Reference Orbit)	Cost FY2004	Cost FY2015
Angara [52]	Russia	1270 kg (800x800 km, i = 93.4°)	25 M$	31.5 M$ (est.)
Rockot [52]	Russia	1340 kg (800x800 km, i = 90°)	13 – 15 M€	16.3 – 18.9 M€ (est.)
Vega [46]	Europe	1430 kg (700x700 km, i = 90°)	18.5 M$	23.3 M$ (est.)
PSLV-C3 [52]	India	1200 kg (800x800 km, i = 99.8°)	20 M$	25.2 M$ (est.)

The final choice has become the Vega launcher of Arianespace[3]. Vega is developed by Arianespace for European Space Agency (ESA) and is able to launch a payload of 1430 kg into a circular polar orbit at 700 km altitude [46]. The launch site is located at ESA's Guiana Space Centre facility[4] in French Guiana. This location allows for launches to orbits with inclinations ranging from 5.2° to 100.5° [15].

[1] http://www.usinflationcalculator.com/ [Accessed on 21/06/2015]
[2] http://www.rateinflation.com/inflation-rate/euro-area-historical-inflation-rate?start-year=2004&end-year=2015 [Accessed on 21/06/2015]
[3] http://www.arianespace.com/launch-services-vega/vega_overview.asp [Accessed on 02/06/2015]
[4] http://www.esa.int/Our_Activities/Launchers/Europe_s_Spaceport/Europe_s_Spaceport2 [Accessed on 02/06/2015]

The Vega is chosen because it is a flight-proven European platform and its performance fulfils launch requirements **LCH-01**, **LCH-02** and **LCH-03**. Because the scope of this report is focused on the design of the S/C and space segment of the mission, it is assumed that the availability of launchers meets **LCH-04** and that launch costs are no problem. The Vega upper stage can be provide five burns and because no further information could be found it is assumed to be able to comply with requirement **LCH-05**.

23.1.3 Launcher Parameters

An overview of the most important parameters is given in Table 23.2. All values listed in this table are taken from the Vega User's Manual [46].

Table 23.2: Summary of Vega launcher injection errors, pointing accuracies, and frequency requirements.

Orbit injection errors ($\pm 3\sigma$)		
Semi-major axis	15	km
Eccentricity	0.0012	–
Inclination	0.15	°
RAAN	0.2	°
Separation mode and pointing accuracy ($\pm 3\sigma$)		
Geometrical axis depointing	1.5	°
Longitudinal angular tip-off rate	≤ 1.5	$^\circ\,s^{-1}$
Lateral angular tip-off rate	≤ 1.5	$^\circ\,s^{-1}$
Frequency requirements		
Lateral	≤ 15	Hz
Longitudinal	$20 < f < 45$ or $f > 60$	Hz

23.2 Operations and Logistics

The section below provides an overview of the mission's operations and logistics. Figure 23.1 shows the logistics after the design phase followed by the actual mission operations including the interaction between the space and ground segment. For the latter, a division has been made between on ground and on board processing, since this distinction changes the type of data exchanged, and the data routing.

After the development phase, the space segment needs to be built. This is initiated during phase C and continues in phase D as defined by the ECSS-M30-A standards [53]. Mission specific components can be developed or outsourced while COTS components can simply be ordered. All these components need to be transported to an assembly and test facility. After completion of Manufacturing, Assembly, Integration, and Test (MAIT), these parts need to be shipped to Kourou, French Guiana, launched and eventually be injected into its designated orbit.

Parallel to the space segment development, the ground support needs to be initialised. This includes building a ground station in the Caribbean special municipalities of the Netherlands, and if required, adapting the ground station in Breda to accommodate the additional operations. Once in operation, the constellation needs to be monitored and maintained from the command centre. This can be outsourced to third parties or done by the RNLAF themselves. Since there is no current experience in this field, training and hiring qualified staff is also part of this pre-operational phase.

During real time operations (Phase E), there is a delicate interaction between the command centre, the RNLAF and the spacecraft constellation. The constellation does onboard processing and thus sends level 3 data packages to the ground station. This data will be analysed and software or library updates can be transferred to the command centre if necessary.

The command centre is responsible for the flight planning and maintenance of the constellation and will thus send commands and pass plans to the constellation. These plans are based on customer needs, regulations and S/C constraints.

Phase F includes the disposal of the space segment and termination of the operations.

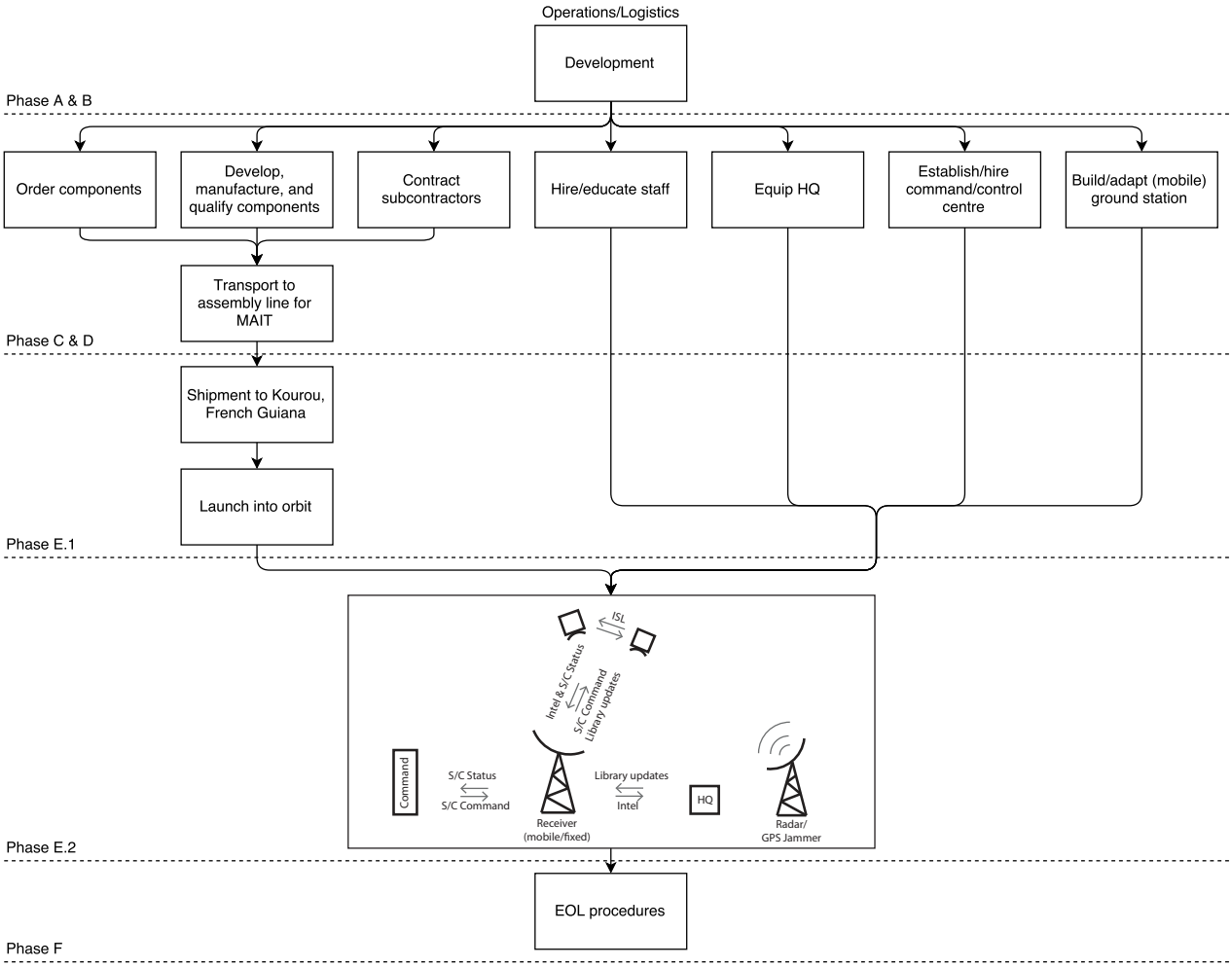

Figure 23.1: Operational flow diagram.

23.3 End-of-Life

At the end of the mission the S/C need to be disposed. This section details the operations in the EOL phase. The EOL process consists of two elements: disposal of the S/C itself and passivation of the on-board systems.

23.3.1 Disposal

To reduce the amount of space debris the S/C should either move into a graveyard orbit or re-enter the Earth's atmosphere. Since the mission takes place in the lower regions of LEO, getting the S/C into a graveyard orbit, which is between 2000 km and 35586 km altitude, would take a lot of time and cost a lot of ΔV. Consequently it is better to dispose the S/C by re-entry into the Earth's atmosphere.

Re-entry can be accomplished in two ways:

- **Controlled:** This method is also known as active de-orbiting. It is done by a long thruster burn at the end of the mission, so it does require some ΔV. Consequently it would increase the required propellant mass as was explained in Section 18.2. Not always do all parts of the S/C fully burn up during re-entry. As this can pose a problem for people on the ground, the main advantage of controlled re-entry is that the location of re-entry can be chosen such as to minimise the risk to people.

- **Uncontrolled:** This method is also known as passive de-orbiting. It is done by letting the orbits of the S/C decay by the atmospheric drag until the S/C re-enter into the atmosphere. The advantage of this method is that no extra propellant is required. The main disadvantage is that it is not known where the S/C will re-enter the atmosphere so people on the ground may be at risk. Another disadvantage is that the S/C still remains in orbit for the duration of the passive de-orbiting process, which could take a long time.

Because of the possible danger to people on the ground and the time it takes to passively de-orbit a S/C, it was decided to use the propulsion system to actively de-orbit the S/C at the end of the mission.

23.3.2 Passivation

Before a S/C re-enters the atmosphere it usually first needs to be passivated. Passivation means the depletion of all on-board sources of energy. However since the non-toxic xenon gas is used for propulsion, which does not pollute the Earth's atmosphere, the propellant tanks do not need to be cleared before re-entry. Because the S/C are re-entered into the atmosphere directly after the mission there is no need to passivate any other subsystems like batteries.

Part IV

Systems Engineering

24 | Final Budget Breakdown

This chapter elaborates on the technical resources of this project, mass and electrical power. Updated figures for mass and power are given at the unit and subsystem level as well as on the system level. Also, a cost estimation is made for the satellites. Instead of a top-down approach, a bottom-up approach is used to generate the new mass and electrical power budgets. The obtained values are compared with the values established in the Baseline Report [4] to assess how the project has developed since the Baseline Report was published.

24.1 Final Electrical Power Budget

In this section the power demand throughout the mission of the satellites is identified to give an updated electrical power budget for the system. An analysis of the power demand of the spacecraft is performed, including peak power for all the loads installed either in the platform or as payload. An overview of the average and peak power consumption per subsystem and the total consumption of the system are given in Table 24.1. The subtotal gives the power budget as established at this stage, while the total gives the power budget including a margin of 15% for the remaining development of the spacecraft.

Table 24.1: Summary of final electrical power budget breakdown

Subsystem	P_{avg}	P_{peak}
Positioning	5.8 W	5.8 W
Attitude determination	14.8 W	15.6 W
Attitude control	12.2 W	45.8 W
Propulsion	36.9 W	184.8 W
TT&C	9.8 W	45.7 W
Thermal	0 W	0 W
Power	30.5 W	36.8 W
Payload	180 W	240 W
C&DH	10.5 W	10.5 W
Subtotal	**300.4 W**	**584.9 W**
Contingency of 15%	**45.1 W**	**87.8 W**
Total	**345.5 W**	**672.7 W**

A detailed version of the power budget breakdown is given in Appendix C, where the power budget is decomposed to the unit level per subsystem. In this appendix every unit includes a specific margin to account for potential extra power consumption. The margins stated in Appendix C are set considering the following criteria:

- 20% margin with respect to expected power demand if the unit design is new.
- 10% margin if the unit design has a heritage from a previous similar one.
- 5% margin if the unit is recurrent.

The system power in the preliminary electric budget was estimated to be 812 W. After the preliminary design was finished, an average power of 346 W and a peak power of 699 W were calculated. The peak power comes out a little lower than the preliminary estimation of 812 W. The thermal subsystem does not use any power, although it was estimated in the preliminary electrical power budget that 56 W would be required.

24.2 Final Mass Budget

This section presents the mass budget after the preliminary design is completed. It contains the estimated masses of all the selected units. A detailed version of the mass budget is provided in Appendix D. A summary of the mass budget down to the subsystem level is given in Table 24.2. A contingency margin of 15% is applied to account for the remaining development of the satellites.
The new mass budget is lower than mass allocated at the beginning of the preliminary design. Two parts of the system mainly contribute to the decrease of the mass budget. Firstly, the propellant mass was budgeted at 38 kg in the preliminary budget, while the required propellant mass was determined to be 5.39 kg. This can be explained by the fact that the satellite has an electrical propulsion system which uses less propellant. Secondly, the payload was initially estimated to weigh approximately 36 kg. However, the updated payload weight is around 13 kg. The new mass budget suggest the design will be compliant with requirement **GEN-03-C02**, which puts a constraint of 200 kg on the S/C mass.

Table 24.2: Summary of final mass budget breakdown

Subsystem	Mass
Positioning	1.1 kg
Attitude determination	8.3 kg
Attitude control	5.5 kg
Propulsion (incl. propellant)	14.4 kg
TT&C	4.4 kg
Thermal	0 kg
Power	33.0 kg
Payload	13.2 kg
Structure	31.3 kg
C&DH	1.5 kg
Subtotal	**112.6 kg**
Contingency of 15%	**16.9 kg**
Total	**129.5 kg**

24.3 Final Cost Estimation

With the newly established mass budget for the ELINT satellite, a new cost estimate can be made. Similar to the preliminary cost budget presented in Chapter 7, the costs are estimated using the Small Spacecraft Cost Model. To account for lower non-recurring costs per unit for COTS products, the cost of the spacecraft bus components are decreased with 20%. The updated cost estimation for four ELINT satellites is given in Table 24.3.

Table 24.3: Final SSCM cost estimation

Cost contributors	Cost estimate FY15
AOCS	€ 11,568,000
Propulsion	€ 3,354,000
TT&C	€ 2,331,000
Thermal	€ 1,185,000
Power	€ 22,116,000
Structures	€ 6,460,000
C&DH	€ 2,049,000
Spacecraft bus	**€ 49,062,000**
Payload	€ 24,531,000
Integration & assembly	€ 8,525,000
Program level	€ 3,511,000
Flight support	€ 920,000
Ground support equipment	€ 1,012,000
Total	**€ 87,561,000**

The total costs for the development and production of four satellites is estimated to be under € 88 million. This is a large increase compared to the preliminary cost estimation established in Section 7.3, which was € 45 million. Since this estimation takes into account the fact that multiple spacecraft will be produced, the resulting estimation is higher. It is therefore assumed that this cost estimate is more accurate than the preliminary cost budget. This cost estimation suggests that there will be non-compliance with requirement **GEN-05**. This requirement puts a constraint of € 45 million on the cost of the satellites. To comply with the initial requirement of € 25 million, one S/C can be built. When producing two S/C, the costs will comply to the loosened cost requirement of € 45 million.

24.4 Results

In short, updated values of the mass, power and cost budget were presented in this chapter. After the preliminary design, the mass and power budgets came out lower than the preliminary budgets established before the design. The lower power budget resulted mainly from the fact that the thermal subsystem uses no power. The mass budget turned out lower due to less required propellant and a lighter payload. The cost estimation turned out higher than the preliminary budget, because the development of multiple spacecraft was taken into account. This will mean that the design will most likely be non-compliant with the cost requirement (**GEN-05**).

25 | Sensitivity Analysis

This chapter aims at evaluating the impact that a change in requirements could have on the design presented in this report. Below, a list of requirements is shown that have a high potential impact on the design, not only are the requirements listed, but their potential impact is described as well. Finally, the overall robustness of the design is analysed.

- **Mission lifetime:** An increase in the mission lifetime has a significant impact on most subsystems. The most influential factor causing this impact is the lifetime of the subsystem components. Their lifetime may be inadequate for missions longer than five years and especially moving parts can fail because of material wear. The propulsion components are designed for ten years, whereas the AOCS components are designed for seven years, just like the S-band downlink chain. The components that are sized depending on the lifetime are the batteries, which would increase in mass by 1 kg (12.5%) if the lifetime were increased by two years. This increase is due to the increase in number of cycle numbers which would decrease the depth of discharge. The lifetime of the UHF transceivers and antennas is unknown. However, the Delfi-C3 hosts a similar system and has been operational for seven years and still operates today. Furthermore, the amount of propellant the S/C needs for orbit maintenance increases with mission lifetime (37% for two more years). Overall, an increase in mission lifetime of two years would increase the S/C total mass by 3.5%.
- **Cost:** The cost requirement (**GEN-05**) is non-compliant. Decreasing the available budget further will thus make the required performance of the system even more unattainable. In order to make the constellation feasible, the budget has to be increased to at least the estimated € 88 million. From the estimate found in Section 24.3, it can be assessed that the S/C buses are the most expensive components (€ 10 million per unit) followed by the payload antennas (€ 25 million total). The cost of the spacecraft bus is dominated by material and development cost. The material cost is invariant however, the development cost could be reduced if an already existing bus were to be used even though this is not always the case (see SSTL-150 for S/C bus with similar characteristics and price € 16 million). The payload antenna costs, similarly to the S/C bus, could be reduced by avoiding development. This would most certainly reduce the performance of the antennas since antennas with angular accuracies smaller than 0.5° are usually custom made. An antenna with angular accuracy of 0.5° would decrease the geolocation accuracy of radars by 63%.
- **Launch window:** An earlier launch window will cost a lot more money to get the S/C manufactured in time. The rest of the planning will also increase in complexity and vulnerability. However, postponing the launch window will make the planning easier. Besides that, the launch window also influences the time frame in which the mission takes place. This might imply different solar conditions during the mission. As the current launch window is scheduled to allow operations during solar minimum, changing the schedule will lead to operations during less optimal solar conditions. Consequently more propellant mass would be required. If the launch window were to start during the next solar maximum (2023), the propellant mass would increase by 1 kg. The system is therefore, robust to the launch window.
- **Geolocation accuracy:** Increasing the required geolocation accuracy will have two effects on the S/C. For the detection of GPS jammers a larger separation between the satellites is required. This implies that a larger aperture angle of the antennas is necessary, and the antennas have to be larger since the maximum separation between the emitter and receiver is greater. For the detection of radars antennas with more angular discrimination are needed which implies that the antenna array shall be larger. Referring back to Chapter 11, it was seen that the accuracy of the AOA method is highly dependent on altitude. This may lead us to consider lower altitudes to avoid an increase in antenna costs.
- **Frequency band detection capability:** To detect larger frequency bands more antenna elements are required. This may create issues for the S/C architecture in terms of space allocation. Furthermore, a sophisticated system of oscillators would need to be implemented or more channels to the electronic support measures would have to be placed. Finally, a more elaborate signal library would have to be implemented. All of these measures would increase the complexity of the system and its cost.
- **Signal power detection capability:** To detect signals emitting at a lower power, larger antennas with higher gains are needed. This however, reduces the viewing angle. Alternatively, up to a certain extent, a higher sensitivity on the receiver could be used.

From this analysis, the system is found to be most robust to launch window and mission lifetime changes (up to seven years). However, changes in required geolocation accuracy and frequency band detection capability would lead to extensive changes in the design on the highest levels.

26 | Deviations and Non-Conformance

In this chapter the compliance to the preliminary and system requirements is evaluated. For the non-compliant requirements an estimate for the severity of non-compliance is made.

26.1 Deviations and Non-Conformance Matrix

In this section the deviations and non-conformance matrix is displayed. Table 26.1 displays only the requirements that are not compliant and the the level of non-compliance of each of the preliminary and system requirements. This structure was chosen instead of a compliance matrix to reduce the size of this chapter and since no explanation has to be given for compliant requirements explaining the non-compliant ones is more informative.

In the deviations and non-conformance table, the column compliance displays an "E" if the system is expected to be compliant but has not been evaluated yet, "P" if the requirement has been achieved partially, and "N" in case of non-compliance. The description of non-compliance column describes why the requirement has not been met or if it is partially met, what is the range of compliance.

Table 26.1: Deviations and non-conformance table of the preliminary and system requirements.

Identifier	Requirement description	Compliance [E/P/N]	Description of non-compliance
GEN-01	The constellation shall consist of 5 to 7 S/C.	N	The formation requires only four S/C to achieve the requirements successfully.
GEN-05	The maximum cost of the mission shall be € 45 million, excluding launch and operations costs.	N	The arrays for the four S/C cost € 25 million. The busses cost € 10 million per unit. As a result, an estimate of € 90 million has been calculated.
PAY-03	RF signal sources shall be located with an accuracy better than 5000 m.	P	Only elevation angles larger than 34° for L-band, 26° for S-band, and 31° for X-band, due to the increase in distance between the emitter and the receiver.
CON-03	The orbit geometry shall provide global coverage for the GPS jammer localisation.	P	Up to 70° latitude because decreasing distance between S/C.
CON-04	The orbit geometry shall provide global coverage for the radar signal localisation.	P	Up to 80° latitude since due to the 100° inclination of the orbital planes, the poles are not covered.

26.2 Criticality Analysis

In this section, the requirements that were not met are analysed to determine the severity of the non-compliance. The analysis is displayed in Table 26.2.

Table 26.2: Criticality analysis of the requirements that are not compliant

Identifier	Criticality
GEN-01	This has a positive impact on the system since more budget can be reserved per S/C.
GEN-05	This killer requirement (as identified in Chapter 4) is not realistic for the required performance of the components. As stated in Section 24.3, the S/C busses cost alone amounts to € 40 million. Furthermore, the required phased array antennas cost € 25 million since the required angle of arrival accuracy is high in order to comply with the geolocation requirement. This has been communicated to the customer but no change has been adopted.
PAY-03	The system is compliant in the range of applicability since the goal is to detect the side-lobes of the radars that are emitted at elevation angles greater than 40°. Taking this into account, the system is compliant but the requirement has to be refined.
CON-03	The system can locate GPS jammers up to 70° latitude, 4° above the arctic circle. This region only excludes the poles, Greenland and a tenth of Russia. This non-compliance is therefore only an issue in case their is a high density of GPS jammers above the latitude threshold. This information is unknown to us.
CON-04	The system can locate radar signals up to 80° latitude. As stated above, the region of applicability includes most of the populated regions of the globe. Furthermore, since launch sites are mainly located at low latitudes to be able to achieve a wide range of inclinations [54], it is probable that the density of launch sites that emit radar signals is low at latitudes above 80°.

27 | Reliability, Availability, Maintainability, and Safety Characteristics

In this chapter, the Reliability, Availability, Maintainability, and Safety (RAMS) characteristics of the system are analysed. First, various reliability philosophies are investigated. This is followed by a list of safety-critical functions implemented in the system of which a Failure Modes Effects Analysis is done. Finally, possible considerations regarding maintenance are discussed.

27.1 Reliability Philosophies

Three different methods can be used to achieve the required reliability of the system. The first is fault avoidance, the second is fault tolerance and the third is functional redundancy.

Fault avoidance is the most basic method. It prevents failure by purchasing high-quality components and by applying design margins. High-quality components have a high reliability, which is favourable. However, usually they are heavy and in general they require expensive resources and inspection during the manufacturing phase, increasing their cost. The large margins used in this philosophy increase the reliability by over-designing the system, requiring more mass, power and a larger cost budget.

Fault tolerance is the ability of the system to continue functioning after failure of a component. This method can be divided into three parts. The first part is the design of redundant components that can accomplish the function of the primary component. The second part is the detection of time at which a primary or redundant component has failed or has diminished performance. Finally, a transfer mechanism is necessary to initiate the transition from the inoperative component to the redundant one [55]. The fault tolerance method adds to the mass, cost and volume of the spacecraft and, unless a power plan is set up, to the power requirements. However, this method is the simplest and can be applied at every level of the design.

The third method is functional redundancy. This approach consists of dissimilar mechanisms that are already placed in the spacecraft for their function but that can also be used to correct the occurrence of failure in another component. This method requires high-level understanding of the system and is usually not a design choice but an option after failure has occurred.

27.2 Safety-Critical Functions

Safety-critical functions are functions that are necessary and irreplaceable for the correct functioning of the system. The hazards that affect these functions can be categorised into safety-critical hardware, software or procedures [56]. The safety-critical functions of the system are listed below, and the system and subsystem hazards related to each of them have been tabulated in Table 27.1. Compared to the risk analysis developed in Chapter 32, the hazards presented in this section occur during the design lifetime and not the development or production phases.

a. Orbital insertion
b. De-tumbling
c. Solar array deployment
d. Antenna array deployment
e. OBC start-up
f. Telemetry downlink
g. Pointing accuracy and attitude knowledge
h. Orbit maintenance
i. Power distribution and generation
j. OBC distribution capability

Table 27.1: List of hazards to the system and their potential countermeasures (function letter corresponds to the list above).

Function	Hazard	Cause category	Potential Countermeasures
a	Faulty orbit insertion	Procedural	Take the insertion error margins of the VEGA launcher into account in the design of the propulsion subsystem
b	Batteries deplete before startup	Hardware, procedural	Design the solar array folding mechanism to have at least one surface in sunlight
c	Solar arrays do not deploy	Hardware	Divide the solar array into two independent arrays; use mechanical, highly reliable deployment mechanisms; program a cyclic duty cycle in case only one array can open
d	Antenna arrays do not deploy	Hardware	Use mechanical, highly reliable deployment mechanisms
e	OBC does not start	Hardware	Launch in sleep mode and connect the system with a timer
f	Telemetry downlink inaccessible	Hardware	Redundancy in the antenna and transponder; use the ISL to do the downlink at a lower data rate
g	GPS data reception disabled	Hardware	Internally redundant receiver
g	Star trackers inoperative	Hardware	Redundant star tracker
h	Thruster failure	Hardware	Internal redundancy in the components and reliable thruster
i	Short-circuit	Hardware	Insert fuses in the circuits to limit the propagation
j	Wire failure in OBC	Hardware	Design cross-redundancy in the OBC and add a redundant OBC

27.3 Safety-Critical Requirements Discovery

At this stage in the design, where the exact configuration of the spacecraft is still open and the components have not yet been selected, the only requirement that can be formulated is a qualitative and functional one: All safety-critical functions shall be designed such as to survive the occurrence of one failure, without loss in performance.

27.4 Maintenance

The maintenance of an orbiting spacecraft is challenging since there is no physical contact with the spacecraft during its lifetime. However, certain aspects of the maintenance need to be addressed. The first being the orbit maintenance that is achieved by the propulsion subsystem. This is done periodically, as stated in Chapter 18, to avoid any interference with the successful execution of the mission. Since the propulsion is only switched on over the poles, where the payload is inoperative since the geolocation accuracy is too low, the total power required remains low. Furthermore, some components require cleaning or purifying to maintain the required performance. This has not been analysed since the components have not yet been selected. The maintenance of the signal library must also be analysed. As described in Chapter 16, the library is fully updateable. Finally, for actual maintenance of the spacecraft two options arise. The first being to design a self-repairing spacecraft (both hardware and software). However, this requires high levels of autonomy which are not in line with the budget of this mission. The second option is on-orbit maintenance. This method is still in the development stage and expensive, therefore it is not a viable option.

28 | Verification and Validation

In this chapter the Verification and Validation procedures for the models used and for the system will be proposed. Throughout the project, the V-model was used to streamline the whole design process. This model is shown in Figure 28.1. This method implies that, after a design, the subsystem and system should be verified. Finally, the system shall be validated when operational.

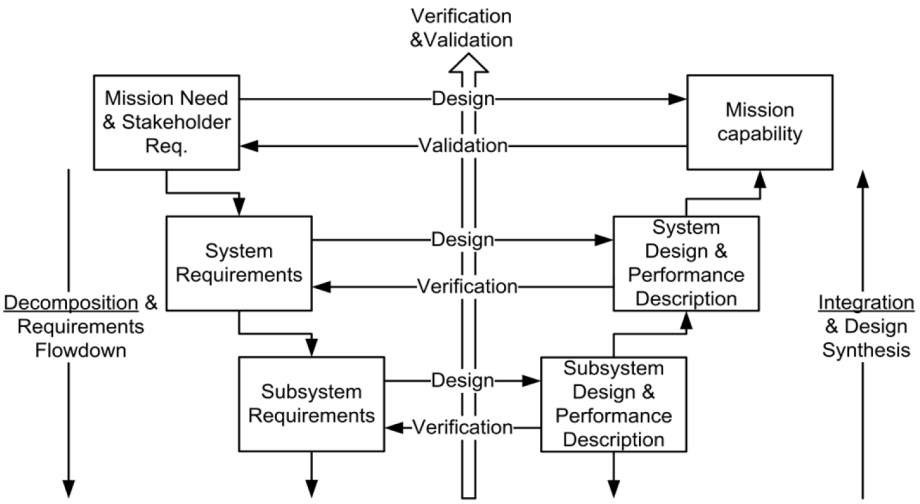

Figure 28.1: The V-model [7].

The definitions of verification and validation are:

Verification "Proof of compliance with design solution specifications and descriptive documents." [57]

Validation "Proof that the product accomplishes the intended purpose based on stakeholder expectations." [57]

28.1 System Verification

To verify and validate the system, different methods can be used. These methods are inspection, analysis, demonstration and testing. For simple requirements, inspection or demonstration can be used. For example, checking if the spacecraft complies with a dimensional requirement is done by inspection. The dimensions of the part are simply measured. For more complex requirements, test or analysis is needed, for example to check whether the propulsion system delivers enough thrust. Though this can be done via analysis, testing is preferred since it gives more accurate results. However, due to time or cost constraints, or practicality or safety problems, testing is not always possible. Sometimes, testing is even not technically feasible, for example simulating the absence of gravity. To do testing, a test model (prototype) is needed. If necessary this model can be refurbished and launched to save costs. The model would be called a Protoflight Model (PFM) [58].

Payload
To verify the antenna array, a test is needed in an anechoic chamber. In this chamber, the walls absorb all reflections from electromagnetic waves, to simulate the space environment. Data from this test is also needed to calibrate the array system for production errors and interference between array and spacecraft. For the signal processing, the verification and validation has to be done by the subcontractor. The geolocation has to be reviewed by analysis, because it cannot be tested until dedicated in-orbit commissioning. Consequently the design for the algorithm has to be thoroughly reviewed.

Propulsion
The propulsion system can be tested on a test bench, preferably in a vacuum chamber. Individual components can be tested as well, for example a destructive pressure test on the fuel tank can be done.

Attitude and Orbit Control System
Perfect simulation of the relevant space environment is impossible on Earth, because continuous free fall is unpractical to simulate, especially for longer periods of time. However, with a Hardware in the Loop Test (HILT), the AOCS can be tested [58]. This involves hooking up the sensors and actuators to a simulator. Output to the actuators is fed into the simulator or computer, and this information is used to simulate the behaviour of the spacecraft. With this simulation, the information is send to the sensors. The on-board AOCS computer calculates new actuators outputs, and the loop is closed. Another option to test the AOCS system is with an air-bearing testbed. This produces even better result, but there are still restrictions [59].

Electric Power System
The EPS should be tested with a solar simulator to ensure the photovoltaic panels deliver enough power (illumination test). Batteries and converters should also be checked [36]. Other important tests are checking for correct connection between all subsystems, so they all receive power, and thermal testing of the solar panels, as they are subject to large thermal shocks when going in or out eclipse.

Telemetry, Tracking, and Command
The TT&C subsystem can be tested in an anechoic test chamber as well, together with the antenna array.

Orbit
Analysis should be performed, since testing on Earth is impossible. Proven models should be used for checking.

Command and Data Handling
To test the C&DH a HILT should be performed, as described above.

Structures and Mechanisms
Structural testing should be done to ensure the spacecraft can withstand all launch loads. This can be thoroughly tested using either a mockup or a full prototype. Vibration testing should be done on a vibrating test bench, for every frequency occurring at launch. Other loads, such as the acceleration loads, can be applied with hydraulics pistons, but it is better to place the prototype in a centrifuge, where all accelerations can be simulated. This should be rather easy since the spacecraft is small. Mechanisms should be tested as well, but it has to be ensured that gravity does not help the deployment of a mechanism, nor obstruct it.

Thermal Control
The thermal control can be tested using special facilities. In order to simulate the space environment, the prototype should be placed in cold room without any air to avoid conduction, and with radiation absorbing walls, to resemble deep space. In this test chamber, different scenarios can be simulated, such as eclipse or full solar radiation. If this cannot be done, analysis offers an alternative.

Electromagnetic Compatibility
An Electromagnetic Compatibility (EMC) test should be performed to check whether different subsystems using electromagnetism, such as the power, communications and payload, do not interfere with each other [60].

28.2 System Validation

The whole system can only be validated when it is operational. This is done by comparing the received data to position data from radars received by other means. A possibility to do this is by setting up a radar by the RNLAF in a known position, and check whether the system intercepts, identifies and localises the signal correctly and within the accuracy margins dictated by the requirements. When the system provides useful intelligence, it is validated, as this is what the customer wants.

28.3 Model Verification and Validation

Another aspect of the project to be verified and validated are the models used. The different options to do this are experience, analysis or comparison with other validated models.

To verify the orbital models created, comparison is done with the validated software package Systems Tool Kit (STK) [61]. The array sizing tool should be verified based on analysis, and afterwards be compared with a more extensive computer simulation. The antenna elements have been simulated with MATLAB Antenna Toolbox [34], which is a tool recently published. The simulations should be checked with a better validated tool, such as FEKO. The geolocation TDOA model was derived from a established model [17]. This model has been verified by comparing it to results published in the same source. The AOA method was verified by checking extreme conditions by hand. This is a check by analysis. For the TT&C, a link budget was established. This was compared with other link budgets and it got the same results. Another piece of software, SPATpro, was used to compare the results with as well. The structural model came from several handbooks. They are verified and validated by experience. The thermal design used Simulink [62]. This thermal model has been verified by hand. This is a check by analysis. The AOCS, EPS and propulsion system all use models from experienced authors [15].

29 | Manufacturing, Assembly, Integration, and Test

Following the detailed design phase as described in ECSS-M30-A [53], the MAIT procedures are started. This chapter gives a general overview of the activities that will have to be carried out during this phase of the design. It focuses on the system level, however most activities have their counterparts at subsystem level.

29.1 Manufacturing

The manufacturing process is generally distributed over multiple subcontractors. They first all perform their own design cycle including conceptual, preliminary, and detailed design. After that they start their MAIT phases in which they test and qualify their components. Based on type test theory this process can be sped up if COTS components are used, as they have already been designed and qualified. Consequently COTS components will only be subjected to less severe acceptance tests [15].

29.2 Assembly

Spacecraft assembly can be planned in different ways. One way is to have all components produced and delivered before the assembly starts. The advantage of this is that every part will be available at the moment it is needed. However, it implies that all subcontractors need to finish at the same time, that the longest manufacturing time determines the start of the assembly phase and that storage costs need to be accounted for.

The other solution would be to use distributed delivery of components. The advantage might be that parts will be kept in stock for shorter times and that the assembly might start earlier. The disadvantage being the risk that if the component delivery scheme is interrupted, the assembly will get delayed. the latter approach to assembly requires sufficient margins and strict schedule compliance.

For this specific mission the possibility exists to combine both approaches and to have the PFM assembled at the beginning when all parts have been produced, and to produce the other three spacecraft using the distributed delivery method.

29.3 Integration and Test

The Integration and Test (I&T) procedures are closely related. Sub assemblies are integrated and tested before being integrated into larger assemblies, etc. This procedure is also described in Section 28.1, where the different verification test are described for the different subsystems. Figure 29.1 shows the standard elements that are carried out during the I&T phase, it was adapted from SMAD [15]. It shows how first the bus is integrated and tested, before the payload is added and tested. Furthermore it presents the different tests such as vibration, shock, and thermal tests that were described in more detail in Section 28.1. It also shows various occurrences of the Comprehensive System Test, a complete system test that may last several days and including subroutines for the different subsystems.

The I&T phase is vulnerable to delays in the other parts of the design chain, as some facilities have to be booked years ahead. This makes I&T costly both with respect to time and costs.

According to the type test theory it is sufficient to qualify a product only once, if it can be guaranteed that the other products are identical. As all S/C are identical, the qualification tests can be conducted on one S/C, the PFM. The other three S/C will only be subjected to the less severe acceptance tests. After refurbishing, if required, the PFM this can be used as the fourth S/C to complete the constellation [15].

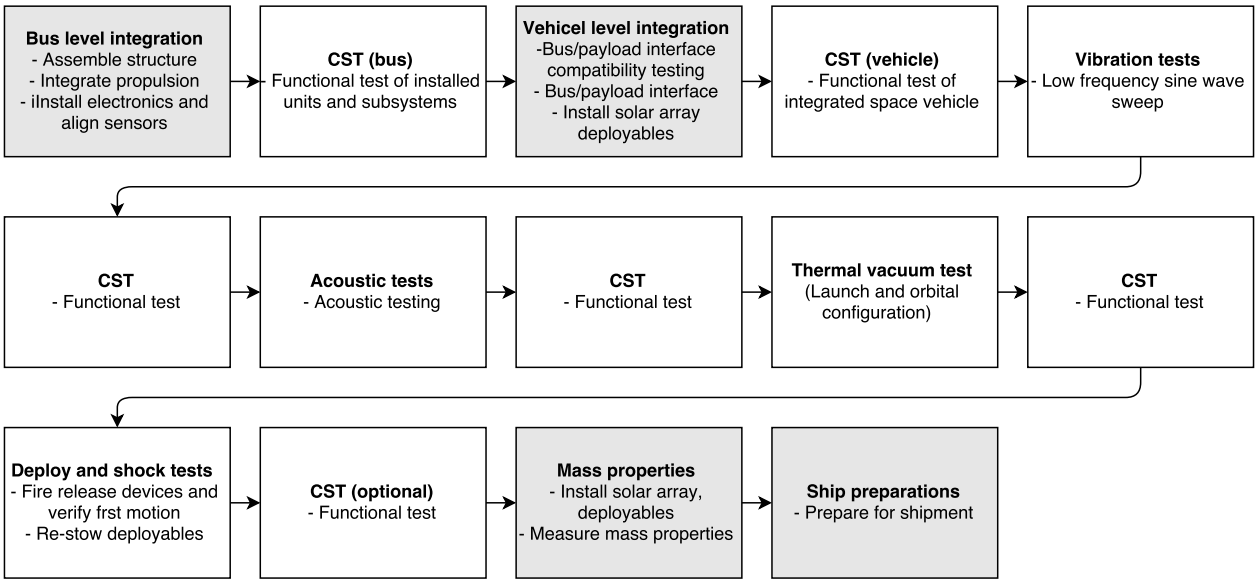

Figure 29.1: S/C integration (grey blocks) and testing (white blocks) flow.

Part V

Project Management

30 | Program Design and Development Plan

This chapter describes the development process of the S/C after the DSE project finishes. It first relates the DSE work to the European Cooperation for Space Standardization (ECSS) standards and from there develops the future activities, presented in a Program Design and Development (PD&D) diagram. Figure 30.3 presents the same activities on the program timescale.

30.1 Status of the Design

This section shows how the work performed so far relates to the ECSS standards for project phasing and planning [53]. Figure 30.1 shows the standard project setup.

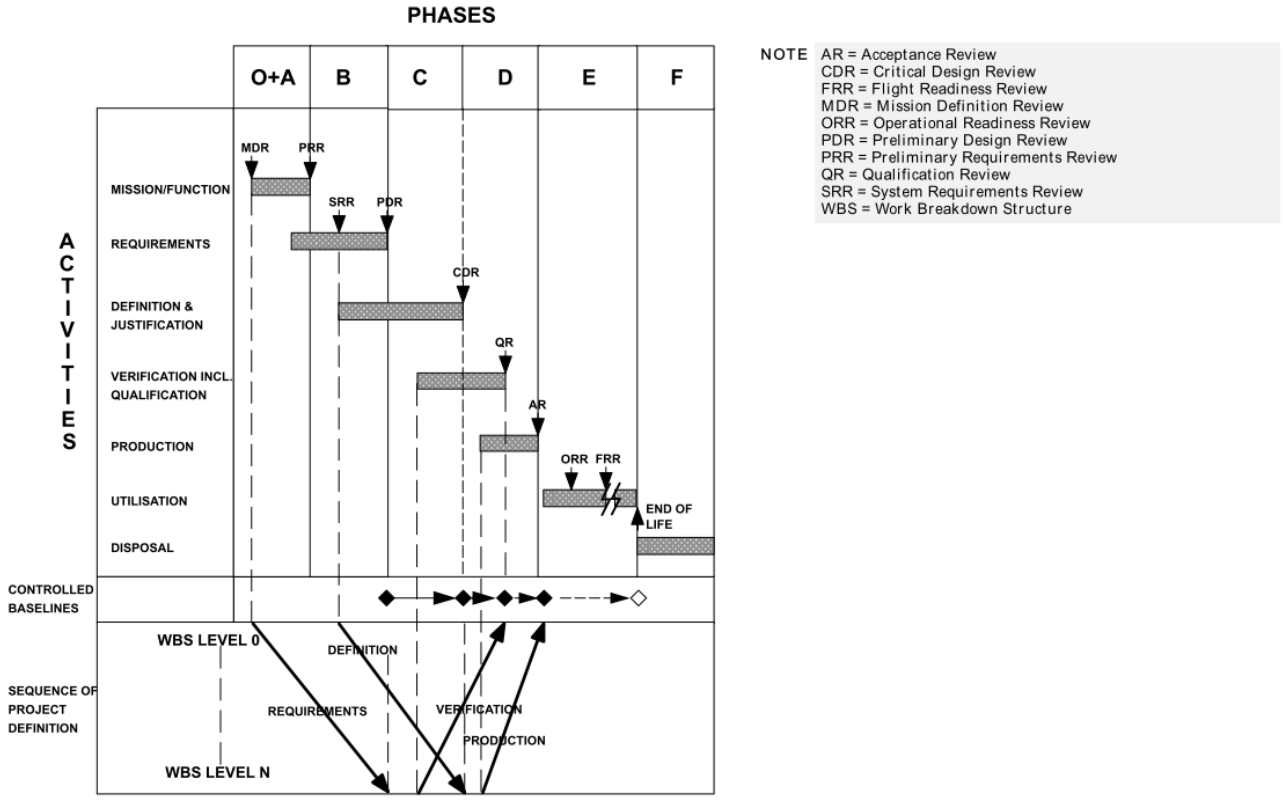

Figure 30.1: Typical project life cycle according to the ECSS-M30-A standard [53].

Phase 0 and phase A focus on project planning, budget allocation, and feasibility study as well as concept generation. These phases resulted in the PP [3], BLR [4] and MTR [5]. These phases together form the conceptual design phase. Phase B is the preliminary design phase, it elaborates on the concept selected at the end of phase A. Besides that it offers a first view on whether or not to use COTS components and it conducts studies into reliability, technological readiness, etc. This phase corresponds to the period following the MTR. Phase C is the detailed design of the selected concept, which ultimately culminates in the Critical Design Review (CDR). This phase is only partially touched upon. The DSE project produces a concept design, provided technical solutions and started a more detailed analysis, but it will not go to the detail required to allow for a CDR or the issue of a Production Master File (PMF).

30.2 Project Design and Development Plan

The PD&D diagram presented in Figure 30.2 shows the phases and activities that have to be performed following the DSE project. It shows the most important activities and reviews stated in the ECSS-M30-A standard [53].

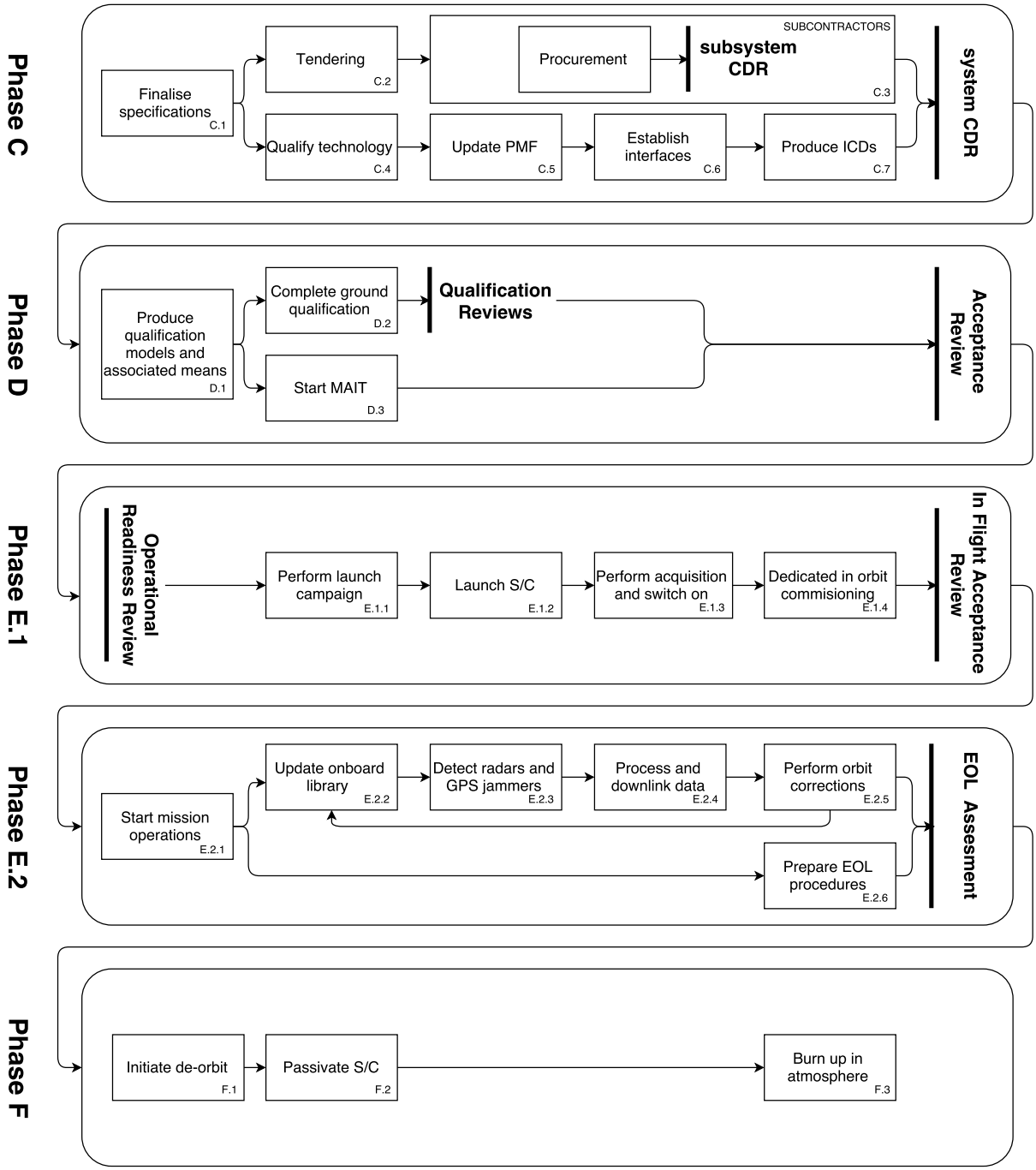

Figure 30.2: The Project Design and Development Plan for the period following the DSE project.

At the start of phase C, the subsystem specifications will be finalised. This has already partially been done, as explained in the previous section. Then subcontractors will be contracted, and they will start their own design program, including a Preliminary Design Review (PDR) and a CDR. If the subcontractors provide COTS products, some of these may be omitted. For brevity only the subsystems' CDR has been presented in Figure 30.2, while in Figure 30.3 the entire phase has been substituted by one entry in the Gantt chart. In the mean time, on the system level, the PMF and Interface Control Documents (ICDs) are issued. Phase D sees simultaneous activities with respect to qualification and MAIT. Phase E.1 comprises the launch campaign, the launch and the in orbit commissioning which has been split in two parts. The first part, acquisition and switch on, checks whether the S/C is still functional. The second part, dedicated in orbit commissioning, takes much longer and can be best described as in orbit validation. Finally, phases E.2 and F are the nominal mission and the EOL procedure. These have been emitted from Figure 30.3 to keep the Gantt chart readable.

Figure 30.3 shows the Gantt chart corresponding to the PD&D. Note how the subsystems' CDR has to be conducted approximately three months before the system CDR to allow for the necessary information and documents to be acquired. Beside the MAIT of the entire system, the subcontractors have to conduct their own MAIT. This has been omitted from both the PD&D and the Gantt chart to maintain the overview. A final note, the three month launch campaign includes not only shipping, but also the month of preparation at French Guiana, which consists of 21 days of preparations after unloading at the port and ten days of common activities carried out by the launch operator [46].

ID	Task Name	Start	Finish	Duration
1	C.1 Finalise Specifications	20-4-2015	20-10-2015	184d
2	C.2 Tendering	20-10-2015	20-11-2015	32d
3	C.3 Procurement	20-11-2015	20-11-2016	367d
4	C.4 Qualify technology	20-11-2015	20-2-2017	459d
5	C.5 Update PMF	20-11-2015	20-2-2017	459d
6	C.6 Establish interfaces	20-11-2015	20-2-2017	459d
7	C.7 Produce ICDs	20-11-2015	20-2-2017	459d
8	CDR	20-2-2017	20-2-2017	0d
9	D.1 Produce qualification methods and associated means	20-2-2017	23-8-2017	185d
10	D.2 Complete ground qualification	20-2-2017	23-8-2017	185d
11	Qualification Reviews	20-2-2017	23-8-2017	185d
12	D.3 Start MAIT	20-2-2017	23-8-2017	185d
13	Acceptance review	23-8-2017	23-8-2017	0d
14	E.1.1 Perform launch campaign	23-8-2017	22-11-2017	92d
15	E.1.2 Launch S/C	22-11-2017	22-11-2017	1d
16	E.1.3 Perform aquisition and switch on	22-11-2017	5-12-2017	14d
17	E.1.4 Dedicated in orbit commissioning	5-12-2017	6-6-2018	184d
18	In Flight Acceptance Review	6-6-2018	6-6-2018	0d

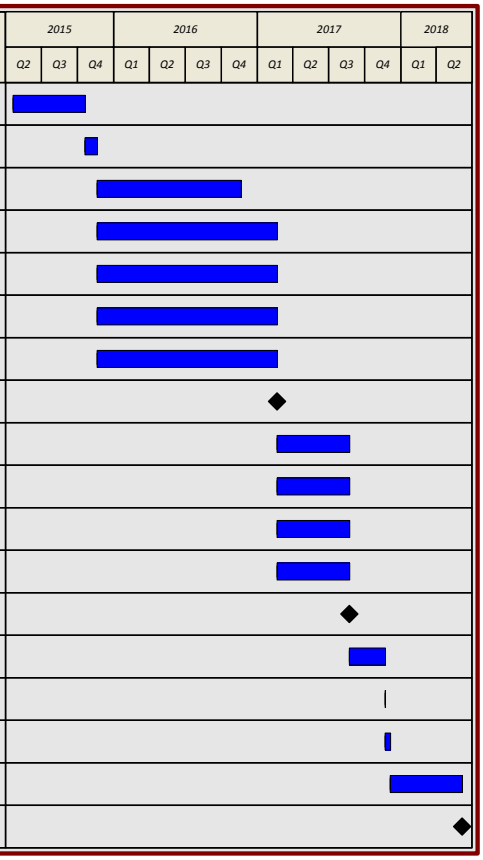

Figure 30.3: The Project Gantt chart for the development following the DSE project.

30.3 Program Cost Breakdown

In this section, a preliminary Cost Breakdown Structure (CBS) is constructed, based on the development proposed above. First, a cost spreading function curve is established [63]. Since the constellation consists of more than two satellites, Equation 30.1 applies [63]. In this cost spreading equation, $F(S)$ is the fraction of cost consumed and S the fraction of total time consumed.

$$F(S) = (10 + S(6S - 15))S^3 \tag{30.1}$$

Using this cost spreading equation and the schedule from the project Gantt chart as presented in Chapter 30, the total cost estimate from Section 24.3, which is approximately € 90 million , is divided over the different project phases C, D and E1, which are shown in Figure 30.3. This breakdown is illustrated in the CBS in Figure 30.4.

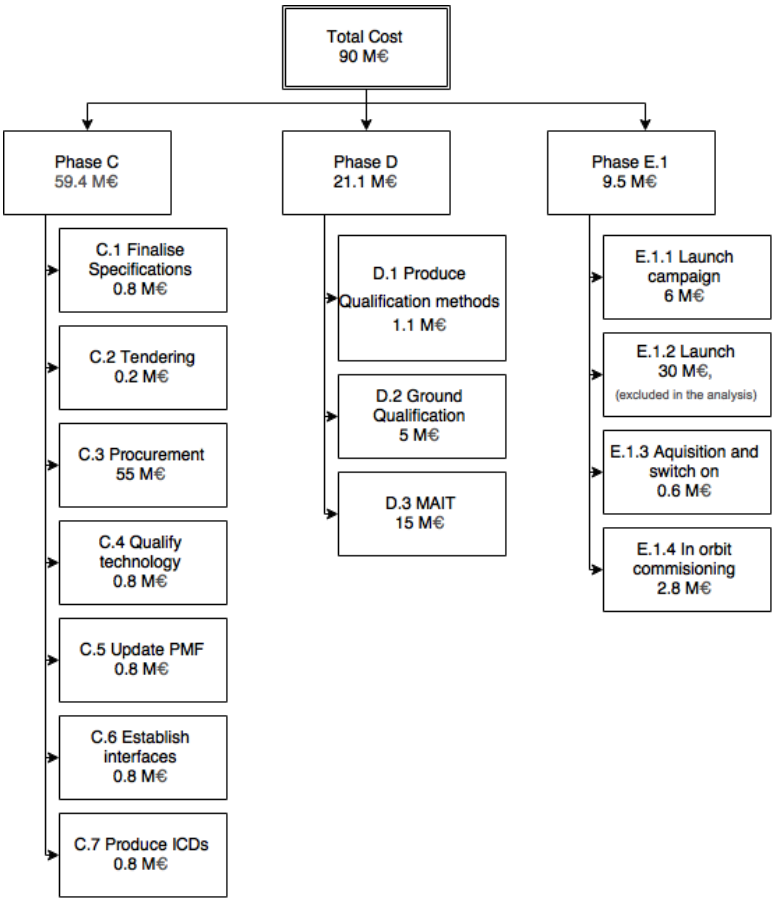

Figure 30.4: Cost breakdown structure.

31 | Market Analysis

This chapter focuses on the market to which this project is dedicated. First of all it describes the general characteristics of the market. After that it looks into the contribution this project offers to this market. Finally it presents the expected development of the market.

General Market Definition
The market under consideration consists in the first place of the RNLAF as this project was inspired by a specific request from the RNLAF. Consequently this project will generate an on-demand, single-use design. As such the market is very restricted. The market could be expanded by considering alternative ways to generate return on investment. Possibilities include offering the constellation's services to other North Atlantic Treaty Organisation (NATO) members.

However, in a more general sense, all small NATO members' MoDs who want to invest in an independent, space based intelligence infrastructure, belong to this market. If the RNLAF succeeds in creating a low cost satellite intelligence mission, this technology can be shared between NATO members to reduce the structural shortage of intelligence capabilities within NATO.

Project Contribution Analysis
The contribution of this project can be split into two main parts. First of all, this project generates an evaluation of the feasibility of creating a low cost, space based intelligence infrastructure. The information generated in this phase serves the market in a broader sense, as the information can be extrapolated to multiple conceptual missions.

The second phase of the project aims at creating a conceptual design for the specific mission the RNLAF requested. This information mainly serves the market in its more restricted notion.

Future Market Development
The potential for using smallsat systems for military applications and surveillance has grown over the past years. The main reasons for this include the shorter development time and the associated reduction in costs. And the potential for the future is still increasing. The reason for this is the increase in technological development focused at smallsat systems. The National Aeronautics and Space Administration (NASA) has invested in the development of special smallsat technology, to increase the potential of smallsat systems for the government and the commercial market. The main obstacle for these systems at this moment is the lack of small launchers that can provide fast and low cost launch capabilities [64].

32 | Risk Analysis

This chapter elaborates on the risk analysis and risk management aspects associated with the presented design. In the first part of this chapter the focus is to explain the methods used, while the second part gives a description of the risks. At this stage of the design only a qualitative assessment of uncertainties is made.

32.1 Risk Identification and Classification

To find the risk associated with the project a brainstorm approach was used. This mainly revealed risks associated with the top level requirements and constraints. Risks that originated from certain aspects of the design had to be reported as they showed up.

To classify the risks they were first identified as either treats or as opportunities. Threats are identified by Arabic numerals while opportunities are identified by Roman numerals. Risks are also labelled using a system identifying the origin of the threat.

The risks were then ordered in a risk map, showing the severity and probability of occurrence of the risk. Due to the fact that the design is still in an early stage, the estimates of impact and probability of occurrence are kept general. The risk map can be consulted in Figure 32.1. Note that the numbers correspond to the numbers displayed in Figure 32.1.

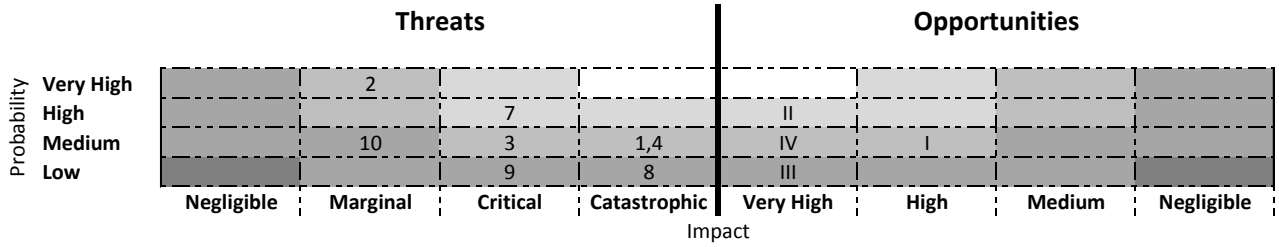

Figure 32.1: Risk map of threats and opportunities derived from the mission statement and top level requirements.

32.2 Risk Response and Mitigation

Multiple possible strategies are available to address risks. Threats can either be avoided, transferred, reduced, or accepted. Avoiding implies adjustment of the project, transferring is done by moving responsibilities to a third party, reducing requires measures that reduce either the impact, the probability of occurrence or both. Accepting the risk on the other hand does not require actions. Opportunities are treated differently. They can be shared, for example with stakeholders, to maximise the benefit. They can be exploited, this requires adjustment of the project. On the other hand it is possible to make a plan to enhance the benefit only when it happens to occur. Finally it is possible to do nothing and to accept the opportunity as it comes.

32.3 Project Related Risks

In Table 32.1 the remaining risks are displayed. It shows their registration number, the nature of the risk, a small description of the risk, the proposed mitigation strategy, and an explanation of the chosen strategy. As can be seen, several risks were deleted. Threat 5 was the dependency on WGS relay for ISL and risk 6 was a unexpected change in requirements. Both were deleted from the risk registry at the moment the concept was selected. The concept did not use WGS and at the MTR the requirements were fixed. Besides that that there were three opportunities removed. Opportunity I was to use piggyback launches. However it was decided to use a shared launch, giving the same benefit, namely cost reduction, but allowing the customer to stay in control with respect to the designated orbit. The second deleted opportunity, II, was to use the constellation for Search and Rescue (SAR). However, the costumer decided that it was not worth pursuing as the RNLAF has sufficient SAR capabilities. Finally, former opportunity IV was to use the constellation to detect radar footprints. This opportunity was ruled out as the feasibility study showed that this was impossible given the constraint on the downlink capacity.

Table 32.1: Overview of the risk identified for the project.

No.	Threat	Impact description	Method	Risk management description
1	Loss of S/C	The constellation will require 4 S/C to meet the geolocation accuracy requirements.	Accept	It is too costly to launch extra S/C for redundancy. Critical systems shall be made as redundant as possible.
2	Exceeding budget	The constellation will not be launched or launch will be delayed.	Accept	It is certain that the cost constraint will not be met. The cost shall be kept to a minimum nevertheless.
3	Failed antenna design	If the antennas do not meet the requirements, the geolocation accuracy cannot be met.	Reduce	Technical experts will be consulted during design.
4	Failed localisation of targets	If the targets are not localised properly, the mission does not fulfil the need.	Reduce	Technical experts will be consulted during design. V&V strategies will be proposed to test the antenna when built.
7	ITAR regulation	If ITAR components are used, the increase in regulations will delay the program	Avoid	The mission will be designed using non ITAR regulated components.
8	Shared antenna for uplink and ISL	If the antenna fails, both uplink and ISL will be unavailable. Consequently no GPS jammers cannot be detected and no software updates can be performed	Reduce	Make a redundant design.
9	Orbit injection error	Deviations in the real and designed orbit may decrease the attainable geolocation accuracy	Reduce	The propulsion system will include enough propellant to compensate for expected orbit injection errors.
10	Launcher availability	A large segment of the launchers on the market do not belong to NATO members or close allies. This could impact the launch schedule.	Transfer	The group will suggest a launcher and launch site but the responsibility will be with the RNLAF.
No.	Opportunity	Impact description	Method	Risk management description
III	Modular bus design	A modular design will allow to add different payloads to the designed bus reducing development of new ELINT missions.	Accept	This possibility, if feasible, can add value to the design. The interest of the customer shall be determined, but unless the customer requests otherwise, this will not be accounted for in the design.

33 | Sustainability

The sustainability of space missions is of growing importance. Throughout the years, awareness has grown on the dangers of the space environment, such as space debris, as well as the effects of greenhouse gases and material disposal. In this chapter, different options are explored that would improve the overall degree of sustainability of a space mission. As can be seen in Figure 33.1 the mission is divided in five elements: production, launch, operations, disposal and spacecraft elements. Each of these five elements are described in a subsection in this chapter.

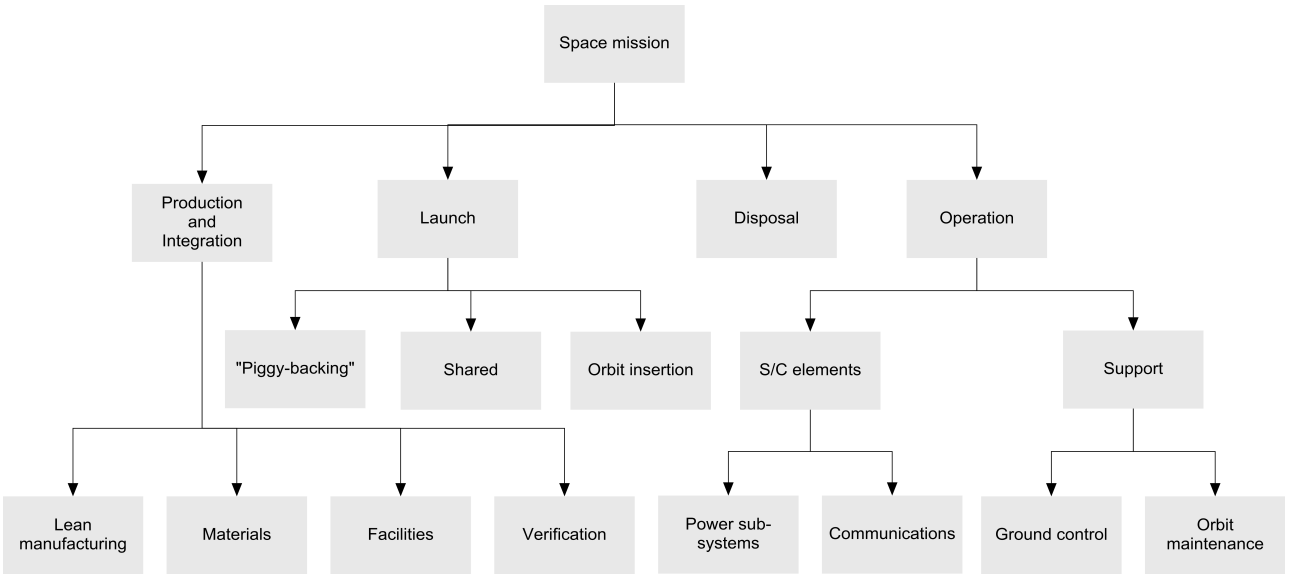

Figure 33.1: Mission breakdown with respect to sustainability.

33.1 Production

The production of the spacecraft is the largest segment that takes place entirely on Earth. Reducing the environmental footprint of this segment will greatly contribute to the overall sustainability of the mission. The production segment has been split into the following parts: materials, processes and facilities. These will be discussed hereafter.

- Materials: When considering the materials that will be used it is important to consider the availability of the materials and try to use as little rare materials as possible. To reduce the environmental impact during and directly after manufacturing the materials should preferably be non-toxic to humans and the environment. To minimise the amount of material wasted during production processes it is preferred to make use of recyclable materials. To ensure sustainability of the mission itself the materials used in the satellites should be able to resist the harsh space environment. At the end of the satellite life, the materials should release as little toxic burn products as possible during re-entry.

  It should be noted that during recycling processes material properties often deteriorate. This means that scrap may not be reusable for space applications but only for sale to other parties. Another important point is that the mechanical properties of materials will probably be more important than toxicity, thus if multiple materials have appropriate mechanical properties the least toxic can be selected.

- Processes: One of the most important aspects of sustainability in manufacturing processes is the elimination of waste, both in a material and immaterial sense. This can be done by implementing a lean manufacturing mindset. Choosing the right methods of manufacturing parts, together with the recyclability of scrap material can reduce the waste of materials. The time required for production might be minimised through the careful implementation of concepts such as Time and Concurrent Manufacturing [65]. The S/C primary structure is designed using composites. This shall not only reduce weight, but also reduce the amount of wasted materials. Composites are build using addition manufacturing and thus less resources are used compared to machining.

- Facilities: To reduce environmental footprint of the facilities required for the production an effort should be made to make use of existing infrastructure whenever possible. In case new facilities have to be built, these should be as environmentally friendly as possible. Furthermore, to reduce emission due to transportation of parts between facilities it could be beneficial to do the production at one site or at sites that are close together.

33.2 Launch

In order to make the launch more sustainable a shared launch has been chosen. All four S/C will be launched using one launcher. The plane changes will be performed by Vega to limit the required on board propellant for the S/C. The weight of the S/C shall also be kept as low as possible to conserve propellant for the launcher and reducing harm full emissions into the atmosphere.

33.3 Operations

Increasing the operational sustainability is achieved by increasing the level of automation of the satellite. An automated satellite requires less frequent and smaller communication with the ground stations, reducing the required surface area of the antennas, the power use of the communications subsystem and the ground system, and the number of operation professionals on the ground [66]. Furthermore, since the workload is decreased, a smaller operations team can track numerous satellites, consequently less human errors are made, improving the efficiency of the mission. To further increase the sustainability of the mission, low thrust electric thrusters were selected. These need longer burn times, but are more efficient.

33.4 Disposal

There are two main parts that have to be considered for the end-of-life disposal of the satellite: de-orbiting and passivisation. Both of these procedures are detailed in Chapter 23.3.

To prevent the constellation from being in its orbit for too long and potentially causing space debris, the S/C are actively deorbited after the end of the mission. This also decreases danger to people on the ground, since the location where the S/C re-enter can be controlled. Since the xenon propellant is not toxic or otherwise harmful for the Earth's environment, there is no need for the S/C to be passivated at the EOL.

33.5 Spacecraft Elements

The spacecraft itself can be divided into separate elements of which the sustainability can be improved. One of the most important systems is the power system. The amount of energy required for the different subsystems determines the energy storage and power generation capacity. Reducing this consumption lowers the overall weight of the satellite, hence making the launch and attitude control more sustainable. One should consider non-toxic materials for the power storage system, since a launch failure could lead to environmental damage.

Looking at the propulsion system, one can directly see that lowering the fuel consumption improves sustainability. Its favourable to have a propulsion system which uses non-toxic propellants and creates no space debris while thrusting. The electric propulsion has a low propellant consumption and uses xenon, which is non-toxic.

The thermal subsystem directly influences the power system. A higher allowable temperature range results in less heating or cooling required. This lowers the power consumption, hence lowers the weight and power consumption of the other subsystems.

The communication system can help lowering the required power and weight by using directional antennas or by distributing the data over a group of satellites. To further optimise this subsystem one can consider data compression, although this might result in higher energy usage by other systems. An additional problem for the communication subsystem is frequency interference[1]. Earth communication and processes can be interrupted by the radio transmission of satellites. To avoid this, one needs to stay in the allocated frequency given by International Telecommunication Union (ITU) regulations[2]. In general, this frequency is in the higher part of the spectrum. One of the benefits is lower transmission power and smaller antennas, but the downside is increased signal attenuation by rainfall.

A final option that needs to be considered is the use of flexible power plans. Not every subsystem needs to be active at all times, and not all activities need the highest possible accuracy.

[1] http://swfound.org/our-focus/space-sustainability/ [Accessed 30/04/2015]
[2] http://www.spectrumwiki.com/wp/allocations101.pdf [Accessed 30/04/2015]

The following list of sustainability improvements should be considered in the design:

- Increase thermal range: possible increase in cost and risk, but large impact on power consumption.
- Non toxic power storage: possible decrease in performance and reliability. Decreased environmental impact in case of launch failure.
- Higher transmission frequency: lower power consumption, but decreased reliability and performance during heavy rainfall near ground station.
- Flexible power plans: more efficient power usage, possible increase in risk and reliability.

All the previously suggested options can contribute to the sustainability of the ELINT mission. However, the mission has a budget constraint. Moreover, sustainable techniques might not be available for certain parts of the mission. Therefore, it is likely that implementing all the proposed sustainable improvements is not possible.

34 | Conclusions

The goal of this project was to study the feasibility of a small satellite constellation with ELINT capability for the RNLAF. A literature study was performed and it was followed by the generation of concepts to perform the mission at hand. After a trade-off, a concept was selected which was worked out in more detail. The result was a preliminary design of an ELINT constellation to which a feasibility study of the requirements set by the RNLAF could be performed. The conclusions drawn from this study are presented in this chapter.

The main conclusion is that the realisation of a constellation of 5-7 small spacecraft with the initial requirements for the geolocation accuracies set by the RNLAF and with a budget constraint of € 25 million is not feasible. An overview of conclusions is given below:

1. The initial budget of € 25 million and the later relaxed budget of € 45 million given by the customer are not sufficient for this mission even when using Commercial Off-The-Shelf components when possible. It is estimated that the cost of development and production is approximately € 88 million, excluding costs of launch and operations.

2. The geolocation of GPS jammers can be done using a Joint Time Difference of Arrival-Frequency Difference of Arrival method and has an accuracy varying between 60 m and 200 m up to 70° latitude. For latitudes higher than 70° the accuracy rapidly deteriorates.

3. It is improbable that multiple satellites in a rectangular formation are able to simultaneously receive the narrow main beams of a radar. This renders the Joint Time Difference of Arrival-Frequency Difference of Arrival method for geolocation of radars virtually useless.

4. To locate radars, the Angle of Arrival method can be used. This requires two mutually perpendicular linear antenna arrays. The initial localisation requirement of 1200 m for radars would drive the design of the system to unacceptable levels, especially considering the cost allocated for this mission. The AOA accuracy to comply with the requirement would be 0.1° which would require two antenna booms of 9.6 m. This yields an antenna design which is too expensive for the allocated cost budget. Therefore, the localisation accuracy was lowered with consent of the RNLAF to bring the payload cost closer to the allocated budget. The new accuracy of the AOA method depends on the elevation of the S/C with respect to the radar and ranges from approximately 1.5 km at high elevation to 5 km at low elevation.

Based on the conclusions given above, in the next chapter some recommendations are made for further investigation by the customer.

35 | Recommendations

In the previous chapter the conclusions were discussed. In this chapter some recommendations are given based on the findings during the project.

1. To decrease the cost of the mission, the requirements on GPS jammer localisation could be loosened, or dropped altogether. Doing this will allow the radar localisation to be performed with just one satellite using the Angle of Arrival method.
2. The constellation's orbital parameters are mainly determined by the requirements imposed by the geolocation algorithms. More coverage would be possible with better antennas, which allow the S/C to orbit at higher altitude with a better view. More S/C in more orbital planes will increase coverage as well, but are costly.
3. For the performance of the payload antennas many assumptions have been used. It is recommended that better antenna designs are investigated to allow for equal or better performance. To do this, the signal characteristics of military radar systems shall be studied in more detail, to determine more optimal antenna properties.
4. Specifications of the signal processing unit have been produced based on a limited literature study. A more thorough investigation of the requirements to operate an Electronic Support Mission in space is required as a basis to develop a suitable payload for the mission.
5. To increase the accuracy of the localisation processes the effects of atmospheric refraction, Earth curvature and signal delay in the ionosphere shall be included in to improve the obtained geolocation accuracy using FDOA and AOA methods.
6. To improve the radar geolocation further, research has to be carried out into the possibility to model frequency hopping. If this can be done, the AOA method can be complemented by the FDOA method.
7. When using Commercial Off-The-Shelf components a strong preference shall be given to components with flight heritage to reduce the risk of unforeseen component failure.
8. The propulsion and AOCS system were designed for a higher system mass. During further iterations in the detailed design it may be possible to decrease the size and mass of these systems.
9. A lot of assumptions have been made in the thermal analysis. Large improvements can be made by expanding the model to incorporate non-homogeneous temperature distribution in side panels, and an increased number of nodes. Furthermore, the analysis did not take into account possible non-nominal operation modes. If the S/C enters into safe mode, the internal temperature will most likely drop below the operational limit. Since additional heaters might become necessary, it is recommended to do further analysis on this. A final recommendation would suggest to use more accurate orbit details and a rotating model of the S/C. This would result in better temperature distribution hence more realistic estimates.

Bibliography

[1] A. de Boer, "Nederlandse stappen richting sterren," *Vliegende Hollander*, Nov. 2014.

[2] J. Klinkenberg, "Space: de logische stap naar het ruimtedomein," *Militaire Spectator*, pp. 83 – 93, Feb. 2015.

[3] T. Benedicto Rinaudo *et al.*, "Signals Intelligence Smallsat Constellation; Low-Cost High-Performance Small Constellation for SIGINT to be Launched by the Royal Netherlands Air Force (Project Plan)," Delft University of Technology, May 2015.

[4] T. Benedicto Rinaudo *et al.*, "Signals Intelligence Smallsat Constellation; Low-Cost High-Performance Small Constellation for SIGINT to be Launched by the Royal Netherlands Air Force (Baseline Report)," Delft University of Technology, May 2015.

[5] T. Benedicto Rinaudo *et al.*, "Signals Intelligence Smallsat Constellation; Low-Cost High-Performance Small Constellation for SIGINT to be Launched by the Royal Netherlands Air Force (Midterm Report)," Delft University of Technology, May 2015.

[6] T. Watts, "Project Guide Design Synthesis Exercise; SIGINT/UHF Smallsat Constellation," Delft University of Technology, Apr. 2015.

[7] E. Gill, "Systems Engineering and Aerospace Design - Systems Engineering Methods," pp. 1–41, Delft University of Technology, Feb. 2015.

[8] Unknown, "Vulnerability Assessment of the Transportation Infrastructure Relying on the Global Positioning System," John A. Volpe National Transportation Systems Center, Office of the Assistant Secretary for Transportation Policy, U.S. Department of Transportation, Aug. 2001.

[9] J. K. Holmes, *Spread Spectrum Systems for GNSS and Wireless Communications*. Boston, MA: Artech House, 1 ed., 2007.

[10] R. H. Mitch *et al.*, "Signal Characteristics of Civil GPS Jammers," in *24th International Technical Meeting of the Satellite Division of the Institute of Navigation*, vol. 3, (Portland, OR), pp. 1907–1919, 2011.

[11] R. H. Mitch *et al.*, "Civilian GPS Jammer Signal Tracking and Geolocation," in *25th International Technical Meeting of the Satellite Division of the Institute of Navigation, ION GNSS*, vol. 4, (Nashville, TN), pp. 2901–2920, 2012.

[12] R. Mitch, M. Psiaki, S. Powell, and B. O'Hanlon, "Signal Acquisition and Tracking of Chirp-Style GPS jammers," 2013.

[13] T. Humphreys *et al.*, "Assessing the Spoofing Threat: Development of a Portable GPS Civilian Spoofer," in *21st International Technical Meeting of the Satellite Division of the Institute of Navigation, ION GNSS*, vol. 2, (Savannah, GA), pp. 1198–1209, 2008.

[14] M. A. Richards, J. A. Scheer, and W. A. Holm, eds., *Principles of Modern Radar*. Raleigh, NC: SciTech Publishing, 2010.

[15] J. R. Wertz, *Space Mission Engineering: The New SMAD*. Hawthorne, CA: Microcosm Press, 2011.

[16] R. G. Wiley, *ELINT The Interception and Analysis of Radar Signals*. Boston, MA: Artech House Publishers, 1 ed., 2006.

[17] Unknown, "JDOP Definition for MEOSAR," Sept. 2013.

[18] D. Mušicki and W. Koch, "Geolocation using TDOA and FDOA Measurements," in *11th Internation Conference on Information Fusion*, (Cologne), pp. 1–8, 2008.

[19] D. Adamy, *EW 102: A Second Course in Electronic Warfare*. Boston, MA: Artech House, 1 ed., 2004.

[20] K. F. Wakker, *Fundamentals of Astrodynamics*. Delft: Delft University of Technology, Jan. 2015.

[21] R. Noomen, "Flight and Orbital Mechanics - Kepler Orbit, Specialized Orbits," pp. 1 – 60, Delft University of Technology, Oct. 2012.

[22] Unknown, "Space Radiation Effects on Electronic Components in Low-Earth Orbit," Johnson Space Center, National Aeronautics and Space Administration, 1996.

[23] M. Pignol, "COTS-based Applications in Space Avionics," in *Design, Automation & Test in Europe Conference and Exhibition*, (Dresden), pp. 1213–1219, 2010.

[24] R. Poisel, *Principles of Electronic Warfare Antenna Systems*. Boston: Artech House, Nov. 2011.

[25] S. E. Lipsky, *Microwave Passive Direction Finding*. Raleigh, NC: SciTech Publishing, 2004.

[26] R. Poisel, *Electronic Warfare Target Location Methods, Second Edition*. Boston: Artech House, 2 ed., 2012.

[27] D. C. Schleher, *Electronic Warfare in the Information Age*. Boston: Artech House Publishers, June 1999.

[28] Unknown, "Attenuation by atmospheric gases," Sept. 2013.

[29] A. Arun and T. Sreeja, "An Effective Downlink Budget for 2.24GHz S-Band LEO Satellites," in *Proceedings of 2013 IEEE Conference on Information and Communication Technologies, ICT*, (JeJu Island), pp. 342–345, 2013.

[30] R. L. Freeman, *Telecommunication System Engineering*. Hoboken, N.J: Wiley-Interscience, 4 ed., 2004.

[31] Unknown, *Electronic Warfare and Radar Systems Engineering Handbook*. United States Navy, Apr. 1999.

[32] D. H. Schaubert and T.-H. Chio, "Wideband Vivaldi Arrays for Large Aperture Antennas," *Perspectives on Radio Astronomy: Technologies for Large Antenna Arrays*, pp. 49–57, 1999.

[33] M. M. Islam, M. T. Islam, M. R. I. Faruque, and W. Hueyshin, "Design of an X-band microstrip patch antenna with Enhanced bandwidth," in *Proceedings of 2013 2nd International Conference on Advances in Electrical Engineering, ICAEE*, (Dhaka), pp. 313–317, 2013.

[34] Unknown, "MATLAB and Statistics Toolbox Release 2015a," 2015.

[35] T. Lavate, V. Kokate, and A. Sapkal, "Performance Analysis of MUSIC and ESPRIT DOA Estimation Algorithms for Adaptive Array Smart Antenna in Mobile Communication," in *2nd International Conference on Computer and Network Technology (ICCNT)*, (Bangkok), pp. 308 – 311, 2010.

[36] M. Patel, *Spacecraft Power Systems*. Boca Raton: CRC Press, 2005.

[37] S. Asif, *Evolutionary computation based multi-objective design search and optimization of spacecraft electrical power subsystems*. PhD thesis, University of Glasgow, 2008.

[38] N. Fatemi, H. Pollard, H. Hou, and P. Sharps, "Solar Array Trades Between Very High-Efficiency Multi-Junction and Si Space Solar Sells," in *Conference Record of the Twenty-Eighth IEEE Photovoltaic Specialists Conference (Cat. No.00CH37036)*, (Anchorage, AK), pp. 1083–1086, 2000.

[39] S. Asif and Y. Li, "Spacecraft power subsystem technology selection," in *2006 IEEE Vehicle Power and Propulsion Conference, VPPC*, (Windsor), 2006.

[40] G. R. Curry, *Radar Essentials: A Concise Handbook for Radar Design and Performance Analysis*. Raleigh, NC: SciTech Publishing, Dec. 2012.

[41] N. Blaunstein and E. Plohotniuc, *Ionosphere and Applied Aspects of Radio Communication and Radar*. Boca Raton: CRC Press, 2008.

[42] S. Cakaj, "Rain Attenuation Impact on Performance of Satellite Ground Stations for Low Earth Orbiting (LEO) Satellites in Europe," *International Journal of Communications, Network and System Sciences*, vol. 02, no. 06, pp. 480–485, 2009.

[43] Unknown, "Integrated On-Board Computer (iOBC) [Personal Communication with G. Colombo]," SSBV, June 2015.

[44] Unknown, "A Satellite Computer Board with optional Mass Memory section (Data Handling) [Personal Communication wit E. Hashem]," DSI Informationstechnik, June 2015.

[45] V. K. Srivastava, Ashutosh, M. Pitchaimani, and B. S. Chandrasekhar, "Eclipse prediction methods for LEO satellites with cylindrical and cone geometries: A comparative study of ECSM and ESCM to IRS satellites," *Astronomy and Computing*, vol. 2, pp. 11–17, 2013.

[46] E. Perez, "Vega User's Manual," No. 3, (Courcouronnes), p. 188, Arianespace, Mar. 2006.

[47] Unknown, "Torquer R10 [Personal Comminucation with M. Pastena]," SSBV, June 2015.

[48] M. Grassi and M. Pastena, "Attitude Acquisition for an Earth Observation Microsatellite," in *48th International Astronautical Congress*, (Turin), 1997.

[49] R. P. Welle, "Propellant Storage Considerations for Electric Propulsion," in *22nd International Electric Propulsion Conference, AIAA-91-2589*, (Viareggio), 1991.

[50] S. S. Pietrobon, "Analysis of Propellant Tank Masses," 2009.

[51] J. J. Wijker, *Spacecraft Structures*. Berlin: Springer, 2008 ed., 2008.

[52] Unknown, "Launch Vehicle Catalogue," European Space Agency, Dec. 2004.

[53] Unknown, "Space Project Management; Project Phasing and Planning," Apr. 1996.

[54] L. Lillard, I. Evans, H.E., and J. Spaulding, "Minimum Variance Missile Launch and Impact Estimation by Fusing Observations From Multiple Sensors," in *1997 IEEE Aerospace Conference*, vol. 3, (Snowmass at Aspen, CO), 1997.

[55] S. R. Starin and J. Eterno, "Attitude Determination and Control Systems," in *Space Mission Engineering: The New SMAD* (J. R. Wertz, ed.), Microcosm Press, 2011.

[56] Unknown, "Guide to the Identification of Safety-Critical Hardware Items for Reusable Launch Vehicle (RLV) Developers," American Institute of Aeronautics and Astronautics, May 2005.

[57] E. Gill and T. Hoevenaars, "Systems Engineering and Aerospace Design - Verification and Validation for the Attitude and Orbit Control System," Delft University of Technology, Feb. 2015.

[58] Unknown, *NASA Systems Engineering Handbook*. National Aeronautics and Space Administration, 2007.

[59] W. Ley, K. Wittmann, and W. Hallmann, *Handbook of Space Technology*. Chichester: John Wiley & Sons, 2009.

[60] J.-L. Suchail, A. Popovitvh, and P. Laget, "Maxwell, the ESA-ESTEC New Large EMC Facility," June 2013.

[61] Unknown, "Systems Tool Kit 10," 2012.

[62] Unknown, "MATLAB and Statistics Toolbox Release 2012b," 2012.

[63] W. J. Larson and J. R. Wertz, eds., *Space Mission Analysis and Design*. Torrance, CA: Microcosm, Inc, 2 ed., 1992.

[64] J. Foust, "Emerging Opportunities for Low-Cost Small Satellites in Civil and Commercial Space," in *24th Annual AIAA/USU Conference on Small Satellites*, (Logan, UT), pp. 1–7, 2010.

[65] J. Sinke, *Production of Aerospace Systems - Reader*. Delft University of Technology, Feb. 2015.

[66] M. Soares *et al.*, "An Approach for Automation the Aatellite of Routine's Operation and Procedures," in *13th International Conference on Space Operations*, (Pasadena, CA), 2014.

Part VI

Appendices

A | Technical Requirements Specification

A.1 General Requirements (GEN)

GEN-01 The constellation shall consist of 5 to 7 S/C.

GEN-02 The constellation shall be capable of accommodating extra S/C.

GEN-03 Each S/C shall meet the requirements specified by the launcher.

- GEN-03-F01: The S/C shall withstand the mechanical loads during launch.
- GEN-03-C01: Each S/C shall fit within a cylinder of 1 m length and 1 m diameter.
- GEN-03-C02: The maximum weight of each S/C shall be 200 kg.

GEN-04 The mission shall have a minimum lifetime of five years.

GEN-05 The maximum cost of the mission shall be € 45 million, excluding launch and operations costs.

GEN-06 The launch window of the mission is between 2017 and 2019.

GEN-07 The satellites shall be removed from orbit no later than 25 years after end of mission.

GEN-08 Intercepted RF signals shall be processed to identify target signals.

- GEN-08-F01: A library of target signals shall be available for the constellation and ground operations system.
- GEN-08-F02: Target signals shall be identified by matching with the signal library.
- GEN-08-F03: The signal library shall be updatable.

A.2 Payload Requirements (PAY)

PAY-01 The constellation shall detect RF signals in the 1-4 GHz and 8-12 GHz bands.

PAY-03 RF signal sources shall be located with an accuracy better than 5000 m.

PAY-04 The constellation shall detect GPS jammers with an EIRP of 40 mW.

PAY-05 GPS jammer positions shall be determined with an accuracy better than 200 m.

A.2.1 Antenna Array Requirements

PAY-06 The antenna array shall provide AOA with an accuracy of 0.4° (1σ) for a viewing angle of ±30° off-boresight.

PAY-07 The antenna array shall accommodate for unambiguous results for the AOA algorithm.

PAY-08 Each L-band antenna element shall have at least −1 dBi gain in the entire L-band, for a viewing angle of ±30° off-boresight.

PAY-09 Each S-band antenna element shall have at least 0 dBi gain in the entire S-band, for a viewing angle of ±30° off-boresight.

PAY-10 Each X-band antenna element shall have at least 1 dBi gain in the entire X-band, for a viewing angle of ±30° off-boresight.

PAY-11 The antenna array structure shall not be effected by thermal expansion.

PAY-12 The antenna element placement shall be precise within 1 mm.

PAY-13 The antenna boom placement shall be 90°, with an accuracy of 1°.

PAY-14 The antenna array shall not be influenced by the TT&C.

PAY-15 The error in frequency detection shall be less than 0.38 Hz.

A.3 Constellation Geometry Requirements (CON)

CON-01 The orbit altitude shall be 500 km.

CON-02 The orbit geometry shall enable the S/C formation to be in view of a ground station on Dutch soil at least once every 6.5 hours.

CON-03 The orbit geometry shall provide global coverage for the GPS jammer localisation.

CON-04 The orbit geometry shall provide global coverage for the radar signal localisation.

CON-05 The orbit geometry shall be such that the minimum in-plane distance between S/C is 500 km.

CON-06 The orbit geometry shall be such that two orbital planes are at least 6° apart at the equator.

CON-07 The orbit geometry shall be such that the S/C nominal orbits do not collide.

A.4 Launcher Requirements (LCH)

LCH-01 The launcher shall be able to lift 648 kg into a 500 x 500 km orbit at 100° inclination.

LCH-02 The launcher shall be able to carry four S/C in one launch.

LCH-03 The S/C shall be separated from the launcher in 3-axis stabilisation mode.

LCH-04 The launch date shall be compliant with GEN-06.

LCH-05 The launcher shall be able to perform a plane change of 6° at 500 km altitude.

A.5 Telemetry, Tracking, and Command Requirements (TTC)

A.5.1 General Requirements

TTC-01 The TT&C subsystem shall receive and demodulate telecommands, modulate and transmit telemetry data, and transpond the ranging signal.

- TTC-01-F01: The TT&C subsystem shall be capable of simultaneously handling telemetry, telecommands, and ranging.
- TTC-01-F02: The TT&C subsystem shall accept uplink signals and provide a demodulated telecommand signal to the C&DH subsystem for further processing.

TTC-02 The TT&C subsystem shall interface exclusively with ground stations on Dutch soil.

- TTC-02-C01: The TT&C subsystem shall use the S-band to transmit payload data and housekeeping data to the ground stations.
- TTC-02-C02: The TT&C subsystem shall use the UHF-band to receive telecommands from the ground station.

TTC-03 The TT&C subsystem shall interface with the other S/C in the constellation.

- TTC-03-C01 : The TT&C subsystem shall use the UHF-band to communicate with the other S/C in the constellation.

TTC-04 The TT&C subsystem shall use TDMA for the uplink and crosslinks.

TTC-05 The TT&C subsystem shall have no requirements for telemetry operation during the launch phase.

A.5.2 Performance Requirements

TTC-06 The TT&C subsystem shall provide the telecommand capabilities in any of the S/C attitudes, at an elevation of at least 10° above the horizon, in any weather conditions.

TTC-07 The TT&C subsystem shall provide the telemetry capabilities at an elevation of at least 10° above the horizon, in any weather conditions.

TTC-08 The TT&C subsystem shall provide a downlink data rate of at least 105 kbps on the S-band.

TTC-09 The TT&C subsystem shall provide a crosslink data rate of 4800 bps on the UHF-band.

TTC-10 The TT&C subsystem shall provide an uplink data rate of 4800 bps on the UHF-band.

TTC-11 The TT&C subsystem shall provide a maximum BER which is better than 10^{-6} on all communications links.

TTC-12 The TT&C subsystem shall have a link margin of at least 10 dB to account for any unexpected attenuations in any of the telecommunications links.

A.5.3 Design Requirements

TTC-13 The TT&C subsystem shall be redundant.

- TTC-13-F01: The TT&C subsystem shall provide hot redundancy for the receiving function when the ground station is in view.
- TTC-13-F02: The TT&C subsystem shall provide cold redundancy for the transmit function during the entire orbit.

TTC-14 The UHF transceivers shall provide a low data rate backup downlink.

TTC-15 The TT&C subsystem shall be able to perform all uplink- and downlink communication during the up- and downlink opportunities provided by the constellation geometry.

A.6 Command and Data Handling Requirements (CDH)

A.6.1 General Requirements

CDH-01 The C&DH subsystem shall decode, validate and distribute telecommands acquired from the TT&C subsystem.

CDH-02 The C&DH subsystem shall acquire telemetry data and format it for transmission by the TT&C subsystem.

CDH-03 The C&DH subsystem shall distribute commands to other subsystems.

CDH-04 The C&DH subsystem shall be able to store software, payload data and housekeeping data.

CDH-05 The C&DH subsystem shall supervise the on-board autonomy.

CDH-06 The C&DH subsystem shall be capable of compressing data.

CDH-07 The C&DH subsystem shall be able to encrypt telemetry data and decrypt telecommands.

CDH-08 The C&DH subsystem shall manage and distribute a time signal.

CDH-09 The C&DH subsystem shall accommodate all interfaces required by the various subsystems.

A.6.2 Performance Requirements

CDH-10 The C&DH subsystem shall have error detection and correction for the Random Access Memory (RAM).

CDH-11 The C&DH subsystem shall have sufficient amounts of storage to store the software, payload data, and housekeeping data.

CDH-12 The C&DH subsystem shall have a low power mode.

A.6.3 Design Requirements

CDH-13 The C&DH subsystem shall not need to download any data to be functional after start up.

A.7 Structural Requirements (STR)

A.7.1 General Requirements

STR-01 The S/C fundamental frequencies shall be different from those of the launcher.

STR-02 The S/C shall have a fundamental frequency in longitudinal direction between 20 and 45 Hz or more than 60 Hz.

STR-03 The S/C shall have a fundamental frequency in lateral direction greater than 15 Hz.

A.7.2 Performance Requirements

STR-04 The structure of the S/C shall be capable of withstanding the loads induced by the launcher during launch.

STR-05 The S/C structure shall be capable of withstanding the loads induced during ground handling before launch.

STR-06 The S/C structure shall be capable of withstanding loads encountered during in orbit operation.

A.7.3 Design Requirements

STR-07 The S/C structure shall not hinder access of ground support equipment to on-board instruments.

STR-08 All component connection contact areas shall be made of three types of material with thermal conductivities of 0.25, 55 and 105.5 $W\,m^{-1}\,K^{-1}$.

STR-09 The S/C structure shall have a thermal conductivity of at most 105.5 $W\,m^{-1}\,K^{-1}$

A.8 Thermal Requirements (TML)

TML-01 The thermal subsystem shall maintain a propellant temperature of at least 17°C at all times.

TML-02 The thermal subsystem shall maintain a temperature range between −20°C and 50°C for the internal parts of the propulsion system.

TML-03 The thermal subsystem shall maintain a temperature range between −40°C and 55°C for the Payload ESM Unit.

TML-04 The thermal subsystem shall maintain a temperature range between −20°C and 65°C for the battery.

TML-05 The thermal subsystem shall maintain a temperature range between −20°C and 50°C for the transmitter.

TML-06 The thermal subsystem shall maintain a temperature range between −100°C and 150°C for the solar panels.

A.9 Attitude and Orbit Control System Requirements (AOC)

A.9.1 General Requirements

AOC-02 The AOCS shall provide hardware and associated on-board software to acquire, control and measure the required spacecraft attitude during all phases of the mission.

AOC-03 The AOCS shall accept ground or on-board telecommands to perform attitude and orbit manoeuvres.

AOC-04 The AOCS shall provide attitude measurement data via telemetry to the ground for attitude reconstitution.

AOC-05 The AOCS shall provide information via telemetry to ground to allow diagnosis of on-board failures.

AOC-06 The AOCS shall perform autonomous attitude adjustment manoeuvres required by the mission operations during periods when ground contact is not available or ground response times are inadequate.

AOC-07 The AOCS shall provide an autonomous Sun-pointing safe mode to ensure the spacecraft systems survival with respect to their thermal environment, and to guarantee power generation.

AOC-08 The AOCS shall be able to perform nominal operations for the minimal lifetime of the mission as specified in GEN-04.

A.9.2 Control Mode Requirements

AOC-09 The AOCS shall provide the required attitude determination and control during acquisition mode.

- AOC-09-F01: Upon separation from the launcher interface the AOCS shall damp out the residual angular rates and acquire the Sun along a specific spacecraft axis before the batteries are depleted.
- AOC-09-F02: After Sun acquisition, the AOCS shall provide stable 3-axes attitude control before and after solar array deployment and during the deployment of the antennas.
- AOC-09-F03: The AOCS shall be able to reacquire Sun pointing attitude and realign solar arrays to the Sun from any initial orientation after initial Sun acquisition, solar array deployment and other acquisition mode activities.

AOC-10 The AOCS shall provide the required attitude determination and control during orbit insertion mode.

AOC-11 The AOCS shall provide the required attitude determination and control during normal mission mode.

- AOC-11-F01: During normal mission mode, the AOCS shall be compliant with the pointing requirements specified in Section A.9.4.
- AOC-11-F02: During normal mission mode, the absolute position knowledge error of the satellite shall not exceed 10 m.

AOC-12 The AOCS shall provide the required attitude determination and control during slew mode.

- AOC-12-F01: The AOCS shall be capable of slewing the payload's line of sight, over 40° while above 80° latitude.

AOC-13 The AOCS shall provide the required attitude determination and control during safe mode.

- AOC-13-F01: Spacecraft shall autonomously manoeuvre into a pre-defined safe mode on determination of an unsafe situation on-board. This autonomous functionality may be disabled by ground command during certain critical manoeuvres.

A.9.3 Design Requirements

AOC-14 The AOCS shall be fully functional at start up after separation.

AOC-15 The attitude control shall be a closed loop design for all three axes in all mission phases.

AOC-16 All attitude control and measurement functions shall be redundant.

AOC-17 The AOCS software shall be reprogrammable in flight.

AOC-18 The AOCS shall transmit via telemetry unambiguous status information of all command and programme controlled variables, modes and of all parameters required for subsystem monitoring and evaluation and for reconstitution on ground of the attitude and attitude control manoeuvres.

AOC-19 The AOCS shall contain a redundant safe mode to recover from any initial attitude at any time in the mission, to guarantee uninterrupted adequate solar power supply and thermal control.

AOC-20 The AOCS shall not include a single point of failure.

A.9.4 Pointing Requirements

AOC-21 The absolute pointing error of the thrust vector during orbital manoeuvres shall be minimal.

AOC-22 The spacecraft shall keep the solar arrays Sun pointing after solar array deployment and initial Sun acquisition apart from preselected periods.

AOC-23 The absolute pointing error of the solar array rotation axis shall not exceed 1°.

AOC-24 The absolute pointing error of the X-band payload antennas during ELINT gathering shall not exceed 1° half cone angle.

AOC-25 The absolute pointing error of the L- and S-band payload antennas during ELINT gathering shall not exceed 1° half cone angle.

AOC-26 The absolute pointing error of the S-band TT&C antenna during downlink communications shall not exceed 60° half cone angle.

AOC-27 The absolute pointing error of the L-band payload antennas during GPS jammer detection and localisation shall not exceed 1° half cone angle.

AOC-28 The absolute pointing error of the UHF-band TT&C antenna during uplink and ISL communications shall not exceed 90° half cone angle.

AOC-29 The absolute pointing knowledge error of the L- and S-band antenna during ELINT gathering shall not exceed 0.04° half cone angle.

AOC-30 The AOCS will provide stability and momentum control for orbit maintenance during 720 s per orbit.

AOC-31 The GPS will provide the velocity with an accuracy of 0.57 $ms^{-}1$

AOC-32 The GPS will provide the time with an accuracy better than 38 μs.

A.10 Propulsion Requirements (PRO)

PRO-01 The propulsion subsystem shall provide the capability to maintain orbit at an altitude of 500 km.

PRO-02 The propulsion subsystem shall be able to correct any errors in orbit injection.

PRO-03 The propulsion subsystem shall be able to perform its tasks for the duration of the mission and the in orbit commissioning.

PRO-03-F01: There shall be enough propellant to perform the mission for the duration of the mission and the in orbit commissioning.

PRO-03-F02: The components used in the propulsion subsystem shall have a lifetime of the duration of the mission and the in orbit commissioning.

PRO-05 The thruster(s) shall cause no electrical interference with other subsystems.

PRO-07 The propellant tank shall be sized large enough to allow for a 20% increase in volume of the propellant.

PRO-08 The thruster and propellant tank placement shall take into consideration the structural parameters of the spacecraft.

PRO-12 The propulsion subsystem shall provide the capability to actively de-orbit the S/C at EOL.

A.11 Power Requirements (PWR)

PWR-01 The power subsystem shall provide all power required by the satellite during all mission phases and for all operation modes through the entire duration of the mission.

PWR-02 The power shall be provided by means of both solar cell array and batteries.

PWR-03 The solar cell array shall be sized with 5% margin for the worst case power situation and provide power up to the end of mission.

PWR-04 The power subsystem shall condition, control, store and distribute electrical power on the spacecraft.

PWR-05 The subsystem shall provide adequate status monitoring and telecommand interfaces necessary to operate the subsystem and permit evaluation of its performance.

PWR-06 The subsystem shall provide adequate failure tolerance and protection circuitry to avoid failure propagation and to ensure recovery from any malfunction within the subsystem and/or load failure.

PWR-07 The power subsystem shall contain all necessary electronics.

PWR-07-F01: The power subsystem shall contain all electronics necessary to provide electrical power from the solar cell generator and/or batteries to all users.

PWR-07-F02: The power subsystem shall contain all electronics necessary to charge, discharge and recondition all batteries.

PWR-07-F03: The power subsystem shall contain all electronics necessary to give the capability for automatic and commanded control of the operation of the subsystem.

PWR-07-F04: The power subsystem shall include all power switching and protection electronics for all spacecraft subsystem users.

PWR-08 The power subsystem shall meet the requirements for average and peak power electrical loads.

A.11.1 Power Conditioning and Distribution

PWR-09 The subsystem shall be capable of operating continuously under all operational conditions of the mission.

PWR-10 The subsystem shall be designed such:

PWR-10-F01: that in all operating modes where the power available from the solar cell generator exceeds the main bus and battery charge demands the surplus of electrical energy is left in the solar arrays.

PWR-10-F02: that in all operating modes where the power demanded from the main bus exceeds the available power from the solar cell generator, the battery charging will be stopped and the solar cell generator is operated in its maximum power point.

PWR-10-F03: that in all operating modes where the power available from the solar cell generator is still insufficient to satisfy the load demand, battery discharge regulators will provide required electrical power from batteries automatically.

A.11.2 Main Bus

PWR-11 No single component failure shall cause an over-voltage or permit short circuit on the main bus.

A.11.3 Batteries

PWR-12 The batteries shall be sized to cover all nominal spacecraft demand during the entire duration of the mission in cases of insufficient or no solar generator power.

PWR-13 The batteries shall be sized to cover all power demands after separation from the launcher until the solar arrays are deployed.

PWR-14 A maximum DOD of 45% in nominal cases shall not be exceeded.

A.12 Harness Requirements (HAR)

A.12.1 General Requirements

HAR-01 The harness shall provide distribution of cabling for power, signals, and data.

A.12.2 Performance Requirements

HAR-02 The harness shall transmit electrical currents in a way that is compatible with both the source and destination.

A.12.3 Design Requirements

HAR-03 Redundant wires shall be routed differently.

HAR-04 The wire-to-pin interfaces shall be covered.

HAR-05 The harness connectors shall be easily accessible, attachable, and removable from the corresponding connectors.

HAR-06 The harness shall be designed such as to minimise the S/C residual dipole moment.

A.13 Requirement Changelog

During the course of this project, some requirements have changed. To keep track of these changes, a changelog has been created. The changelog contains the date on which the change has been made, the old and new requirement code, and the new and old requirement descriptions. If a requirement is slightly changed or appended, it can keep its original requirement code. However, if a requirement is fundamentally changed, it should get a new code. Care will be taken that requirement codes will not be reused during the course of the project.

Table A.1: Requirement changelog.

Date	Old code	New code	Old description	New description
28-04-15	**PAY-05**	**PAY-05**	Jammer position shall be determined with an accuracy better than 1200 m.	GPS jammer positions shall be determined with an accuracy better than 200 m.
29-04-15	**PAY-01**	**PAY-01**	The constellation shall detect RF signals in the 8-12 GHz band.	The constellation shall detect RF signals in the 1-4 GHz and 8-12 GHz bands.
30-04-15	**AOC-02**	**ORB-03**	The position of each S/C should be determined with *To Be Determined (TBD)* accuracy.	The position of each S/C should be determined with *TBD* accuracy.
08-05-15	**PAY-04**	**PAY-04**	The constellation shall detect GPS/Galileo jammers with a power of *TBD* W.	The constellation shall detect GPS jammers with a EIRP of *TBD* W.
08-05-15	**GEN-05**	**GEN-05**	The maximum cost of the mission shall be € 25 million, excluding launch costs.	The maximum cost of the mission shall be € 45 million, excluding launch and operations costs.
13-05-15	**PAY-02**	**GEN-08**	The constellation shall process the detected RF signals. • PAY-02-F01: Constellation will include a library of target signals. • PAY-02-F02: The constellation shall have *TBD* GB of date storage available for the signal library. • PAY-02-F03: The signal library shall be updatable. • PAY-02-F04: Detected signals shall be identified by matching with the signal library.	Intercepted RF signals shall be processed to identify target signals. •GEN-08-F01: A library of target signals shall be available for the constellation and ground operations system. • GEN-08-F02: Target signals shall be identified by matching with the signal library. • GEN-08-F03: The signal library shall be updatable.

13-05-15	**COM-01**	**-**	The satellites shall be able to communicate with each other. • COM-01-F1: Inter-satellite communication shall be encrypted using *TBD* encryption. • COM-01-F2: Inter-satellite communication shall have *TBD* bitrate.	Removed
18-05-15	**AOC-01**	-	The AOCS shall provide a pointing accuracy of *TBD*°.	Removed
27-05-15	**PAY-03**	**PAY-03**	RF signal sources shall be located with an accuracy better than 1200 m.	RF signal sources shall be located with an accuracy better than 5000 m.
29-05-15	**AOC-12-F02**	-	AOC-12-F02: The AOCS shall be able to slew 360° within *TBD* seconds.	Removed
08-06-15	**AOC-xx**	**AOC-xx**	Attitude Determination and Control Subsystem Requirements	Attitude and Orbit Control Subsystem Requirements
08-06-15	**ORB-01**	**CON-01**	The orbit altitude shall be no greater than 650 km.	The orbit altitude shall be 500 km.
08-06-15	**ORB-02**	**PRO-01**	The orbit shall be maintained during the lifetime of the S/C.	The propulsion subsystem shall provide the capability to maintain orbit at an altitude of 500 km.
08-06-15	**ORB-03**	**AOC-11-F02**	The position of each S/C should be determined with TBD accuracy.	During normal mission mode, the absolute position knowledge error of the satellite shall not exceed 10 m.
15-06-15	**AOC-12-F01**	**AOC-12-F01**	The AOCS shall be capable of slewing the payload's line of sight, based on ground update of an on-board path control algorithm.	The AOCS shall be capable of slewing the payload's line of sight, over 40° while above 80° latitude.
19-06-15	**POS-01**	**AOC-11-F02**	The absolute positioning error of the satellite shall not exceed *TBD* m, *@ 10*% confidence level.	The absolute positioning error of the satellite shall not exceed 10 m.
19-06-15	**PNT-01**	**AOC-21**	The absolute pointing error of the thrust vector during orbital manoeuvres shall not exceed *TBD*° half cone angle, *@ TBD*% confidence level.	The absolute pointing error of the thrust vector during orbital manoeuvres shall not exceed 90° half cone angle.
19-06-15	**PNT-02**	**AOC-22**	The spacecraft shall keep the solar arrays Sun pointing after solar array deployment and initial Sun acquisition apart from preselected periods.	-
19-06-15	**PNT-03**	**AOC-23**	The absolute pointing error of the solar array rotation axis shall not exceed *TBD*°, *@ TBD*% confidence level.	The absolute pointing error of the solar array rotation axis shall not exceed 1°.

19-06-15	**PNT-04**	**AOC-24**	The absolute pointing error of the X-band antenna during ELINT gathering shall not exceed *TBD*° half cone angle, @ *TBD*% confidence level.	The absolute pointing error of the X-band antenna during ELINT gathering shall not exceed 1° half cone angle
19-06-15	**PNT-05**	**AOC-25**	The absolute pointing error of the L & S-band antenna during ELINT gathering shall not exceed *TBD*° half cone angle, @ *TBD*% confidence level.	The absolute pointing error of the L & S-band antenna during ELINT gathering shall not exceed 1° half cone angle.
19-06-15	**PNT-06**	**AOC-26**	The absolute pointing error of the TT&C antenna during TT&C communications shall not exceed *TBD*° half cone angle, @ *TBD*% confidence level.	The absolute pointing error of the S-band antenna during downlink communications shall not exceed 60° half cone angle.
19-06-15	**PNT-07**	**AOC-27**	The absolute pointing error of the L-band antenna during GPS jammer detection and localisation shall not exceed *TBD*° half cone angle, @ *TBD*% confidence level.	The absolute pointing error of the L-band antenna during GPS jammer detection and localisation shall not exceed 1° half cone angle.
19-06-15	**PNT-08**	**AOC-28**	The absolute pointing error of the up-/downlink antenna during mission up-/downlink shall not exceed *TBD*° half cone angle, @ *TBD*% confidence level.	The absolute pointing error of the UHF-band antenna during uplink and ISL communications shall not exceed 90° half cone angle.
19-06-15	**PNT-09**	-	The absolute pointing error of the ISL antenna during inter-satellite communications shall not exceed *TBD*° half cone angle, @ *TBD*% confidence level.	Removed
19-06-15	**PNT-10**	-	The absolute pointing error of the radiators shall not exceed *TBD*° half cone angle, @ *TBD*% confidence level.	Removed
19-06-15	**AOC-09-F01**	-	Upon separation from the launcher interface the AOCS shall damp out the residual angular rates and acquire the Sun along a specific spacecraft axis within *TBD* minutes and compatible with the power and thermal requirements for the subsequent deployment of solar arrays and antenna booms.	Upon separation from the launcher interface the AOCS shall damp out the residual angular rates and acquire the Sun along a specific spacecraft axis before the batteries are depleted.
22-06-15	**AOC-21**	-	The absolute pointing error of the thrust vector during orbital manoeuvres shall not exceed *TBD*° half cone angle.	The absolute pointing error of the thrust vector during orbital manoeuvres shall be minimal.

B | Electrical Block Diagram

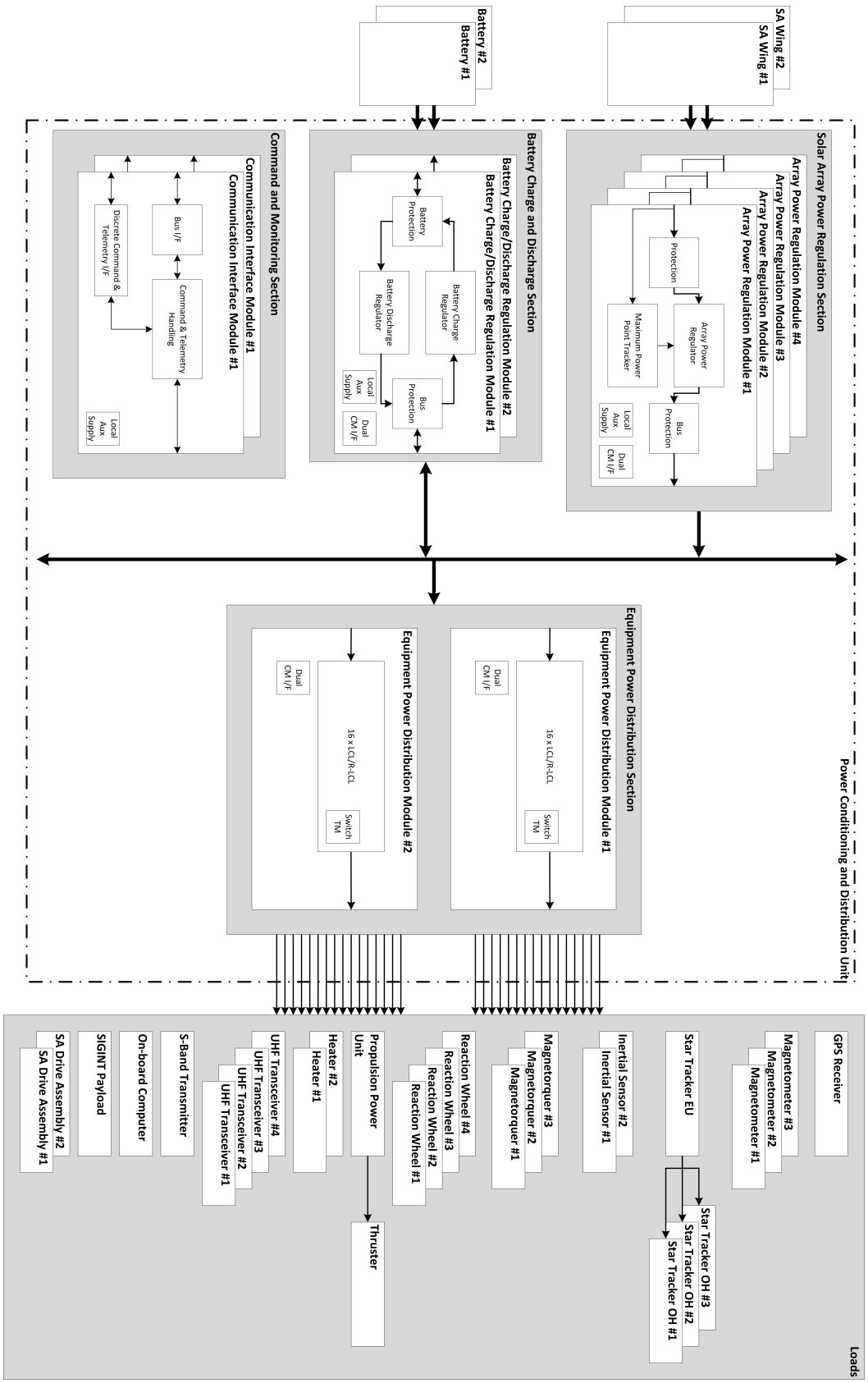

Figure B.1: Electrical block diagram.

C | Electrical Power Budget Breakdown

This chapter provides a detailed overview of the required power per subsystem component.

Table C.1: Detailed power budget of LEOPARDSAT

Positioning subsystem	**Power**	**Quantity**	**Duty cycle**	**Margin**	P_{avg}	P_{peak}
GPS receiver	5.5 W	1	100%	5%	5.8 W	5.8 W
Subsystem total					**5.8 W**	**5.8 W**
Attitude determination subsystem						
Magnetometer	0.3 W	3	12%	5%	0.11 W	0.9 W
Star tracker OH	1 W	3	100%	5%	3.2 W	3.2 W
Star tracker EU	8 W	2	50%	5%	8.4 W	8.4 W
Inertial sensor	1.5 W	2	100%	5%	3.2 W	3.2 W
Subsystem total					**14.8 W**	**15.6 W**
Attitude control subsystem						
Magnetorquer	1.2 W	3	12%	5%	0.5 W	3.8 W
Reaction wheel	2.8 W	4	100%	5%	11.8 W	42 W
Subsystem total					**12.2 W**	**45.8 W**
Propulsion subsystem						
PPU	161 W	1	12.5%	5%	21.1 W	169.1 W
Heater 1	15 W	1	100%	5%	15.8 W	15.8 W
Heater 2	15 W	1	12.5%	5%	2.0 W	15.8 W
Subsystem total					**36.9 W**	**184.8 W**
Telemetry, Tracking, and Command subsystem						
UHF transceiver	5.5 W	4	25%	5%	5.8 W	5.8 W
S-band transmitter	38 W	2	5%	5%	4.0 W	39.9 W
Subsystem total					**9.8 W**	**45.7 W**
Power subsystem						
PCDU	19.0 W	1	100%	5%	19.0 W	19.0 W
SADA	5 W	2	100%	5%	10.5 W	16.8 W
Subsystem total					**30.45 W**	**36.75 W**
Payload						
ELINT Payload	150 W	1	100%	20%	180 W	240 W
Subsystem total					**180 W**	**240 W**
Command and Data Handling subsystem						
On-board computer	10 W	1	100%	5%	10.5 W	10.5 W
Subsystem total					**10.5 W**	**10.5 W**
Subtotal					**300.4 W**	**584.9 W**
Contingency						**15%**
Total					**345.5 W**	**672.7 W**

D | Mass Budget Breakdown

This chapter provides a detailed overview of the mass per subsystem component.

Table D.1: Detailed mass budget of LEOPARDSAT

Positioning subsystem	**Mass**	**Quantity**	**Total mass**
GPS antenna	0.05 kg	2	0.1 kg
GPS receiver	0.95 kg	1	0.95 kg
Subsystem total			**1.1 kg**
Attitude determination subsystem			
Magnetometer	0.06 kg	3	0.18 kg
Star Tracker OH	1.41 kg	3	4.23 kg
Star Tracker EU	1.9 kg	2	3.8 kg
Inertial sensor	0.055 kg	2	0.11 kg
Subsystem total			**8.3 kg**
Attitude control subsystem			
Magnetorquer	0.55 kg	3	1.65 kg
Reaction wheel	0.96 kg	4	3.84 kg
Subsystem total			**5.5 kg**
Propulsion subsystem			
PPU	1.61 kg	1	1.61 kg
Thruster	1.8 kg	1	1.8 kg
Propellant tank & propellant	6.0 kg	1	6.0 kg
Feed system	5.0 kg	1	5.0 kg
Subsystem total			**14.4 kg**
Telemetry, Tracking, and Command subsystem			
UHF transceiver	0.07 kg	4	0.28 kg
UHF antenna	0.03 kg	4	0.12 kg
S-band patch antenna	0.08 kg	2	0.16 kg
S-band transmitter	1.8 kg	2	3.6 kg
RF switch	0.08 kg	3	0.24 kg
Subsystem total			**4.4 kg**
Power subsystem			
Solar array	8.04 kg	2	16.1 kg
Batteries	8.02 kg	1	8.02 kg
PCDU	7.86 kg	1	7.86 kg
SADA	0.5 kg	2	1 kg
Subsystem total			**33.0 kg**
Payload			
Vivaldi antenna	0.2 kg	14	2.8 kg
X-band patch antenna	0.1 kg	18	1.8 kg
GPS patch antenna	0.3 kg	2	0.6 kg
ESM	8 kg	1	8 kg
Subsystem total			**13.2 kg**
Structure			
Bus	22.06	1 kg	22.06 kg
Antenna boom	4.6	2 kg	9.2 kg
Subsystem total			**31.26 kg**
Command and Data Handling subsystem			
On-board computer	1.5 kg	1	1.5 kg
Subsystem total			**1.5 kg**
Subtotal			**112.6 kg**
Contingency			**15%**
Total			**129.5 kg**

E | Thermal Model

The full model explained in Chapter 20 is provided below in Figure E.1. Table E.1 show the final values used in the model, or the reference to the location where these values can be found.

Table E.1: Input values

Inputs		
Solar flux	1367	$W\,m^{-2}$
Albedo	212	$W\,m^{-2}$
Eclipse time	$0-35$	minutes
Thruster burn time	300	s
Mass components	See Chapter 24.2	
Power components	See Chapter 24.1	
Contact area components	$0.001-0.1$	m^2
Conduction	See Chapter 20	

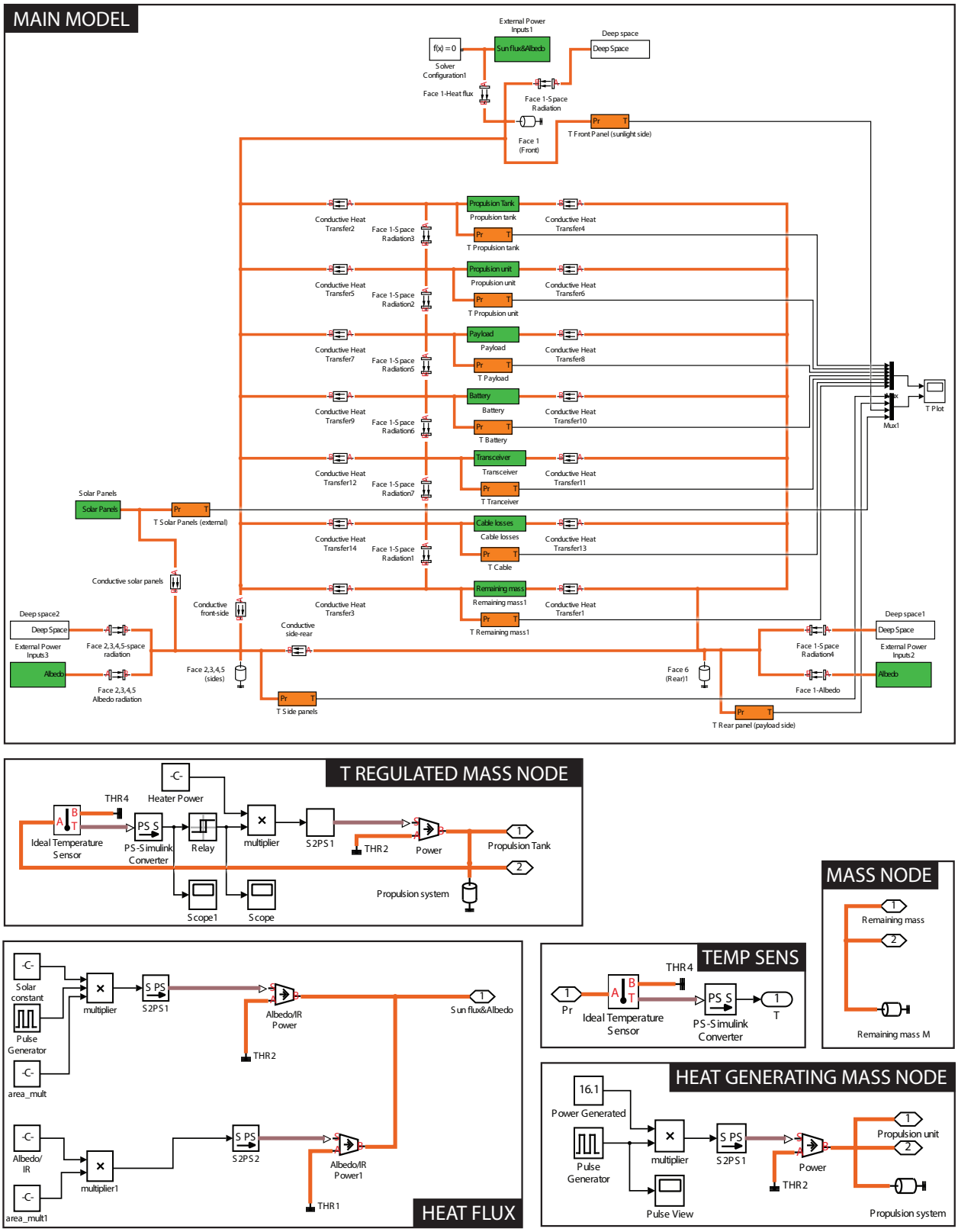

Figure E.1: Full thermal model overview

F | Work Division

Table F.1: Work division of the Final Report

Chapter	Author(s)
Preface	Danny
Summary	Tomas, Tom
1	Danny
2	Willem
3	Willem
4	Tomas, Willem
5	Willem
6	Ruben, Salwan
7	Danny, Dries
8	Willem
9	Willem
10	Tom, Maarten
11	Tomas, Jeffrey
12	Ruben
13	Salwan, Dries
14	Danny
15	Tom
16	Tom
17	Danny, Willem
18	Maarten
19	Salwan

Chapter	Author(s)
20	Jeffrey
21	Tom
22	Jeffrey, Willem, Tomas
23	Ruben, Maarten, Willem
24	Danny
25	Maarten, Tomas
26	Tomas
27	Tomas
28	Dries
29	Willem
30	Willem, Dries
31	Willem
32	Willem
33	Willem, Maarten
34	Ruben
35	Danny, Ruben
Appendix A	All
Appendix B	Danny
Appendix C	Danny
Appendix D	Danny
Appendix E	Jeffrey

Note that the following work also had to be done:

- Quality control : Ruben, Danny, Maarten, Tom
- CATIA models: Jeffrey, Tomas
- Time management: Dries